ER-6643
January 1964

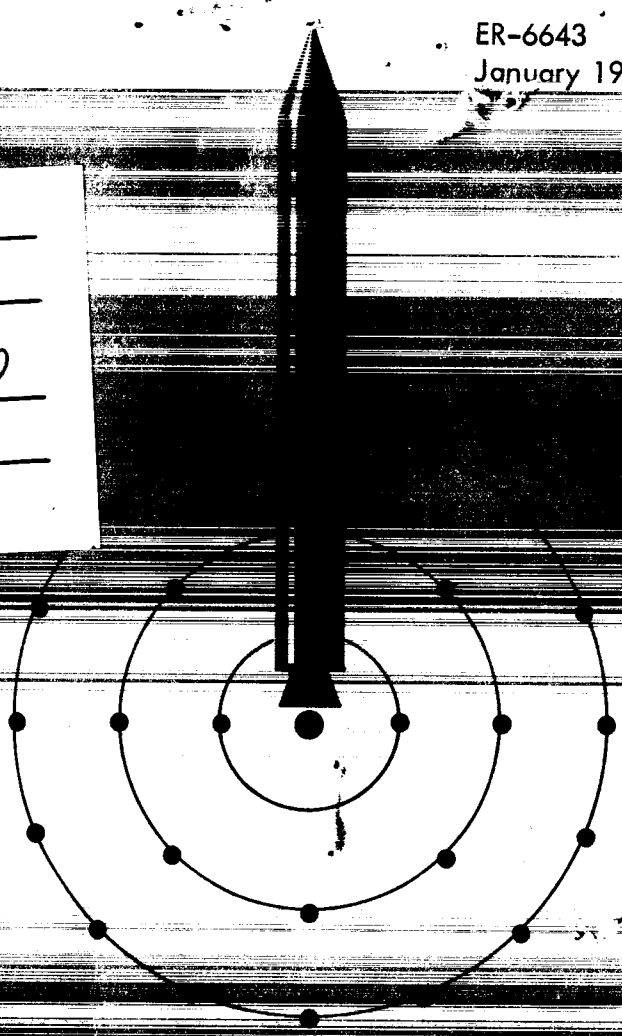

Computer Programs for Shielding Problems in Manned Space Vehicles

NASA CONTRACT NO. NAS 8-5180

Copy No. ____

ER-6643

January 1964

COMPUTER PROGRAMS FOR SHIELDING PROBLEMS IN MANNED SPACE VEHICLES

Prepared By:

C. W. Hill
C. C. Douglass, Jr.
W. B. Ritchie
K. M. Simpson, Jr.

Prepared For:

George C. Marshall Space Flight Center
National Aeronautics and Space Administration
Huntsville, Alabama

NASA Contract NAS 8-5180

LOCKHEED NUCLEAR PRODUCTS
Lockheed-Georgia Company -- A Division of Lockheed Aircraft Corporation

If this document is supplied under the requirements of a United States Government contract, the following legend shall apply unless the letter U appears in the coding box:

This data is furnished under a United States Government contract and only those portions hereof which are marked (for example, by circling, underscoring or otherwise) and indicated as being subject to this legend shall not be released outside the Government (except to foreign governments, subject to these same limitations), nor be disclosed, used, or duplicated, for procurement or manufacturing purposes, except as otherwise authorized by contract, without the permission of Lockheed-Georgia Company, A Division of Lockheed Aircraft Corporation, Marietta, Georgia. This legend shall be marked on any reproduction hereon in whole or in part.

The "otherwise marking" and "indicated portions" as used above shall mean this statement and includes all details or manufacture contained herein respectively.

Code: U Contract: NAS 8-5180

FOREWORD

This report is submitted to the George C. Marshall Space Flight Center, National Aeronautics and Space Administration, Huntsville, Alabama, in accordance with the requirements of Contract NAS8-5180.

SUMMARY

This report describes the results of an effort to extend and refine certain space radiation shielding codes and to provide detailed code descriptions and operating instructions so that the codes may be used at other installations. In particular, the approximations in the proton penetration code have been examined and improved where possible. Changes include a better attenuation kernel for evaporation neutrons, parabolic rather than linear interpolation in tables, arbitrary angle of incidence for monodirectional proton beams, removal of the assumption of constant cross section within a layer, and inclusion of a source term calculation for secondary gamma rays.

Three new codes were written during the present effort. Program LIGHT computes gamma ray cascades from excited nuclei. Program MSGAM computes gamma ray dose due to the distributed sources developed in the proton penetration code. Program LRSPC computes improved proton range and stopping power data for use in the proton penetration code.

The production of cascade gamma rays arising from inelastic nucleon collisions with shield nuclei was examined because of conflicting results of other investigators. Madey et al. found that the gamma ray component overshadows the primary proton component in certain cases of interest. Alsmiller et al., using a different approach, estimated a gamma ray component which was smaller by a factor of ten. Results presented herein, based on a third approach, tend to agree with those of Alsmiller et al. A discussion of the discrepancies and their possible origin is given.

TABLE OF CONTENTS

LIST OF FIGURES

LIST OF FIGURES (Continued)

1. GAMMA RAY PRODUCTION IN PROTON SHIELDS

The question of secondary production in proton shields has been investigated during the past several years in order to assess its importance for space radiation shielding. Secondary component calculational methods have been developed for cascade protons, cascade neutrons, and evaporation neutrons. Estimates have shown that meson production in shields up to 100 grams per square centimeter is insignificant. However, estimates of gamma ray production and transport indicate that this component may be as important as other secondary components and should, therefore, be considered in dose calculations.

Experimental data concerning gamma ray production due to nucleon bombardment is scant and incomplete. A calculational method based on direct experimental results would, of necessity, incorporate several gross assumptions. The two limiting features of such a method would be the assumption of gamma ray spectrum and yield with bombarding energy and the difficulty of extending the calculation to materials for which no experimental data exists.

In view of the difficulties connected with the utilization of present experimental data on gamma ray production, a model has been constructed which will predict gamma ray yield from basic nuclear data, much of which is available in the literature or may be calculated. The data obtained from the model should yield space radiation shielding results as reliable as those obtained from the present experimental data. In addition, this approach permits investigation of a wide variety of shielding materials.

The calculation of gamma ray yield is based on the statistical model of the nucleus. Consider a nucleus composed of A nucleons. Nuclide A is normally in the ground state, but may be excited to a higher state by an inelastic collision with a high energy nucleon. The distribution of excited states is taken from the Nuclear Data Sheets[35] for low-lying levels, and is calculated from Bethe's equation using Varshni's fit[45] for higher levels. The probability of exciting a particular level is based upon statistical considerations.

The excited nucleus may decay in several ways. It may emit a gamma ray and go to a lower level. A series of such transitions is termed a gamma ray cascade and is pictured in Figure 1. The dashed vertical arrow represents

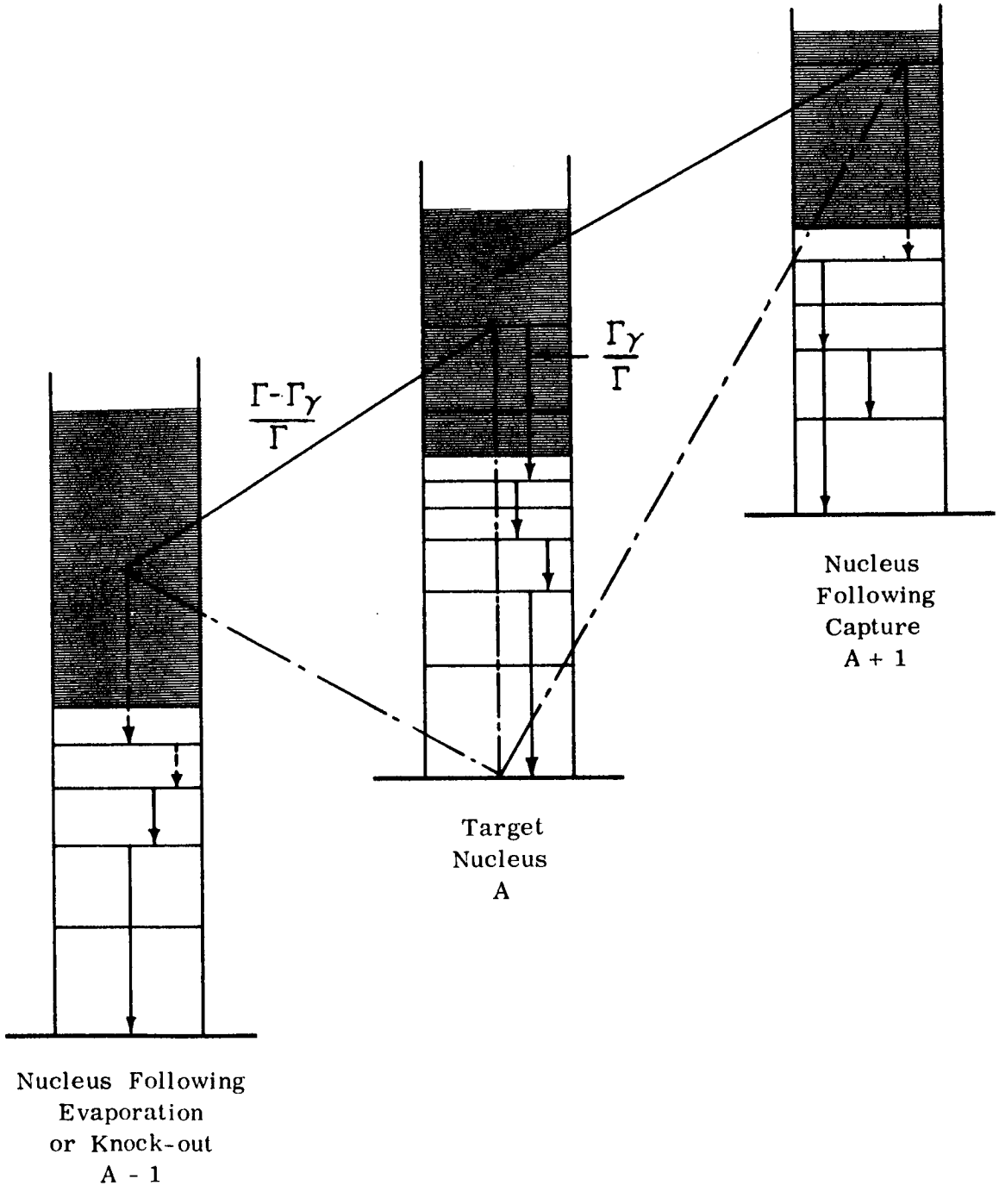

FIGURE 1 EXCITATION AND DE-EXCITATION SCHEME FOR BOMBARDED NUCLEUS

excitation and the solid vertical arrows represent a particular cascade mode. At each step in this process, gamma ray emission competes, usually weakly, with particle evaporation until the excitation energy is lower than the threshold for particle emission. The total gamma ray production in nuclide A is computed according to a method outlined by Troubetzkoy.[44] Further details are given in Section 4, the description of computer program LIGHT which traces the cascade.

Program LIGHT ignores gamma rays which may be emitted following direct knock-on processes and particle evaporation as illustrated in the formation of nuclide A-1 in Figure 1. These gamma rays are estimated in the following way. It is assumed that no gamma rays are emitted until a sequence of evaporations leaves the residual nucleus in a state just above the threshold for particle emission. From this point, the residual nucleus, A-N where N is the number of particles which have left, is assumed to emit gamma rays similar to those of the parent nucleus, A, which is also several Mev above particle emission threshold. The overestimate arising from the fact that the last evaporation is not permitted to take the nucleus to the ground state is partially compensated for by permitting a fraction of the residual nuclei to evaporate a final particle, giving rise to no gamma rays at all.

In the case of nucleon capture, also shown in Figure 1, the nucleus A + 1 is assumed to decay similarly to nucleus A.

The proton penetration code, LPPC, uses spectral yield data developed by LIGHT to calculate and sum gamma ray production as a function of incident particle energy and the type of target nucleus. Interactions produced by primary protons, cascade protons, and cascade neutrons are taken into account. The resulting gamma ray sources are output on punched cards in the form of energy and depth distributions.

Gamma ray dose is computed by program MSGAM using source data from the proton penetration code. A calculation is performed for each of ten gamma ray energies for which isotropic sources are distributed throughout the shield. Moments method buildup factors[12,19] are used for the gamma ray transmission calculations.

Several calculations have been performed for three shield materials; carbon, aluminum, and iron. The results for carbon should be regarded as tentative; since many aspects of the statistical model are violated by light nuclei.

Figure 2 shows a comparison of the present results with those of Madey, et al.,[30] and of Alsmiller, et al.[7] Madey based his gamma ray yield data upon experimental data for protons in aluminum at 14 Mev. He assumed that gamma ray production was constant for bombarding energies up to 50 Mev and zero thereafter. Gamma rays arising from secondary protons and neutrons were ignored. The Alsmiller results are based upon a theoretical model which yields gamma production cross sections for inelastic (n, n') reactions. The neutron cross sections are assumed to apply to proton reactions after an adjustment is made for the coulomb barrier. Two upper cut-off energies are shown, 22.3 Mev and 50 Mev, yielding a factor of two or three difference. All gamma rays are assumed to be emitted straight ahead in the Alsmiller calculation so that contributions arise from protons entering along the shield normal only. Gamma rays arising from secondary protons and neutrons are ignored.

The data presented in Figure 2 show that the Lockheed results agree with the Alsmiller, et al., calculations for shield thicknesses greater than 20 grams per square centimeter. Above 70 grams per square centimeter, the Lockheed curve changes slope, reflecting the contributions due to cascade nucleons. It is significant that the dose at the larger thicknesses of aluminum is primarily due to gamma rays generated by low energy protons in the first centimeter of shielding. This fact indicates that proton experiments below 50 Mev would be of great value in confirming secondary gamma ray dose calculations for the relatively soft proton spectrum of most flares.

At small shield thicknesses, the Lockheed results are appreciably higher than those of Alsmiller, et al. A portion of the discrepancy may be due to the gamma ray transport calculation. Alsmiller, et al., used the straight-ahead approximation which assumes that only those protons entering the shield along the normal contribute to the dose at the center of the spherical shell shield. A second possibility is that the low energy gamma ray yields may be larger in the Lockheed calculation, leading to a higher dose estimate near the entry face of the shield. A third possible explanation of the discrepancy may be in the choice of thickness mesh size near the entry face. In the Lockheed calculation, a mesh size of 0.1 was required in the first 0.5 grams per square centimeter of aluminum to yield an accurate dose estimate. The mesh size would be less important if the low energy portion of the gamma ray spectrum were small or if a hard proton spectrum were analyzed.

Both the Alsmiller results and the Lockheed results are generally much lower than the dose estimates of Madey, et al. The difference is thought to

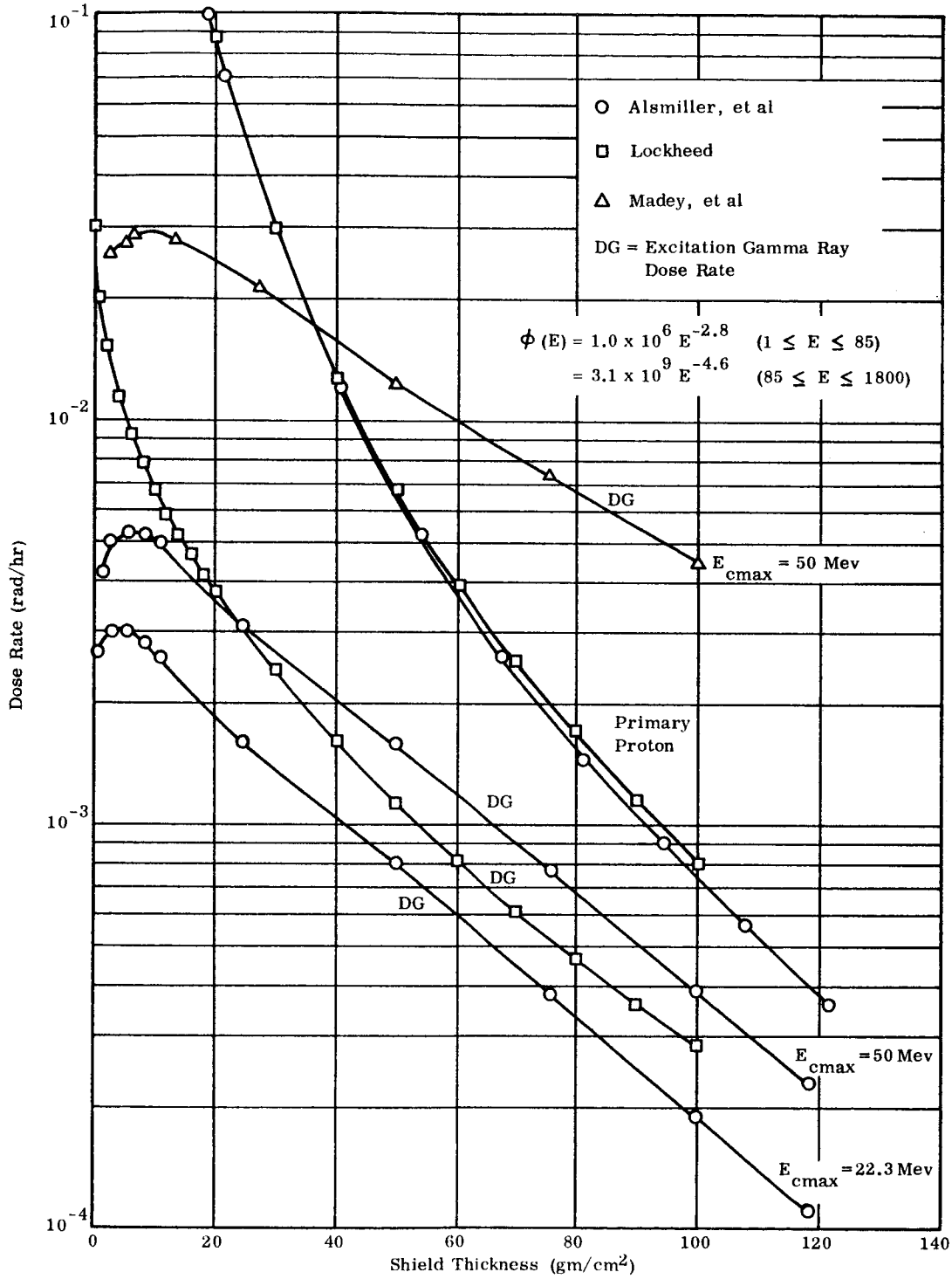

FIGURE 2 COMPARISON OF GAMMA AND PRIMARY PROTON TISSUE DOSE RATES AT CENTER OF SPHERICAL ALUMINUM SHIELD FROM ISOTROPIC SOLAR FLARE PROTONS

be due to two factors. First, Madey et al. assumed the gamma ray yield per unit proton flux is constant from the Coulomb barrier energy to 50 Mev. This procedure probably overestimates the gamma ray yield for protons whose energy is between 4 and 12 Mev. Second, the Lockheed gamma ray spectrum has less low energy photons than the 14 Mev proton data indicate.[46] If this difference is the same at other bombarding energies, the Lockheed dose results may be low by a factor of two.

Figure 3 shows a second comparison with the results of Alsmiller et al. In this case the disagreement is only a factor of two at small thicknesses, perhaps due to the use of a harder spectrum.

The importance of gamma ray secondaries compared to other dose components may be seen in Figures 4 through 9. Doses are plotted for carbon, aluminum, and iron shields for the Freden-White spectrum and for an imaginary envelope solar flare.[51]

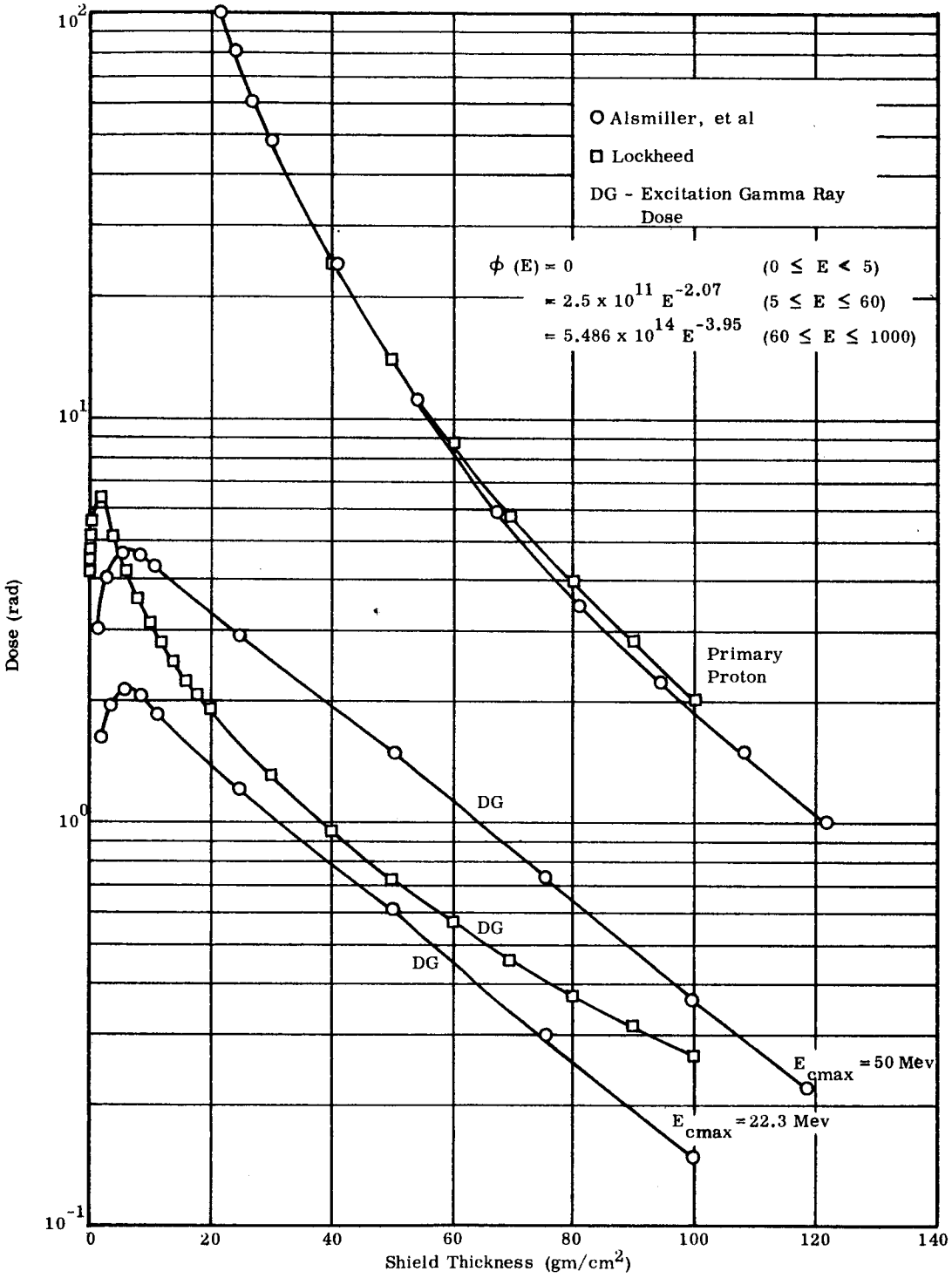

FIGURE 3 COMPARISON OF GAMMA AND PRIMARY PROTON TISSUE DOSES AT CENTER OF SPHERICAL ALUMINUM SHIELD FROM ISOTROPIC SOLAR FLARE PROTONS

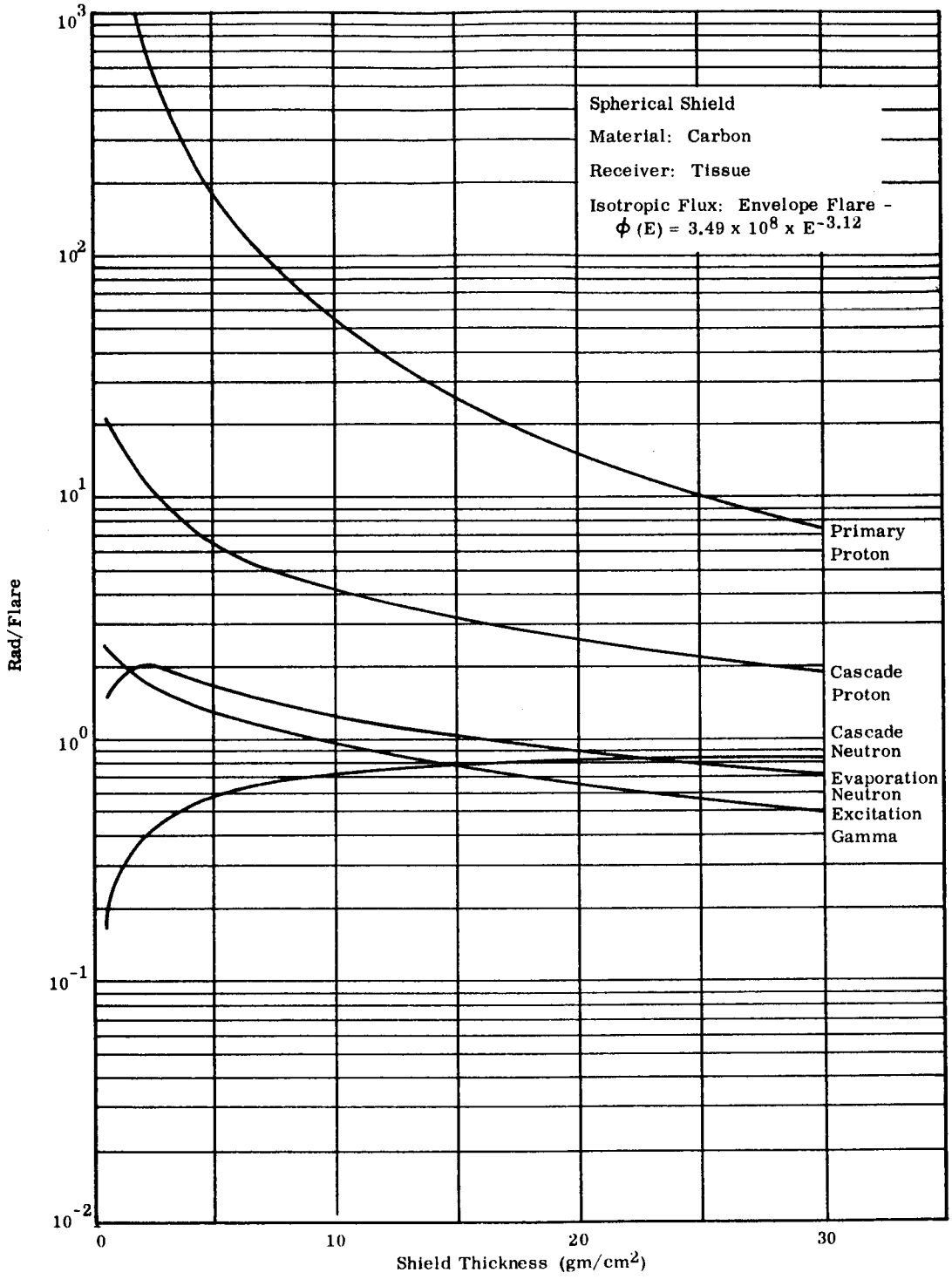

FIGURE 4 DOSE PER FLARE

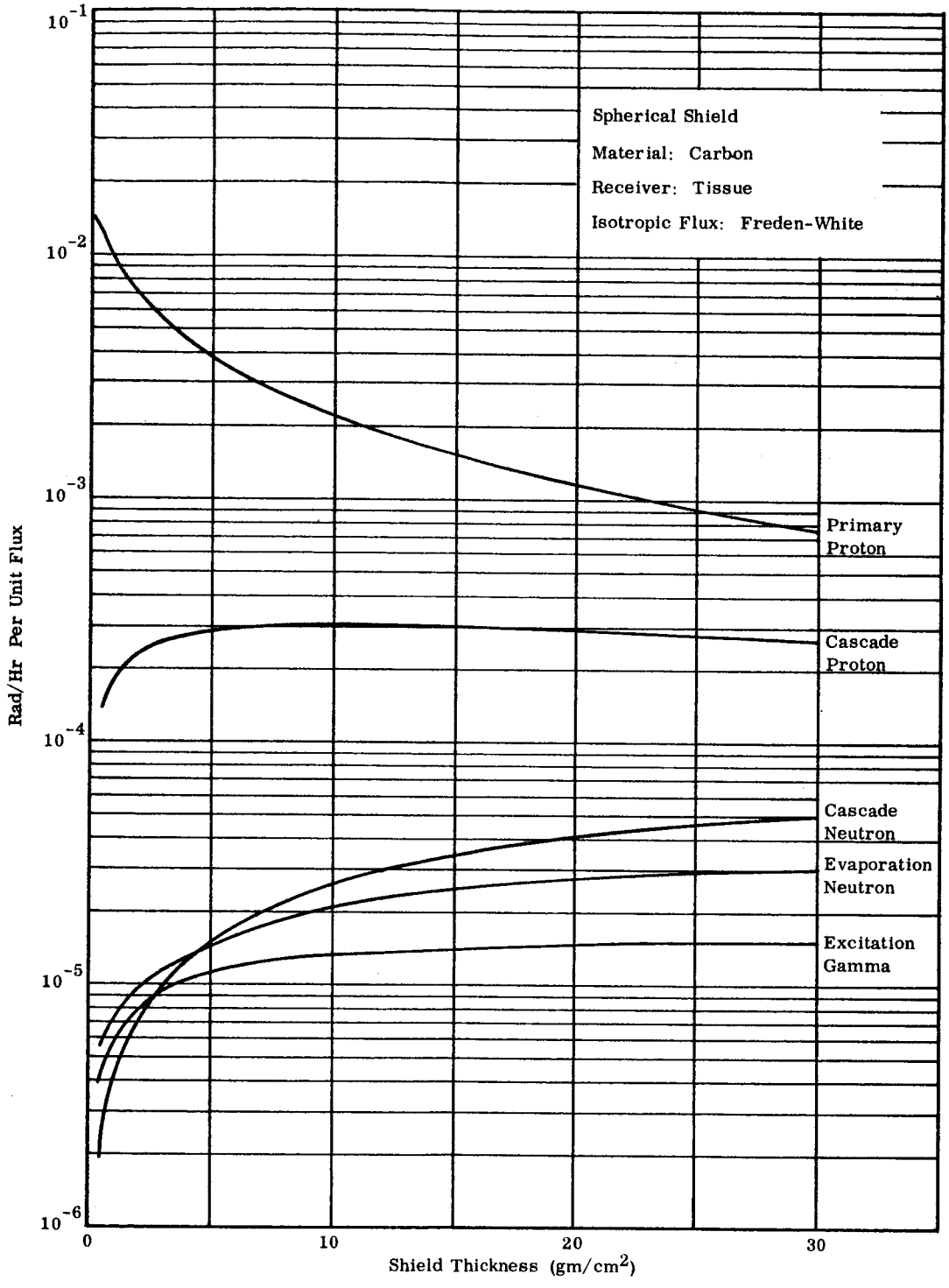

FIGURE 5 DOSE RATE PER UNIT FLUX ABOVE 40 MEV

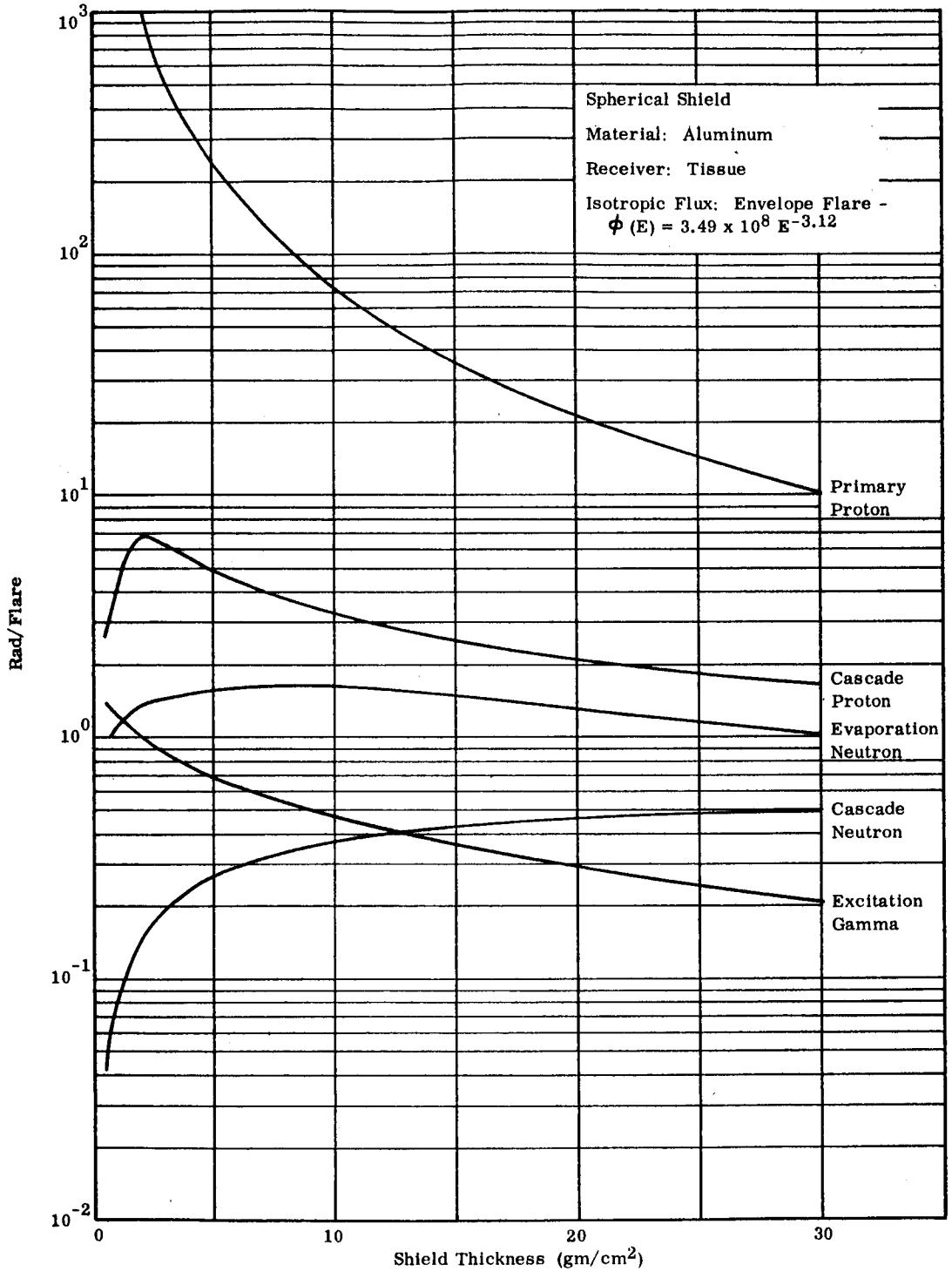

FIGURE 6 DOSE PER FLARE

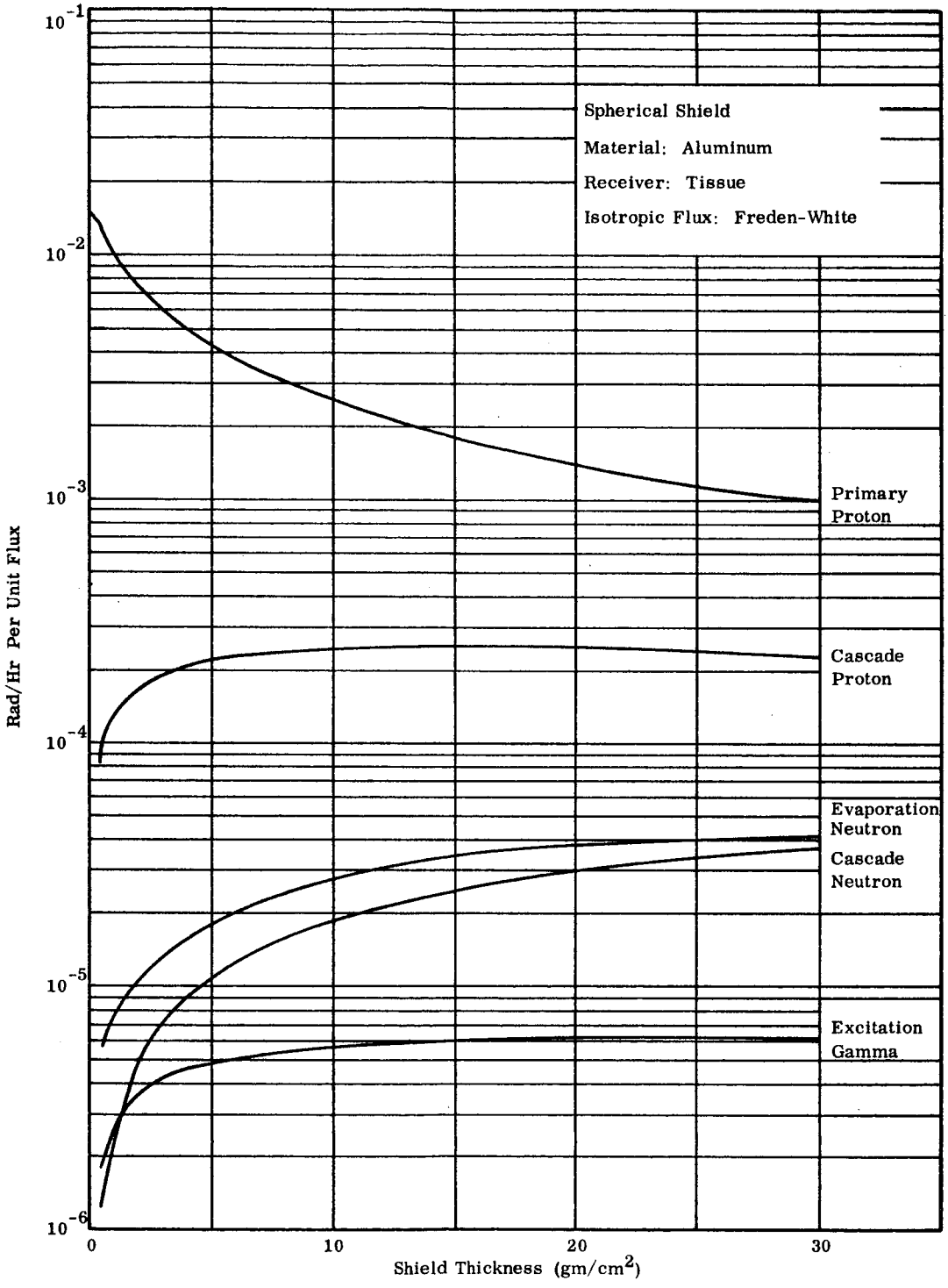

FIGURE 7 DOSE RATE PER UNIT FLUX ABOVE 40 MEV

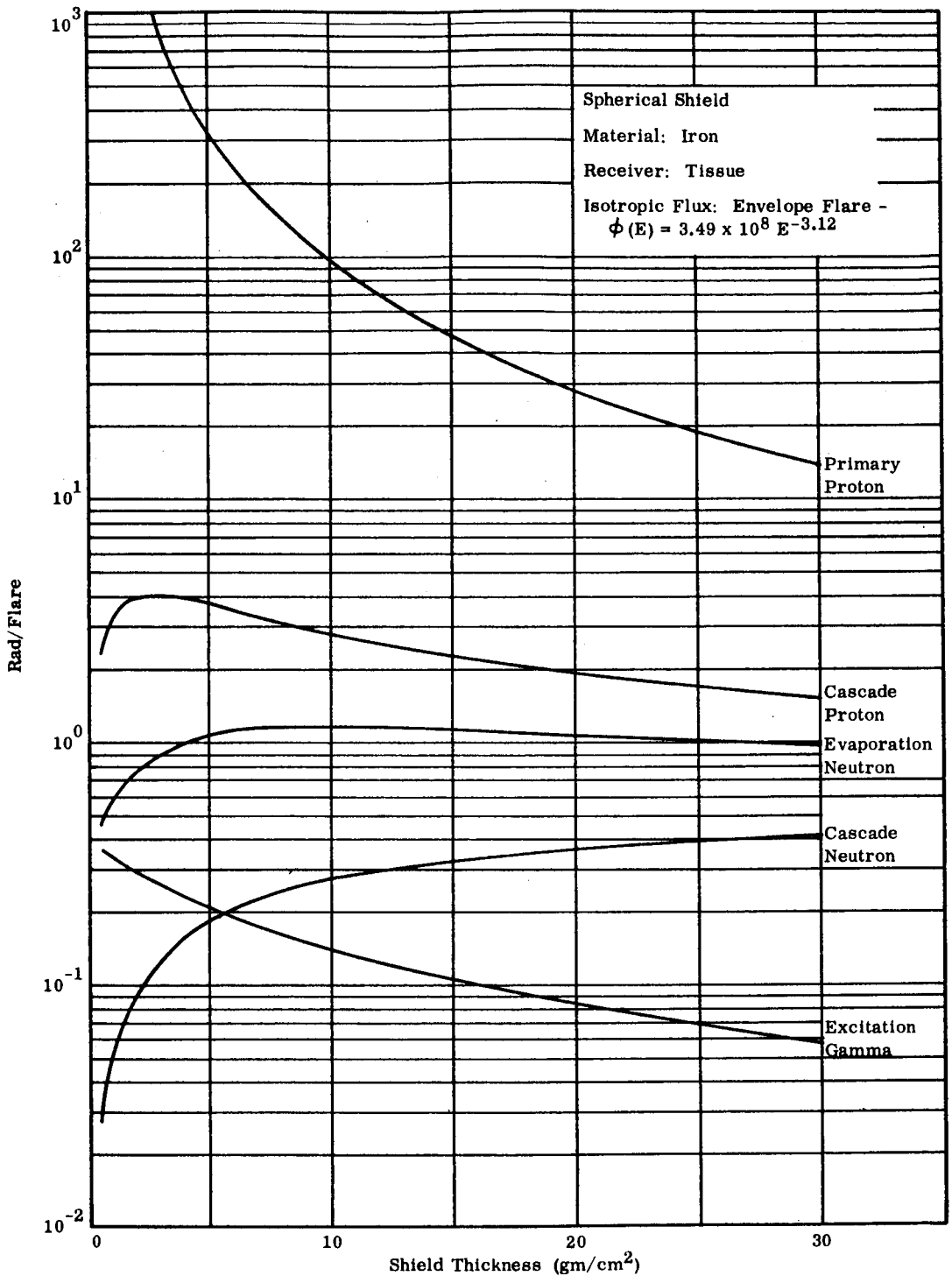

FIGURE 8 DOSE PER FLARE

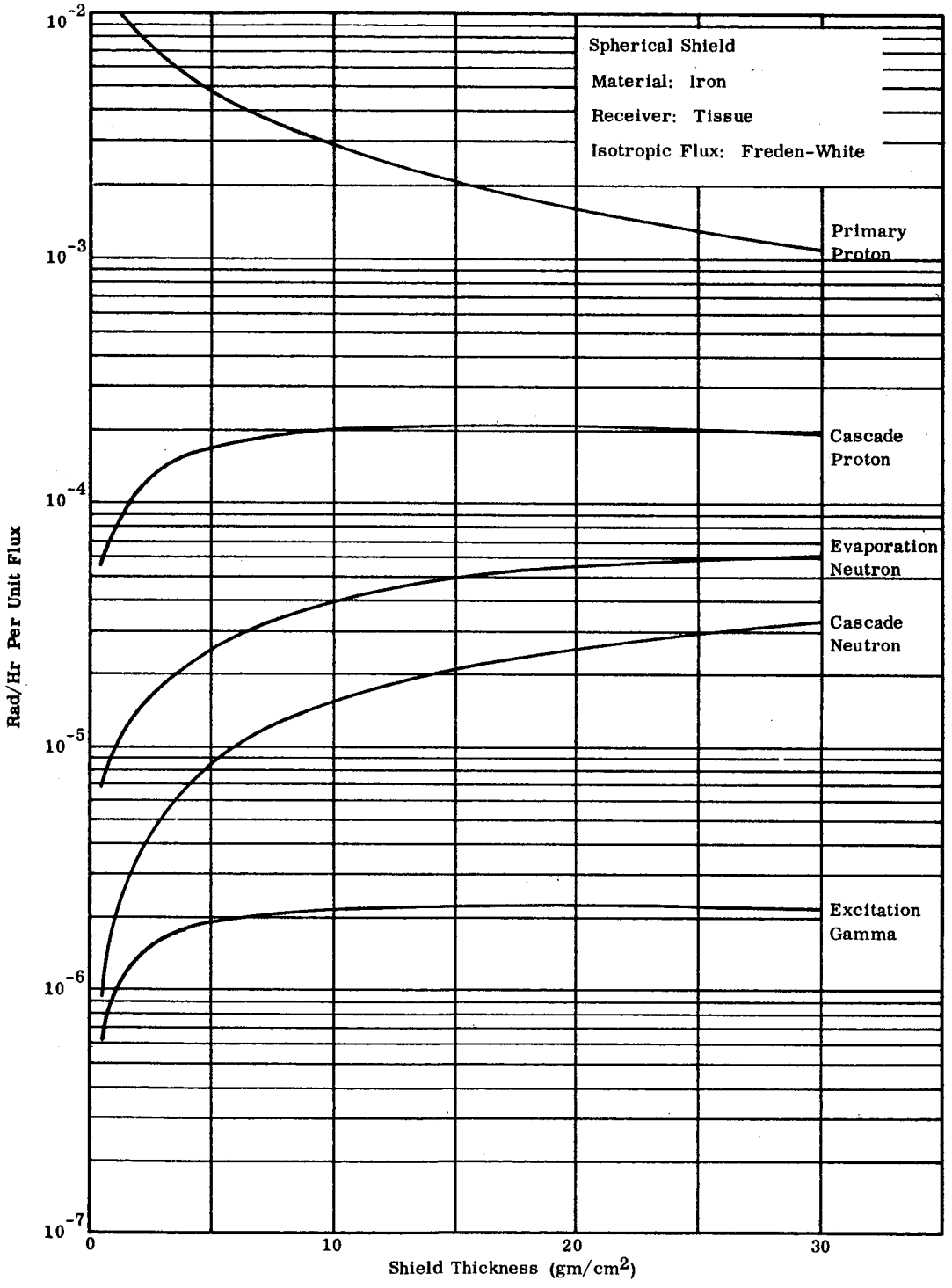

FIGURE 9 DOSE RATE PER UNIT FLUX ABOVE 40 MEV

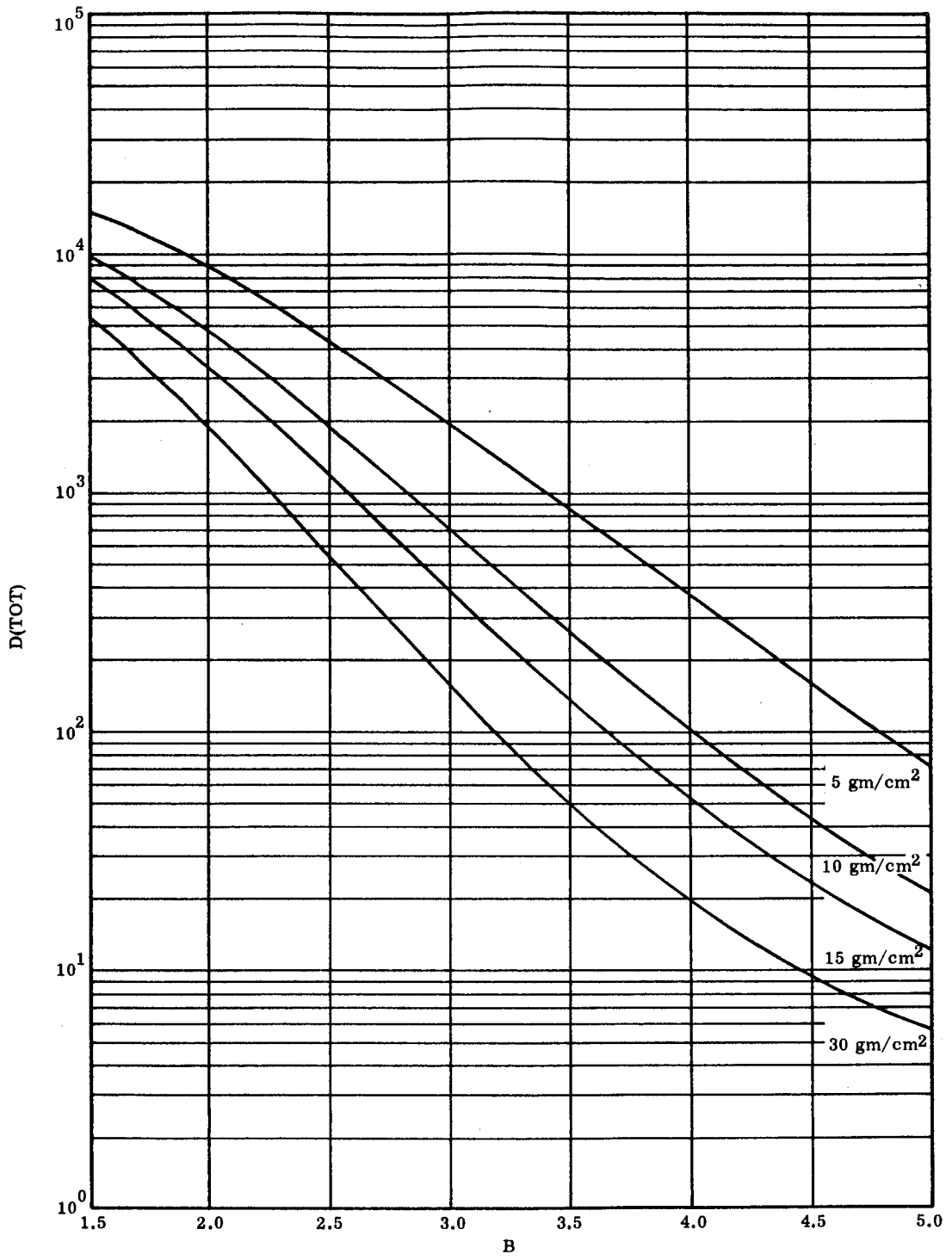

FIGURE 10 TOTAL DOSE VERSUS SPECTRUM SHAPE - ALUMINUM SHIELD

2. PARAMETRIC STUDY OF PROTON PENETRATION CODE

The dose rate, D(TOT), calculated by LPPC is extremely sensitive to the incident proton spectrum shape. This is indicated by the data displayed in Figure 10; the dose rate is plotted versus B, the parameter in the power law spectrum AE^{-B}, for four shield thicknesses. The coefficient A is determined such that

$$A \int_{10(\text{Mev})}^{\infty} E^{-B}\, dE = 1.0 \times 10^{8}$$

that is, the integral flux is constant over the range of B. The shield material used for this presentation is aluminum, and the receiver is water.

To determine the effect of the energy table mesh size on the LPPC calculations, an extensive program of varying the step size within each energy group and varying the sizes of the four energy groups in the table was performed. Fine mesh steps for the low energies in the table and coarse mesh steps for the high energies were found to be most suitable. A satisfactory arrangement is 1 Mev steps from the minimum energy to 20 Mev, 2 Mev steps from 20 Mev to 50 Mev, 10 Mev steps from 50 Mev to 300 Mev, and 50 Mev steps from 300 Mev to the maximum energy. This arrangement provides a relatively short energy table, which results in shorter times on the computer. A finer mesh does not improve the LPPC calculations to an appreciable degree.

The effect of the step size used in stepping through the shield material is indicated in Tables A and B. The incident proton spectrum is the "imaginary flare enevelope" with isotropic distribution;[51] the isotropic incidence is used because the calculations are most sensitive to step size in this mode. The maximum percent difference in the total dose rate is less than 1.2 percent, and the maximum percent different in the total proton number flux is less than 1.1 percent. Hence, the LPPC calculations are not very sensitive to step sizes between 1 and 10 gm/cm^2 in thickness.

Table C indicates the effect on the total dose rate, of step size through an extremely thick cesium shield. It is to be noted that the percent difference remains less than 10% for shields up to 300 gms/cm^2 in thickness. Apparently, large step sizes tend to underestimate the dose rate for shields

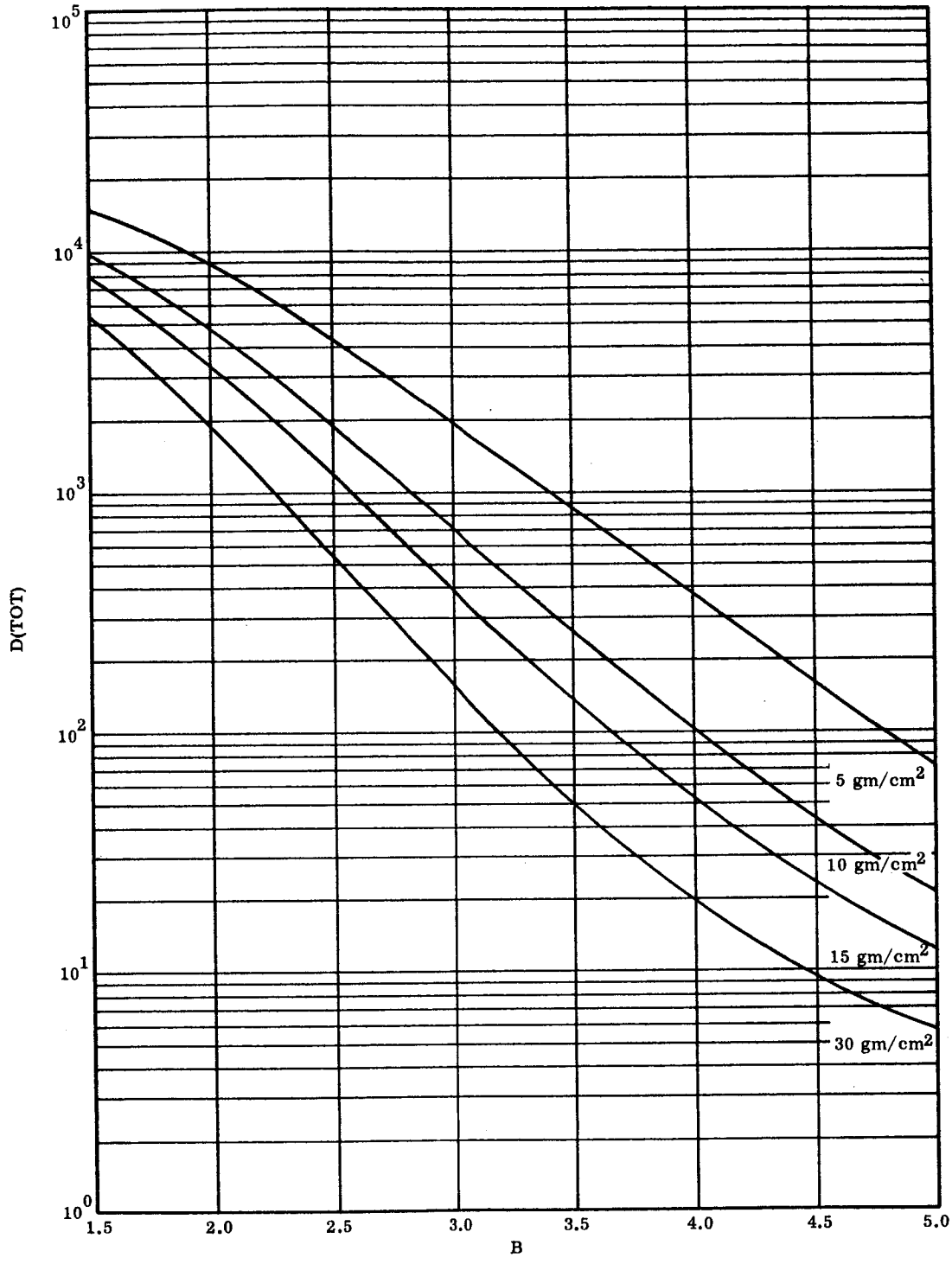

FIGURE 10 TOTAL DOSE VERSUS SPECTRUM SHAPE - ALUMINUM SHIELD

less than 30 gm/cm^2 thick and overestimate the dose rate for shields greater than 30 gm/cm^2 thick.

TABLE A

TOTAL DOSE RATE - ALUMINUM

X \ ΔX	1.0 gm/cm^2	2.0 gm/cm^2	5.0 gm/cm^2	10.0 gm/cm^2
0.0 gm/cm^2	3.30×10^4	3.30×10^4	3.30×10^4	3.30×10^4
0.5	1.20×10^4	1.20×10^4	1.20×10^4	1.20×10^4
2.0	1.20×10^3	1.20×10^3	1.20×10^3	1.20×10^3
4.0	3.95×10^2	3.91×10^2	3.91×10^2	3.91×10^2
10.0	9.38×10^1	9.30×10^1	9.29×10^1	9.27×10^1
20.0	3.44×10^1	3.43×10^1	3.43×10^1	3.42×10^1
30.0	1.97×10^1	1.97×10^1	1.98×10^1	1.98×10^1

TABLE B

TOTAL PROTON NUMBER FLUX - ALUMINUM

X \ ΔX	1.0 gm/cm^2	2.0 gm/cm^2	5.0 gm/cm^2	10.0 gm/cm^2
0.0 gm/cm^2	1.58×10^7	1.58×10^7	1.58×10^7	1.58×10^7
0.5	4.26×10^6	4.26×10^6	4.26×10^6	4.26×10^6
2.0	8.12×10^5	8.09×10^5	8.09×10^5	8.09×10^5
4.0	3.55×10^5	3.51×10^5	3.51×10^5	3.51×10^5
10.0	1.14×10^5	1.13×10^5	1.13×10^5	1.13×10^5
20.0	4.68×10^4	4.63×10^4	4.63×10^4	4.63×10^4
30.0	2.68×10^4	2.66×10^4	2.66×10^4	2.67×10^4

TABLE C

TOTAL DOSE RATE - CESIUM

X \ ΔX	5.0 gm/cm^2	20.0 gm/cm^2	% Difference
20.0 gm/cm^2	54.0	53.3	-1.3
40.0	16.8	16.8	0.0
60.0	8.57	8.64	0.82
80.0	5.36	5.40	1.9
100.0	3.75	3.86	2.9
200.0	1.19	1.27	6.7
300.0	0.56	0.61	8.9

3. PROTON PENETRATION CODE (LPPC)

CODE DESCRIPTION

The Lockheed Proton Penetration Code (LPPC) is an IBM-7094 program which calculates primary and secondary doses behind multistrata slab shields due to an incident proton flux. A number of options are available to treat diverse proton angular and energy distributions and to provide several types of output data. Early versions of this code have been reported in several previous reports.[5, 6, 38]

Incident Flux

The incident proton flux may be monodirectional or isotropic. The monodirectional flux option treats protons impinging on a slab shield at an arbitrary angle. The isotropic flux option considers isotropic protons incident on a slab shield and applies a transformation to convert to a spherical shell shield. The slab doses are available as intermediate output, if desired.

The energy spectrum of the initial protons is specified as the number flux, differential in energy, or as monoenergetic. Spectrum option 1 computes the spectrum from the power law given in Equation 3-1.

$$\Phi(E) = A \cdot E^{-B} \tag{3-1}$$

A and B are input constants and E is the energy in Mev. Spectrum option 2 computes the spectrum from an exponential form given in Equation 3-2.

$$\Phi(E) = A \cdot \mathrm{Exp}(-E/B) \tag{3-2}$$

Low and high energy cutoffs may be applied to spectrum options 1 and 2. Spectrum option 3 causes the code to read a table of the number flux, differential in energy, versus energy. A parabolic interpolation routine automatically computes the flux at the energy mesh points used in the calculation. Spectrum option 4 treats a monoenergetic proton flux.

Shield Composition

The shield is composed of one to ten homogeneous strata. A stratum may contain a single element, compound, or mixture. Each stratum may be subdivided into a number of layers. The layer size defines the thickness mesh used in solving the transport equations. The total number of layers in a shield may be as large as one hundred.

The nuclear and atomic parameters required for each material are stored on a library tape. At present, the library contains data for the nine elements and five compounds listed in Table D.

TABLE D

MATERIALS CONTAINED IN THE LPPC LIBRARY

Number	Material
1	Hydrogen
4	Beryllium
6	Carbon
7	Nitrogen
8	Oxygen
13	Aluminum
26	Iron
55	Cesium
74	Tungsten
201	Water
202	Hydrogen Peroxide
203	Polyethylene
204	Hydrazine
221	Tissue

Dose Components

Dose components are computed for zero shield thickness and after each layer. These doses include primary proton dose, cascade proton dose, cascade neutron dose, and evaporation neutron dose. In addition, gamma

ray source terms as a function of energy and depth may be calculated and output on punched cards. These data may be used in conjunction with program MSGAM (Section 5.) to obtain gamma ray dose as a function of shield thickness.

Radiation Transport

The computational model applies to a beam of protons incident on a slab shield. Isotropic flux is approximated by taking eleven beams at equal intervals in the cosine of the incident angle and performing a numerical integration over solid angle. The calculation proceeds by treating in sequence the penetration of radiation through successive shielding layers, each of which is of thickness substantially smaller than the mean free path for nuclear collisions. Given the absolute energy spectrum of nucleons incident on the first layer, the spectra of emerging nucleons are calculated on the basis of the ionization energy losses and nuclear collisions within the layer. These spectra are then taken to represent the spectra of protons and neutrons incident on the second layer, and the calculations are repeated until the desired range of shield thicknesses has been covered.

Inelastic nuclear collisions within a layer remove nucleons from the beam but may produce secondary nucleons which must be considered. These collisions are treated in accordance with the direct interaction model first proposed by Serber.[39] The nuclear reaction proceeds in two stages. In the first stage, the bombarding nucleon makes collisions with individual nucleons; and these in turn have further collisions within the nucleus, thus generating a cascade of nucleons. Since the energies of the bombarding particle and the first few nucleons involved in the cascade are large compared to the binding energy of a nucleon, this stage of the reaction may be considered to consist of collisions between free nucleons. The Pauli exclusion principle should be taken into account in that collisions that would lead to nucleons in otherwise occupied states are forbidden. Energies of the first few particles involved in the cascade are typically large enough so that these emerge from the nucleus. After a few collisions, however, the energies of the remaining nucleons involved in the cascade are reduced below that necessary for escape. At the end of the cascade stage, a residual nucleus remains, usually in a highly excited state. Further particle emission can then follow by the comparatively slower second stage of the reaction, the evaporation process.

The generation of secondary nucleons within the shield presents a complex shielding problem because of the energy and angular distribution of these particles. An approximate computational method has been devised on the

basis of the simplifying assumtpion that the high energy neutrons and protons resulting from the initial stage of the nuclear reaction are emitted in the direction of the incident nucleon giving rise to the reaction. An energy distribution of these straight-ahead nucleons is derived from the Metropolis data.[31,32] The more nearly isotropic evaporation nucleons are treated in a separate calculation.

The spectrum of primary and cascade nucleons is calculated after each layer by evaluating the solution to a pair of coupled, integro-differential equations, represented by Equations 3-3 and 3-4.

$$\frac{\partial \Phi_P(E,X)}{\partial X} + \Sigma_P(X) \cdot \Phi_P(E,X) = \frac{\partial \left[\Phi_P(E,X) \cdot S(E)\right]}{\partial} + \Phi_{PP}(E,X) + \Phi_{NP}(E,X) \tag{3-3}$$

$$\frac{\partial \Phi_N(E,X)}{\partial X} + \Sigma_N(E) \cdot \Phi_N(E,X) = \Phi_{PN}(E,X) + \Phi_{NN}(E,X) \tag{3-4}$$

$\Phi_P(E,X)$ = primary plus secondary proton differential energy flux. The code actually treats each component separately.

$\Phi_N(E,N)$ = cascade neutron flux.

E = energy.

X = position in shield.

$\Sigma_P(E)\ \Sigma_N(E)$ = inelastic cross section for protons (neutrons).

$S(E) = \frac{dE}{dX}$, proton stopping power.

$\Phi_{AB}(E,X)$ = cascade production term, or particles of type B produced by particles of type A in the shield layer.

Solutions to Equations 3-3 and 3-4 are given by Equations 3-5 and 3-6.

$$\Phi_P(E, X + \Delta X) = \Phi_P(E', X) \frac{S(E')}{S(E)} \mathrm{Exp}\left[-y(E') + y(E)\right] + \Phi_{PP}(E,X) + \Phi_{NP}(E,X) \tag{3-5}$$

$$\Phi_N(E, X + \Delta X) = \Phi_N(E, X)\ \mathrm{Exp}\left[- \Sigma_N(E) \cdot \Delta E \right] + \Phi_{PN}(E, N) + \Phi_{NN}(E, X) \tag{3-6}$$

where ΔX = layer thickness, and E' is defined in terms of the range, R(E).

$$R(E') = R(E) + \Delta X \tag{3-7}$$

The terms in the exponent of Equation 3-5 are defined in Equation 3-8.

$$y(E) = \int_0^E \frac{\Sigma_P(E'')}{S(E'')}\, dE'' \tag{3-8}$$

The production terms, $\Phi_{AB}(E, X)$, are given in Equations 3-9 through 3-12.

$$\Phi_{PP}(E, X + \Delta X) =$$

$$\int_X^{X+\Delta X} \left[\int_{E'}^{\infty} \Phi_P(E_I, x) \cdot \Sigma_P(E_I) \cdot \tau_{PP}(E_I, E_S) dE_I \right] \frac{S(E_S)}{S(E_I)}\, dx \tag{3-9}$$

$$\Phi_{NP}(E, X + \Delta X) =$$

$$\int_X^{X+\Delta X} \left[\int_{E_S}^{\infty} \Phi_N(E_I, x) \cdot \Sigma_N(E_I) \cdot \tau_{NP}(E_I, E_S) dE_I \right] \frac{S(E_S)}{S(E_I)}\, dx \tag{3-10}$$

$$\Phi_{PN}(E, X + \Delta X) =$$

$$\int_X^{X+\Delta X} \left[\int_{E}^{\infty} \Phi_P(E_I, x) \cdot \Sigma_P(E_I) \cdot \tau_{PN}(E_I, E_S) dE_I \right] dx \tag{3-11}$$

$$\Phi_{NN}(E, X + \Delta X) =$$

$$\int_X^{X+\Delta X} \left[\int_{E}^{\infty} \Phi_N(E_I, x) \cdot \Sigma_N(E_I) \cdot \tau_{NN}(E_I, E_S) dE_I \right] dx \tag{3-12}$$

where E_I = energy of incident particle suffering an inelastic collision at x, $X \leq x \leq X + \Delta X$

E_S = energy of secondary particles emerging from inelastic collision

$\tau_{AB}(E_I, E_S)$ = number of secondary particles of type B per unit energy at E_S resulting from the inelastic collision of a particle of type A with energy E_I.

The reduction of Equations 3-9 through 3-12 to a more tractable form is explained in an earlier report.[6] The assumptions used in the derivation are listed below.

- The flux of particles available for producing inelastic collisions is unaffected by nuclear collisions within the layer.
- The flux of cascade particles generated throughout a layer is not attenuated by nuclear collisions. Layer thickness is generally a few percent of the inelastic mean free path inside the layer and does not produce additional cascade particles within the layer.
- The cascade nucleon sources are distributed realistically through the layer.
- The effect of energy losses due to ionization within the layer is taken into account, both for proton initiated reactions and for cascade protons produced in the layer.
- The effect of nuclear attenuation and ionization losses is considered in attenuating particles which are incident on the layer.
- Finally, it is assumed that the cascade nucleon production function is separable as in Equation 3-13.

$$\tau_{AB}(E_I, E_S) = F_{AB}(E_I) \cdot G_{AB}(ES) \tag{3-13}$$

The final form of Equations 3-9 through 3-12 is given below.

$$\Phi_{PP}(E, X + \Delta X) = R_{PP}(E') \frac{1}{S(E)} \int_{E}^{E'} F_{PP}(E_S) dE_S \tag{3-14}$$

$$R_{PP}(E') = \int_{E}^{E_{max}} G_{PP}(E_I)\, \Phi_P(E_I, X)\ \Sigma_P(E_I) dE_S \tag{3-15}$$

$$\Phi_{NP}(E, X + \Delta X) = \frac{1}{S(E)} \int_{E}^{E'} R_{NP}(E_S) F_{NP}(E_S) dE_S \tag{3-16}$$

$$R_{NP}(E_S) = \int_{E_S}^{E_{max}} G_{NP}(E_I)\, \Phi_N(E_I, X)\ \Sigma_N(E_I) dE_I \tag{3-17}$$

$$\Phi_{PN}(E, X + \Delta X) = F_{PN}(E) \int_{E}^{E_{max}} G_{PN}(E_I) R_{PN}(E_I, X)\ \Sigma_P(E_I) dE_I \tag{3-18}$$

$$R_{PN}(E_I, X) = \frac{1}{S(E_I)} \int_{E_I}^{E'} \Phi_P(E'', X) dE'' \tag{3-19}$$

$$\Phi_{NN}(E, X + \Delta X) = \Delta X\, F_{NN}(E) \int_{E}^{E_{max}} G_{NN}(E_I) \cdot \Phi_N(E_I, X) \cdot \Sigma_N(E_I) dE_I \tag{3-20}$$

The code proceeds step by step through the shield, calculating the energy spectra of primary protons and cascade protons and neutrons after each layer. The energy mesh may contain up to 250 points divided into four ranges with constant energy spacing within each range. The shield may contain up to 100 layers divided into ten or fewer homogeneous strata.

The monoenergetic spectrum case is treated in a straightforward manner by adding a single term to Equations 3-3 and 3-4 to account for secondaries produced by the monoenergetic beam. The monoenergetic option is exact in the sense that a true line spectrum is used for primary protons while a continuous spectrum is used for cascade secondaries. Further details may be obtained from an earlier report.[38]

Evaporation Neutron Dose

Protons and neutrons incident on a layer may suffer inelastic collisions with the shield nuclei. The treatment of cascade nucleons ejected in the first stage of the de-excitation process has been described in the preceding section. The residual nucleus is left in a highly excited state and more particles may be emitted. Since these evaporation particles possess relatively little energy, charged nucleons are stopped quickly. However, the evaporation neutrons may increase the transmitted dose significantly for shields of moderate to large thickness.

The energy spectrum of the evaporation neutrons is continuous with an upper bound of 10 to 20 Mev. The data[15,16,21,26,27,28] available indicate that the spectrum peaks below one Mev and resembles the fission spectrum within experimental error.

The evaporation neutron source term as a function of shield thickness is computed according to Equation 3-21.

$$S_{ev}(X)dX = \frac{dX}{\cos\theta}\int_0^{E_{max}} \Phi_P(E,X)\ \Sigma_P(E)\ Y_P(E)dE + \frac{dX}{\cos\theta}\int_0^{E_{max}} \Phi_N(E,X)\ \Sigma_N(E)\ Y_N(E)dE \qquad (3\text{-}21)$$

where $S_{ev}(X)$ = evaporation neutron source density at X, (n/gm-sec)

$\Phi_P(E,X)$, $\Phi_N(E,X)$ = total proton (neutron) number flux, differential in energy, at X, (particles/cm^2-sec-Mev)

$\Sigma_P(E)$, $\Sigma_N(E)$ = inelastic cross section for protons (neutrons), (cm^2/gm)

$Y_P(E)$, $Y_N(E)$ = average isotropic evaporation neutron yield per inelastic collision

θ = angle of incidence.

If the incident proton flux is isotropic, the evaporation neutron source term is computed according to Equation 3-22.

$$S_{ev}(X)dX = dX\, 2\pi \int_0^1 \frac{d(\cos\theta)}{\cos\theta} \int_0^{E_{max}} \left[\Phi_P(E, X, \theta) \cos\theta \cdot \Sigma_P(E)\, Y_P(E) + \Phi_N(E, X, \theta) \cos\theta \;\; \Sigma_N(E)\, Y_N(E)\right] dE \qquad (3\text{-}22)$$

where the explicit flux angular distribution is considered.

The evaporation neutron dose, $D_{ev}(X)$, at shield thickness X is given by Equation 23.

$$D_{ev}(X) = \int_0^X T(X - X')\, S_{ev}(X')\, dX' \qquad (3\text{-}23)$$

where $T(X - X')$ is the dose transmission function for neutrons emitted isotropically from a plane source at X' to the exit surface at X. Both the dose transmission function and the source function are assumed to vary exponentially within each layer. With this approximation, Equation 3-24 may be integrated analytically to yield the dose after m layers.

$$D_{ev}\left(X = \sum_{i=1}^{m} \Delta X_i\right) = \sum_{i=1}^{m} \Delta X_i \frac{\left[T(X_m - X_i)S_{ev}(X_i) - T(X_m - X_{i-1})S_{ev}(X_{i-1})\right]}{\ln\left[T(X_m - X_i)S_{ev}(X_i) \,/\, T(X_m - X_{i-1})S_{ev}(X_{i-1})\right]} \qquad (3\text{-}24)$$

In the case where the denominator vanishes for, say the j^{th} term, the dose contribution becomes

$$\Delta D_{ev}(X,\ X_{j-1} \text{ to } X_j) = \Delta X_j\, T(X - X_j)\, S_{ev}(X_j) \qquad (3\text{-}25)$$

The quantity still to be determined is the dose transmission function, $T(X - X')$. Even with the assumption that evaporation neutrons are emitted isotropically with a fission spectrum, the transmission function is difficult to evaluate. Moments method data[14,18] are available for a few elements and compounds. However, these data apply to an infinite homogeneous medium so that material changes and boundaries are not taken into account properly. Monte Carlo data[2,3,4,10,29] are available for a few elements and compounds; but, again, data are not available for material changes and the particular boundary conditions of interest. Further, the incorporation of a neutron Monte Carlo penetration computation into the code would be quite prohibitative from the standpoint of computer time.

The neutron attenuation scheme incorporated into the proton penetration code is a point kernel approach based upon experimental removal cross sections for non-hydrogenous materials proposed by Albert and Welton.[1] Certain constants in the equations are adjusted to normalize to moments method data for light elements and water and to Monte Carlo data for iron and other heavy elements.

The evaporation neutron dose transmission function is given in Equation 3-26:

$$T(X - X') = \frac{1}{2} \int_0^1 \frac{G(X - X', \theta)}{\cos \theta} d(\cos \theta) \qquad (3\text{-}26)$$

where $G(X - X', \theta)$ represents the material attenuation kernel. For non-hydrogenpus shields:

$$G(X - X', \theta) = C_o \, Exp(- \sum_i K_i S_i r_i) \qquad (3\text{-}27)$$

where $C_o = 1.5 \times 10^{-5}$ rad/hr per n/cm^2-sec

i = layer number describing layers between X' and X

$K_i = 1$ for elements with atomic number 2 through 6

S_i = removal cross section for the i^{th} layer (cm^2/gm)

r_i = slant penetration distance in the i^{th} layer (gm/cm^2).

The values of K_i are chosen to improve the fit to moments method data for beryllium and carbon and to Monte Carlo data for iron.

For hydrogenous shields:

$$G(X-X', \theta) = C_1 \left(\sum_i H_i \frac{r_i}{P_i} \right)^{C_2} Exp \left[-C_3 \left(\sum_i H_i \frac{r_i}{P_i} \right)^{C_4} \right] \cdot Exp(- \sum_i S_i r_i) \qquad (3\text{-}28)$$

where $C_1 = 8.86 \; 10^{-5}$

$C_2 = 0.29$

$C_3 = 0.83$

$C_4 = 0.58$

H_i = hydrogen density in layer i relative to the hydrogen density in water

P_i = density of the material in layer i (gm/cm^3).

The intermediate case, where some layers contain hydrogen and some do not creates a special problem. This case is treated somewhat arbitrarily as follows. The material attenuation kernel is approximated by Equation 3-28 with the value of S_j replaced by $L_j S_j$. The quantity L_j equals K_j if no hydrogenous material follows layer j. However, if hydrogenous layers follow layer j, the value of L_j is chosen according to the recipe:

$$L_j = 1. \text{ for } K_j = 1$$

$$L_j = 0.5 + \left(\sum_{i=j+1}^{i_{max}} \frac{H_i r_i}{P} \right) \Big/ 15 \text{ or } 1., \text{ whichever is less, for } K_j = 0.5 \qquad (3\text{-}29)$$

The above procedure assumes that the equivalent of six inches of water will reestablish the water equilibrium fast neutron spectrum.

The methods described above enable the code to treat attenuation of evaporation neutrons in non-hydrogenous and hydrogenous shields or in multistrata shields of arbitrary composition. Further experimental and theoretical work is required to test the validity of the attenuation calculation and to examine the variation in evaporation neutron spectra as a function of atomic number and bombarding energy.

Cascade Gamma Ray Source

Protons and neutrons incident on a layer may suffer inelastic collisions with the shield nuclei. The treatment of cascade nucleons and evaporation nucleons which are ejected in the first two phases of the de-excitation process has been described in preceding sections. Gamma rays are emitted in competition with the evaporation phase and are the dominant decay mode when residual excitation energy falls below the nucleon emission threshold. Evaluation of the gamma ray source distribution in the shield is described below. The evaluation of gamma ray dose is relegated to a separate program, MSGAM.

The model used in calculating cascade gamma ray spectra is detailed in the description of the LIGHT program. The method develops a discrete spectrum arising from transitions between discrete excited states, and a continuum spectrum arising from transitions originating in the continuum of excited states. The discrete spectrum is assumed independent of bombarding energy except that the gamma ray energy must be smaller than the bombarding energy. The discrete gamma ray yield which is generated at a layer interface is given by Equation 3-30.

$$P_D(E_{Gi}, X) = G_3(E_{Gi}) \int_{E_{Gi}}^{E_{max}} \left[\Phi_P^*(E, X)\, \Sigma_P(E) + \Phi_N^*(E, X)\, \Sigma_N(E) \right] dE \tag{3-30}$$

where $P_D(E_{Gi})$ = number of discrete photons per gram-sec at energy E_{Gi} and at position X

$G_3(E_{Gi})$ = number of discrete photons at energy E_{Gi} per inelastic collision

$\Phi_P^*(E, X)$, $\Phi_N^*(E, X)$ = total proton (neutron) number flux, differential in energy, at position X

$\Sigma_P(E)$, $\Sigma_N(E)$ = inelastic proton (neutron) cross section.

The total proton number flux at energy E and position X is, for the isotropic case:

$$\Phi_P^*(E, X) = 2. \cdot 2\pi \int_0^1 \Phi_P(E, X, \theta)\, d(\cos\theta) \tag{3-31}$$

where the factor of 2 is due to the transformation from the slab to the spherical shield. For monodirectional beams:

$$\Phi_P^*(E, X) = \Phi_P(E, X, \theta) \tag{3-32}$$

Similar equations define the total neutron number flux.

The continuum gamma ray yield is obtained in a somewhat different way. Analysis of a large quantity of data produced by program LIGHT reveals that the continuum gamma ray yield from a single inelastic collision, $Y_G(E_G, E_B)$ may be represented by a product of two functions.

$$Y_G(E_G, E_B) = G_1(E_B)\, G_2(E_G) \tag{3-33}$$

where E_G is the gamma ray energy and E_B is the nucleon bombarding energy. This separability condition permits a simple solution to the continuum gamma ray source equation.

$$P_C(E_{Gi}, X) = E_{Gi} \int_{E^*_{Gi}}^{E^*_{Gi+1}} \frac{G_2(E)}{E} dE \cdot \int_{E_{Gi}}^{100} \left[\Phi^*_P(E_B, X) \Sigma_P(E_B) + \Phi^*_N(E_B, X) \Sigma_N(E_B) \right] G_1(E_B) dE_B \quad (3\text{-}34)$$

The first integral in Equation 3-34 reduces the photon spectrum, which is differential in energy, to a line spectrum similar to the discrete spectrum. The discrete energies and the continuum range boundaries are given below.

$$E_{Gi} = 1, 2, 3, \ldots 9, 10$$

$$E^*_{Gi} = 0, 1.5, 2.5, 3.5, \ldots 8.5, 9.5, 50$$

The proton penetration code computes and sums the discrete and continuum gamma ray spectra and, upon request, outputs the data on punched cards. This output consists of ten source terms, one per energy, at the entrance and exit faces and at each layer interface. The units of each source are photons per gram-second.

INPUT DATA PREPARATION

LPPC is a set of subroutines linked by an editor. Input will be divided among the routines; there are 3 routines that require input: (1) the editor, MNGR90, (2) the library routine, PPCLIB, and (3) the execution routine, EXE.

Input to MNGR90

There are eight cards that may be interpreted by MNGR90. Seven are macro-instructions to control flow of data between various routines in the system and the eighth is a comment card.

The card form is $ in column 1 and an instruction beginning in column 7. Comments may begin in any column in the comment card, other than column 1.

The instructions and their functions are:

1. WRITE LIBRARY - PPCLIB is instructed to read library data from cards and prepare a library tape.

2. EDIT LIBRARY - PPCLIB is instructed to update the library tape by replacing old data and/or inserting new data from cards.

3. EXECUTE - EXE is instructed to perform a shield calculation.

4. PRINT LIBRARY - PPCLIB is instructed to print the contents of the library tape on the off-line printer.

5. EXIT - MNGR90 will relinquish control to MONITOR after completion of current group of macro-instructions.

6. DUMP - MNGR90 will, after completion of current group of macro-instructions, dump the contents of the core and then relinquish control to MONITOR.

7. TAPE (XXXXXX) - MNGR90 notes that the tape is stored or is to be stored in a tape bin whose name is XXXXXX.

8. Comment card.

Input to PPCLIB

PPCLIB has three entry points, LIB, EDT, and PRT. PRT is the entry for printing the contents of the library and requires no input cards. LIB and EDT are the write and edit entries respectively and require an A type card described below.

See Figure 11 for illustration of A type and associated cards.

IATNUM is the number assigned to the material for recognition.

NEVAL is the number of entries in the EI, SI, RI table. Note that exactly NEVAL cards must follow the A card. NEVAL must be 60 or less.

RHO is the density of the material, TC is its removal cross section and HP is the hydrogen density in the material divided by the hydrogen density in water.

EI, SI, and RI are energy mesh points, stopping powers at the mesh points, and ranges at the mesh points. The KPP card follows the last EI card. The quantities are developed by program NCON.

NGV is the number of mesh points at which the production constants for secondary particles are tabulated. NGV is 20 or less.

Exactly NGV cards must follow the NGV card.

EEGV is the energy at the mesh point. The four G's are provided by NCON. TSCV is the inelastic mean free path; P and N are production constants for evaporation neutrons due to proton and neutron interactions respectively.

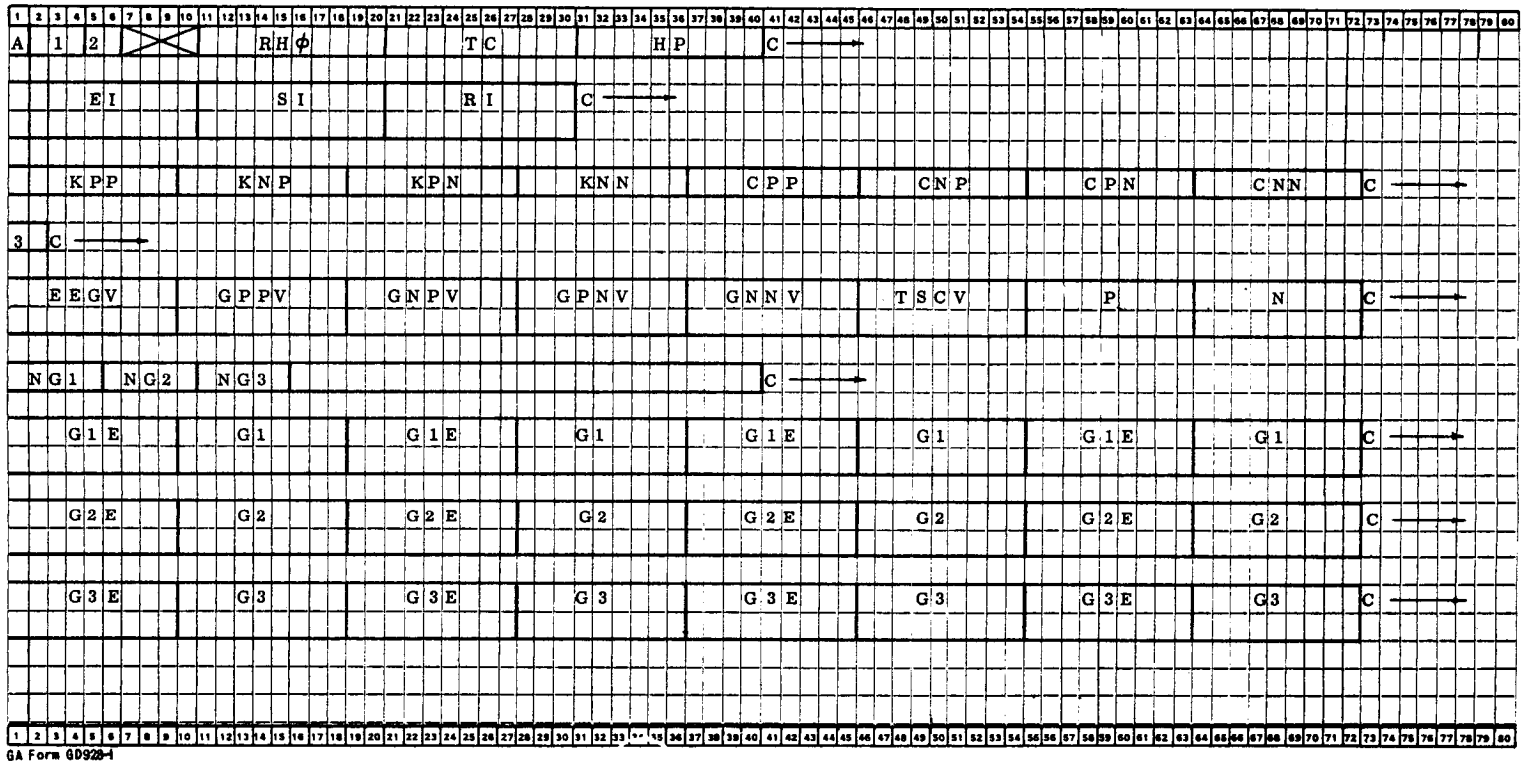

GA Form GD928-1

1 IATNUM
2 NEVAL
3 NGV

C ⟶ indicates remainder of card may be used for comments.

FIGURE 11 DATA INPUT FORMAT - LIBRARY ROUTINE

NG1, NG2, and NG3 are the number of entries in the G1, G2, and G3 tables respectively. The G1 table represents the function, $G_1(E_B)$, the G2 table represents the function, $G_2(E_G)$, and the G3 table represents the function, $G_3(E_{Gi})$; these three functions are described in the "Cascade Gamma Ray Source" part of the LPPC section. G2E is the energy entry, and G1 is the associated value of $G_1(E_B)$; G2E is the energy entry, and G2 is the associated value of $G_2(E_G)$; G3E is the energy entry, and G3 is the associated value of $G_3(E_{Gi})$. The entries in these three tables are determined from the output data of program LIGHT.

Blank cards are permitted between data blocks, but none should be placed within a data block.

Input to **EXE**

Five types of cards are required: An I card, an option card, an EMAX card, a DX card, and a XMAX card. A sixth card, indicating the cosine of the incident angle, and a seventh card or set of cards contining the desired proton spectrum, may be required. The prerequisite for six or more cards in a data set is the use of the pertinent option in the option card. See Figure 12.

1. The I card

   Column 1 contains an I, and columns 2-73 are alphameric data used as a heading.

2. The option card (all numbers are integers)

   Columns 1-5 LDS, problem number

   Columns 6-7 ISPTO; 1, 2, 3, or 4, spectrum type

   - 1 Power law
   - 2 Exponential law
   - 3 Read tabulated table
   - 4 Monoenergetic

   Columns 8-9 IOUT1; 0 or 1 (nonisotropic option)

   - 0 Do not print
   - 1 Print spectrum between layers

   Columns 10-11 IOUT2; 0 or 1

   - 0 Do not print
   - 1 Print input spectrum

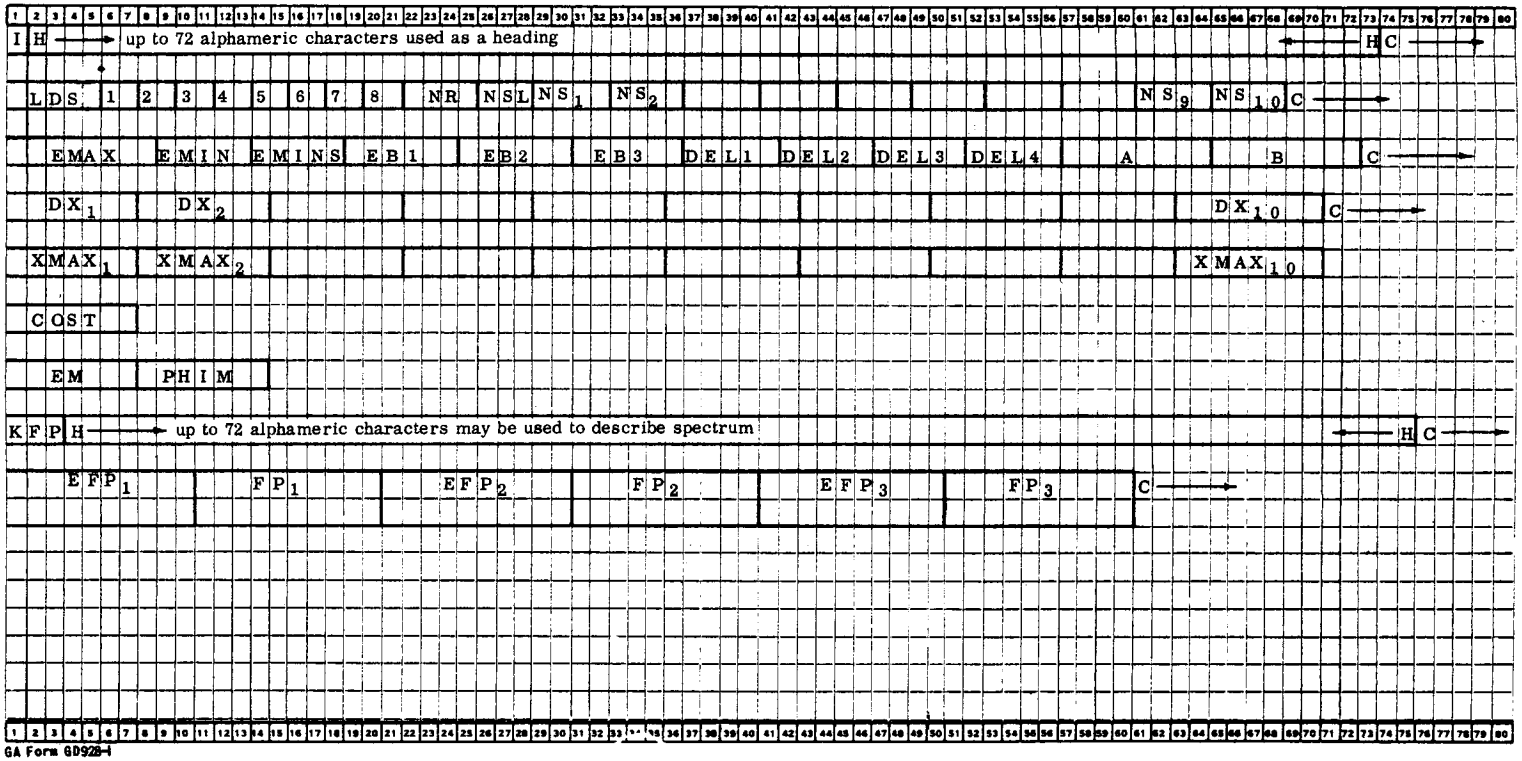

GA Form GD928-1

1 ISPTO
2 IOUT1
3 IOUT2
4 IOUT3
5 ISO
6 PRTISO
7 PCHISO
8 GAMS

C ——→ indicates remainder of card may be used for comments.

FIGURE 12 DATA INPUT FORMAT - EXECUTE ROUTINE

Columns 12-13 IOUT3; 0 or 1, incident angle option

0 Cosine of incident angle equals 1.
1 Cosine of incident angle to be read from data card.

Columns 14-15 ISO; 0 or 1, isotropic switch

0 Incident angle of monodirectional beam determined by IOUT3
1 Incident proton flux is isotropic

Columns 16-17 PRTISO; 0 or 1 (isotropic option only)

0 Do not print
1 Print angular dose after each layer

Columns 18-19 PCHISO; 0 or 1 (isotropic option only)

0 Do not punch
1 Punch isotropic data

Columns 20-21 GAMS; 0 or 1, gamma source option

0 Do not punch gamma source data
1 Punch gamma source data

Columns 22-25 NR; material number of receiver

Columns 26-28 NSL; number of layers in the shield (this number must equal the number of entries in the DX card)

Columns 29-32 NS_1; material number of outermost (incident face) material.

Columns 33-36 NS_2; material number of next material.

Continue with 4-column fields until NSL NS_i values are entered. The option card format is (I5, 8I2, I4, I3, 10I4).

3. The EMAX card (all numbers must have a decimal point).

Columns 1-8 EMAX; maximum energy considered

Columns 9-13 EMIN; minimum energy considered

Columns 14-18 EMINS; minimum energy for input spectrum tabulation

Columns 19-24 EB1;)
25-30 EB2;) These are exactly as described for the
31-36 EB3;) spectrum converter (LSSC).
37-41 DEL1;)

Columns 42-46 DEL2;)
47-51 DEL3;)
52-56 DEL4;)
These are exactly as described for the spectrum converter (LSSC).

Columns 57-64 A;)
65-72 B;)
Constants for power or exponential spectra.

4. The DX card; step sizes for stepping through the various layers.

   Columns 1-7 DX_1 step size in first layer

   Columns 8-14 DX_2 step size in second layer

   Entries are continued until all desired step sizes and/or all layers are satisfied. The DX card format is (10E7.).

5. The XMAX card; the thickness of each layer

   Columns 1-7 $XMAX_1$, the thickness of the first layer (incident face)

   Columns 8-14 $XMAX_2$, the thickness of the second layer

   Entries are continued until the number of entries equals NSL (i.e., the number of entries in the DX card). The XMAX card format is (10E7.).

Note: The units for the entries in the DX and XMAX cards are grams per centimeter squared.

6. The COST card; the cosine of the incident angle for a monodirectional proton beam

   Columns 1-7 COST

   The COST card format is (E7.).

7. Spectrum cards

   The type of spectrum cards to be read depends on ISPTO. No cards will be read for ISPTO = 1, 2; and EM type card will be read for ISPTO = 4; and KFP type cards will be read for ISPTO = 3.

   a. EM card (10E7.)

      Columns 1-7 EM; energy of monoenergetic input

      Columns 8-14 PHIM; flux at energy EM

   b. KFP cards

      Card 1

         Columns 1-3 KFP; number of mesh points

Columns 4-75 72 alphameric heading characters

Following cards:

Columns 1-10 EFP_1; energy at mesh point 1

Columns 11-20 FP_1; flux at energy EFP_1

Columns 21-30 EFP_2; energy at mesh point 2

Columns 31-40 EP_2; flux at energy EFP_2 (see Figure 1).

Continue as above until KFP spectrum mesh points have been read.

Blank cards may be used between data sets, but should not be used within a data set, multiple data sets may be used.

Stops and Error Types

LPPC has 2 programmed stops

If sense switch 2 is down at the beginning of the run, a comment to lift sense switch 2 will appear on the printer and the program will halt with HPR 77776 in the storage register. Lift sense switch 2 and press start.

The "Break In" stop is HPR 77777. Mount library tape on B6 and press start. If the library tape is being mounted for editing, a comment to insert ring in reel will appear on the printer.

A mispunched data card may cause a comment to be listed off line, along with the bad card and the format being used; the program then exits to the 1-CS record of the FORTRAN MONITOR through subroutine NLIXIT.

An error in LIB, EDT, PRT, EXE will cause a printed diagnostic, and execution will continue if possible. The error types are listed below:

(1, L) EOF while reading library tape

(2, L) Failure to read library tape in 10 tries

(3, L) Failure to write a legible record on the library tape in 5 tries

(4, L) Failure to erase properly

(5, L) No library input data on input tape (A2)

(0, E) EOF while reading library tape

(1, E) Error while reading receiver data

(2, E) Error while reading shield data

Error types with a tag of L denote errors while in LIB, EDT, or PRT; those with a tag of E denote errors in EXE.

Miscellaneous Comments

A job which is overtime should be stopped by depressing sense switch 2. Information that has been calculated will be printed. There is no restart procedure. Since LPPC outputs to A3 by channel trapping, it is possible to lose up to 399 lines of output if the above procedure is not followed.

The system tape is A1, input tape A2, output A3, punch tape B4, the library tape B6. Tape B3 is used as a scratch tape by EDT.

If the above tape assignments are changed, one must not assign A3 as a new input tape.

The present editor, MNGR90, permits multiple processing and will process successive blocks defined by appropriate "$" cards until $ EXIT or $ DUMP is encountered.

A $ DUMP or $ EXIT will cause a PM and/or exit when the current pass is completed.

Tape bin locations should not be changed by subsequent $ TAPE (XXX) cards.

The procedure used by MNGR90 in routing program control is to read all instruction cards containing a $ in column 1 until a non $ card is encountered. MNGR90 then rearranges the instructions in logical order and initiates a pass. If one of the instructions is an EXIT or DUMP card, all other instructions will be processed first. If no EXIT or DUMP instruction is given, control will return to MNGR90 after current instructions are executed. MNGR90 will then search the input tape for the next group of $ instruction cards. If an end of file is encountered before a "$ EXIT" card, all unprocessed macro-instructions will be processed and then control will be passed to the MONITOR system.

OUTPUT FORMAT

With the option to print the spectrum after each layer of the shield "on":

a. The top left-hand section of the page contains Hollerith information from the I-card.

b. The top right-hand section of the page identifies the RECEIVER material, the SHIELD material, the LAYER from which the

spectrum is emerging, the THICKNESS of the shield up to and including this layer, and the date.

Note: The date may or may not print properly depending on the monitor system at the installation.

c. The rest of the page contains the number flux versus energy, E, for PRIMARY proton, TOTAL proton (i.e., primary plus cascade proton), and cascade NEUTRONS. The energy points are determined from values given on the "EMAX card".

Note: The spectrum after each layer is obtainable only with the normally incident flux option.

With the initial spectrum print option "on":

a. The top left-hand section of the page contains Hollerith information from the I-card.

b. The top right-hand section of the page contains the words - INPUT SPECTRUM - and the date.

c. The rest of the page contains the incident proton number flux, PHI(E), versus energy, E. The energy points are determined from values given on the "EMAX card".

With the option to print data, resulting from isotropically incident flux, after each layer:

a. The top left-hand section of the page contains Hollerith information from the I-card.

b. At the top right-hand side of each block of data (usually 3 to a page, each block representing a layer) is information identifying the RECEIVER material, the SHIELD material, the LAYER, and the shield THICKNESS up to and including the layer in question.

c. Each layer is represented by a block of information containing 11 rows and 11 columns plus column headings. The column headings are as follows:

(1) THETA - The cosine of the angle between the particle velocity vector and the slab normal.

(2) FPMAX - Total proton number flux.

(3) FNMAX - Total neutron number flux.

(4) SEVAP - Evaporation neutron source strength (n/gm-sec) at the layer exit face due to protons and neutrons travelling through the layer in the direction THETA.

(5) PNUC - Dose rate (rad/hr) corresponding to energy removal from the proton beam minus PRIMARY minus SECONDARY (local deposition assumption).

(6) NNUC - Dose rate (rad/hr) corresponding to energy removal from the neutron beam minus NEUTRON (local deposition assumption).

(7) PRIMARY - Dose rate (rad/hr) due to primary protons.

(8) SECONDARY - Dose rate (rad/hr) due to cascade protons.

(9) NEUTRON - Dose rate (rad/hr) due to cascade neutrons.

(10) TOT. ION. - Dose rate (rad/hr) due to primary plus cascade protons.

(11) PRI + CASC - Dose rate (rad/hr) due to primary and cascade protons plus cascade neutrons.

The data on the summary page are as follows:

a. The top left-hand section contains Hollerith information from the I-card.

b. The top right-hand section identifies the RECEIVER material; the SHIELD material(s); the number of LAYERS in each shield material; and whether the incident flux is isotropic, in which case ISOTR is printed, or monodirectional, in which case the cosine of the angle is printed.

c. Directly below a. and b. is the following information:

(1) SPECT. - Indicates incident spectrum option.

(2) E(MAX) - Maximum incident particle energy (Mev).

(3) E(MIN) - Minimum energy to be considered, not necessarily minimum source energy (Mev).

(4) EB1, EB2, EB3, DEL1, DEL2, DEL3, and DEL4 are explained in the "input data" section.

(5) X(MAX) - Thickness (gm/cm^2) of each material in the shield, and total thickness of shield.

(6) DELTA(X) - Step size (gm/cm^2) in each shield material.

(7) A - The coefficient "A" in the power law spectrum AE^{-B}, or the coefficient "A" in the exponential law spectrum $Ae^{-E/B}$.

(8) B - The parameter "B" in the power law spectrum or the exponential law spectrum.

d. The rest of the page(s) contain 13 columns with the following headings:

(1) LAYER - Indicates the layer exit face to which the data pertains.

(2) X - Thickness (gm/cm^2) of the shield, up to and including this layer.

(3) FP(MAX) - Total proton number flux.

(4) FN(MAX) - Total neutron number flux.

(5) S(EVAP) - Evaporation neutron source strength (n/gm-sec) at the layer exit face due to proton and neutron interactions with nuclei.

(6) PRI. ION - Dose rate (rad/hr) due to primary protons.

(7) SEC. ION - Dose rate (rad/hr) due to cascade protons.

(8) P(NUC) - Dose rate (rad/hr) corresponding to energy removal from the proton beam minus PRI. ION minus SEC. ION (local deposition assumption). *

(9) N(NUC) - Dose rate (rad/hr) corresponding to energy removal from neutron beam minus D(NEUT) (local deposition assumption). *

(10) D(NEUT) - Dose rate (rad/hr) due to cascade neutrons.

(11) D(EVAP) - Dose rate (rad/hr) due to evaporation neutrons.

(12) D(TOT) - Total dose rate (rad/hr); the sum of PRI. ION, SEC. ION, D(NEUT), and D(EVAP).

---

* See Page 129, Reference 38.

(13) D(MAX) - Total dose rate (rad/hr); the sum of D(TOT), P(NUC), and N(NUC).

4. INELASTIC GAMMA PRODUCTION CODE (LIGHT)

CODE DESCRIPTION

The LIGHT code estimates gamma ray spectra resulting from inelastic nucleon-nucleus collisions. Gamma ray transitions from excited levels of the nucleus are traced, and an estimate of gamma ray production following direct interactions and nucleon evaporation may be made. Gamma rays due to proton bremsstrahlung, beta ray bremsstrahlung, annihilation radiation, and collective dipole effects are not considered.

The excited residual nucleus following inelastic scattering may decay through a number of channels provided that sufficient energy is available.[8,22,33,37] Nucleon evaporation is usually the dominant decay mode above the nucleon emission threshold but exceptions have been observed. For example, the 15.1 Mev level of C^{12} decays by gamma ray emission 80% of the time.[35] For excited states below the nucleon binding energy, gamma ray emission generally proceeds much faster than beta ray emission or internal conversion.

A complete calculation of gamma ray de-excitation should consider the different nuclei possible following direct or knock-on processes. Each residual nucleus would then be traced through the cascade and evaporation stage until a stable configuration is achieved. It is possible to do such a calculation by Monte Carlo methods, but the lack of nuclear level data and the effort required militate against this detailed procedure at the present time.

The present calculation is based upon a simple statistical model of the nucleus supplemented by knowledge of the low-lying nuclear levels. The method is based upon the work of Troubetzkoy.[44]

Level Density

The level distribution of the target nucleus is shown in Figure 1. Discrete levels are taken from the Nuclear Data Sheets.[35] In the continuum, the level density is taken from Bethe's equation, 4-1, with constants derived from the fit of Varshni.[45]

$$\rho(E) = \frac{1}{P}(AE)^{-2}\,\mathrm{Exp}\left[2(\mu AE)^{1/2}\right] \qquad (4\text{-}1)$$

where $\rho(E)$ = level density

A = mass number

E = excitation energy

$\mu = 0.1023$

$$P = \begin{cases} 0.03583 \text{ for even A, odd Z} \\ 0.07630 \text{ for odd A} \\ 0.2592 \text{ for even A, even Z} \end{cases}$$

Transition Probability

A highly excited nucleus may decay through a series of electric and/or magnetic multipole transitions. Theoretical arguments[8] indicate that low order multipole transitions are favored over the next higher one by factors ranging from 10^3 to 10^6 although smaller factors are observed. Similarly, electric transitions are favored over magnetic transitions of the same multipole order except for parity unfavored cases. These trends, together with a desire for simplicity, lead to a choice of electric dipole-type transitions in the model.

The assumption of electric dipole transitions leads to the following transition probabilities:

$$S_1(E, E') = f_1(E)(E - E')^3 \rho(E')$$

$$S_2(E, E_i) = f_2(E)(E - E_i)^3 \qquad (4\text{-}2)$$

$$S_3(E_j, E_i) = f_3(E_j)(E_j - E_i)^3$$

where $S(E, E')$ = radiative transition probability from a state at E to a state between E' and E' + dE'

f(E) = normalization factor

E = energy of initial state in the continuum

E' = energy of final state in the continuum

E_j = energy of initial state in the discrete region

E_i = energy of final state in the discrete region.

The subscript 1 refers to transitions within the continuum; 2, to transitions from the continuum to discrete levels; and 3, to transitions between discrete levels.

The normalizing factors are given by:

$$f_1(E) = \frac{\dfrac{\Gamma_\gamma(E)}{\Gamma(E)}}{\sum_{i=0}^{n}(E - E_i)^3 + \int_{E_c}^{E} \rho(E')(E - E')dE'}$$

$$f_2(E) = f_1(E) \tag{4-3}$$

$$f_3(E_j) = \frac{1}{\sum_{i=0}^{j-1}(E_j - E_i)^3} \cdot \frac{\Gamma_\gamma(E_j)}{\Gamma(E_j)}$$

where $\Gamma_\gamma(E)$ = radiative level width

$\Gamma(E)$ = total level width

E_c = lowest energy in the continuum.

Level Population

The initial level population, $R^o(E)$, is defined as the probability that a level will be occupied immediately as a result of the inelastic collision. According to the statistical model, $R^o(E)$ is given by Equation 4-4.

$$R^o(E) = N \frac{E_m - E}{T^2} \mathrm{Exp}\left(-\frac{E_m - E}{T}\right) \tag{4-4}$$

where $T = \dfrac{E_m}{\sqrt{2\mu A E_m - 2}}$, N = normalizing factor

E_m = nucleon bombarding energy.

The total level population is defined as the probability that a level will be occupied either by the initial excitation or by transitions from higher levels.

This probability may be expressed as an integral equation, Equation 4-5, for levels in the continuum. The subscript c designates continuum values.

$$R_c(E) = R_c^o(E) + \int_E^{E_m} R_c(E')S_1(E', E)dE' \qquad (4\text{-}5)$$

Equation 4-5 may be solved by use of the variable substitution defined in Equation 4-6.

$$\psi(E) = \frac{R_c(E) - R_c^o(E)}{\rho(E)} \qquad (4\text{-}6)$$

Equation 4-5 becomes, after substitution:

$$\rho(E)\ \psi(E) = \int_E^{E_m} R_c(E')f_1(E')(E' - E)^3\ \rho(E)dE' \qquad (4\text{-}7)$$

Differentiating four times with respect to E yields:

$$\psi''''(E) = 6f_1(E)\ \rho(E)\ \psi(E) + 6f_1(E)R_c^o(E) \qquad (4\text{-}8)$$

Equation 4-8 is solved by numerical integration using the boundary conditions:

$$\psi'''(E_m) = \psi''(E_m) = \psi'(E_m) = \psi(E_m) = 0$$

Once Equation 4-8 is solved, the level population in the continuum is found from relation 4-6.

The level population in the discrete region is found from Equation 4-9. The subscript D designates values in the discrete region.

$$R_D(E_i) = R_D^o(E_i) + \sum_{j=i+1}^{n} R_D(E_j)S_3(E_j, E_i) + \int_{E_c}^{E_m} R_c(E')S_2(E', E_i)dE' \qquad (4\text{-}9)$$

The first term in Equation 4-9 represents initial excitation; the second term, transitions from higher discrete levels; the third term, transitions from the continuum.

Gamma Ray Spectrum

Given the level density, level population, and transition probabilities, it is possible to compute the resulting gamma ray spectrum.

A discrete spectrum is obtained by computing transitions between discrete levels as in Equation 4-10.

$$PD(E_j - E_i) = R_D(E_j)S_3(E_j, E_i),\ E_j > E_i \text{ photons} \tag{4-10}$$

Since 50 excited states are permitted by the dimensions in LIGHT, a maximum of (50/2)(50 + 1) or 1275 discrete transitions may be calculated. The largest number of discrete excited states considered to date is 36 for aluminum, leading to 666 lines. The LIGHT program sums these transitions into 10 energy groups ranging from 1 to 10 Mev. The number flux is corrected to insure energy conservation in the summing process.

A continuous gamma ray spectrum is obtained by computing transitions within the continuum and from the continuum to discrete states, as shown in Equation 4-11.

$$PS(E_\gamma) = \int_{E_c+E_\gamma}^{E_m} R_c(E)S_1(E,\ E - E_\gamma)dE + \sum_{i=0}^{n} R_c(E_i + E_\gamma)S_2(E_i + E_\gamma,\ E_i) \text{ photons/Mev} \tag{4-11}$$

The continuous gamma ray spectrum may be integrated over small energy ranges to yield a line spectrum similar to the discrete gamma ray spectrum.

Gamma Ray Emission Following Evaporation and Direct Processes

For excitation energies well above the nucleon binding energy, the radiative width falls to a small fraction of the total level width.[8, 11, 33, 43] The great majority of decays from these levels proceed by evaporation of a nucleon or cluster of nucleons. In general, the residual nucleus is still in an excited state and may decay via gamma ray transitions. The present model discontinues the cascade following particle emission so that the additional contribution is not computed.

Gamma ray production following nucleon evaporation is crudely estimated in the following way. The LIGHT code is run at energies near the nucleon emission threshold where discrete gamma ray transitions are the dominant decay mode. The intensity distribution of these discrete gamma rays is assumed to be valid for neighboring excited nuclei which are the products of nucleon evaporation. At higher bombarding energies, the discrete transition spectrum decreases due to the small Γ_γ/Γ ratio, but the above assumption

partially compensates for the loss. No attempt is made to compute transitions in the continuum after nucleon evaporation because of their minor importance.

Gamma ray production following knock-on processes, in which several nucleons may be ejected, and nucleon capture are treated in a similar way. The residual nucleus is generally left in an excited state. It may decay by evaporation of nucleons or by competitive gamma ray emission. Again, the gamma rays emitted by the highly excited nucleus are ignored following knock-on processes, and the gamma ray spectrum emitted after the evaporation phase is completed is assumed to resemble that of the parent nucleus.

These approximations are illustrated in Figure 13. The dash-dot lines represent, from left to right, a knock-on reaction with two nucleons emerging, an inelastic scatter with one nucleon emerging, and a capture reaction. The solid vertical arrows represent gamma ray cascades. The dashed vertical arrows for nuclei A - 1 and A + 1 represent gamma rays not accounted for in the calculation. The solid vertical arrows for these same nuclei are assumed to be identical with the solid vertical arrows associated with nucleus A which are below the nucleon binding energy.

A sample of the LIGHT code results for aluminum is given in Table E and Figure 14. Table E presents the discrete gamma ray spectrum per inelastic collision for 10 Mev protons on aluminum. The spectrum shown is reduced from 666 discrete lines. Figure 14 illustrates the continuous gamma ray spectrum per inelastic collision as a function of bombarding energy.

TABLE E

DISCRETE GAMMA RAY SPECTRUM

Energy (Mev)	Photons
1	0.506
2	0.163
3	0.208
4	0.230
5	0.244
6	0.209
7	0.092
8	0.047
9	0.033

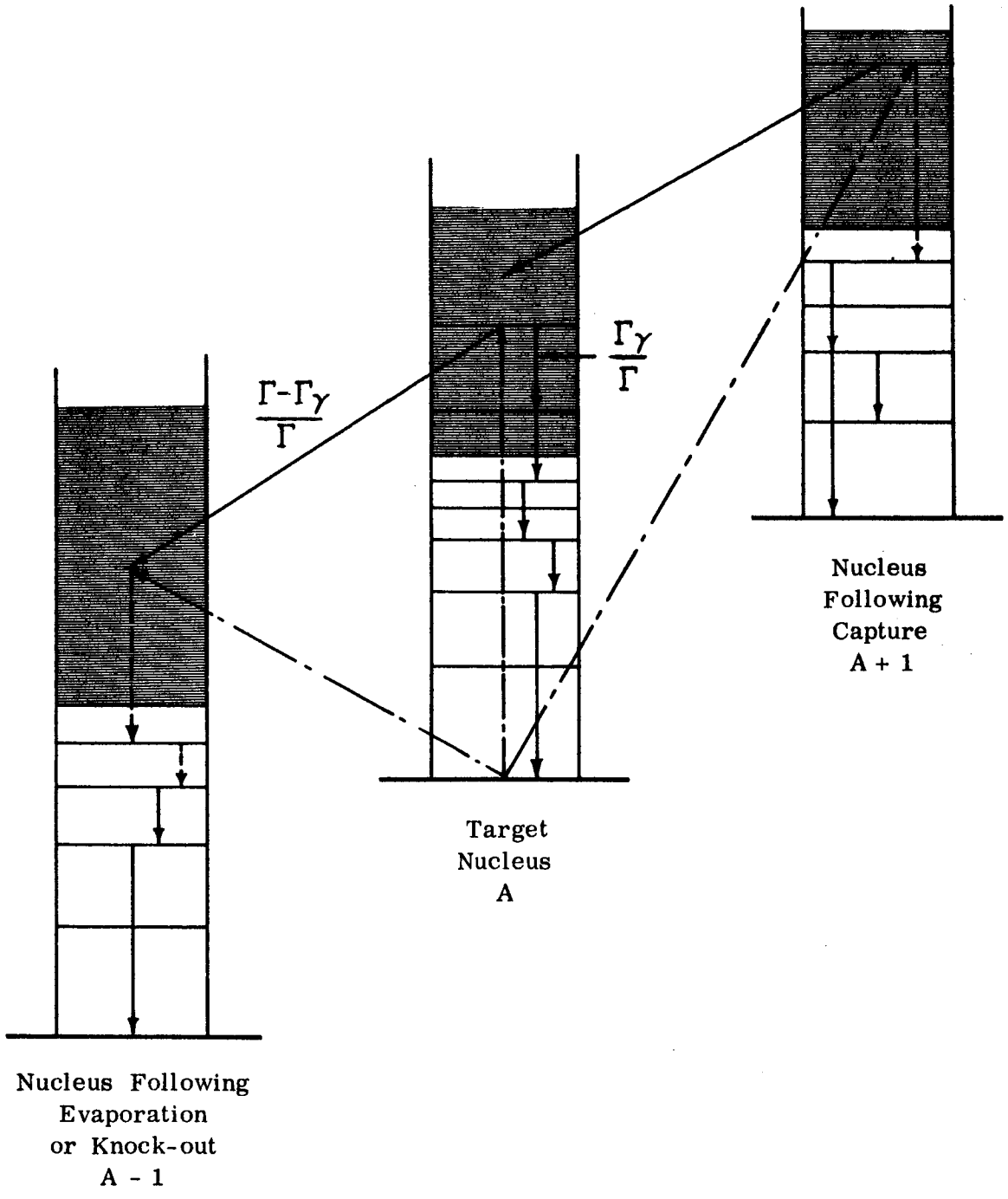

FIGURE 13 EXCITATION AND DE-EXCITATION SCHEME FOR BOMBARDED NUCLEUS

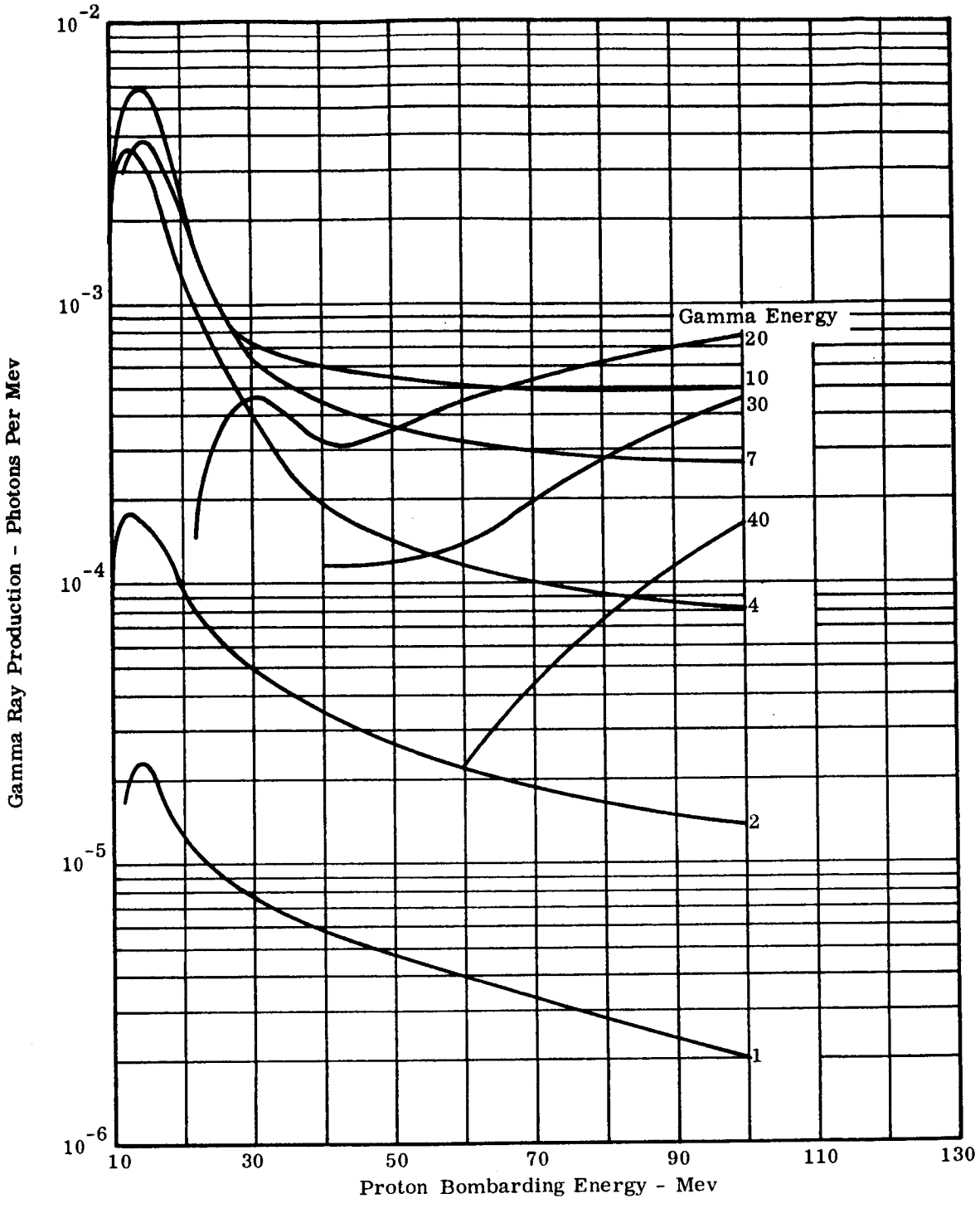

FIGURE 14 CONTINUUM GAMMA RAY INTENSITY AT SEVERAL ENERGIES VERSUS PROTON BOMBARDING ENERGY

GLOSSARY OF INPUT DATA TERMS

IK - An integer indicating the number of different nuclei to be bombarded.

AT(K) - The atomic mass number of the k^{th} nucleus.

FMU(K) - A constant of the level density formula (μ = 0.1023 for all nuclei).

CP(K) - A coefficient of the level density formula for the k^{th} nucleus.[45]

$= 3.583 \times 10^{-2}$ for odd nuclei

$= 7.630 \times 10^{-2}$ for odd-mass nuclei

$= 2.592 \times 10^{-1}$ for even nuclei

HD - Hollerith information (e.g., to identify the nucleus being "bombarded").

NI - An integer indicating the number of discrete energy levels to be read. (Ground state is a level of zero energy and must be counted.)

EI(I) - The energy of the i^{th} level. All levels are of non-negative energy and must be in an increasing sequence with the ground state first. (Mev)

NJ - An integer indicating the number of entries in the Γ_γ / Γ_T-table.

EJ(I) - The i^{th} energy at which the i^{th} Γ_γ / Γ_T is tabulated. (Mev)

G(I) - The i^{th} Γ_γ / Γ_T.

EC - The greatest lower bound energy of the level density continuum. (Mev)

EM - The proton bombarding energy. (Mev)

DEI - The step size to be used in the numerical solution of the differential equation. DEI $\geq (E_m - E_c)/1000$.

INPUT DATA PREPARATION

Card Type 1 - Columns 1-5 contain an integer, IK. This number must be right adjusted in the I-field. This integer must equal the number of cards Type 2 that follow.

Card Type 2 - Columns 1-10, the atomic mass number; columns 11-20, the constant FMU(K); columns 21-30, the coefficient CP(K).

The format for card Types 1 and 2 is (I5/(3E10.)).

The following card types are read in a "DO LOOP" ranging over the number, IK, of nuclei.

Card Type 3 - 72 columns of the Hollerith information to identify the nucleus being investigated. FORMAT (12A6).

Card Type 4 - Columns 1-5 contain an integer, NI. This number must be right adjusted in the I-field. This integer must equal the number of discrete energy levels of the nucleus.

Card Type 5 - Eight fields of nine columns each, containing the energy, EI(I) (Mev), of each energy level of the nucleus. Cards Type 5 are continued until the number of levels indicated in card Type 4 has been satisfied.

The format for card types 4 and 5 is (I5/(8E9.)).

Card Type 6 - Columns 1-5 contain an integer, NJ. This number must be right adjusted in the I-field. This integer must equal the number of entries in the Γ_γ / Γ_T table.

Card Type 7 - Eight fields of nine columns each; the 1st, 3rd, 5th, and 7th fields contain the energies, EG(I) (Mev); the 2nd, 4th, 6th and 8th fields contain the Γ_γ / Γ_T ratio, G(I), corresponding to the preceding energy. Cards Type 7 are continued until the number of entries indicated in card Type 6 is satisfied.

The format for card Types 6 and 7 is (I5/(8E9.)).

Card Type 8 - Columns 1-9, the value of EC for the nucleus being considered; columns 10-18, the bombarding energy, EM;

columns 19-27, the step size, DEI. Cards Type 8 should be repeated for each bombarding energy to be considered. The last card Type 8 for each nucleus should be a blank card. FORMAT (8E9.).

OUTPUT FORMAT

The information output is data from the heading card, card Type 3. Next, the greatest lower bound energy (EC) of the continuum and the nuclear bombarding energy (EM) are indicated. Beneath EC and EM is a tabulation of the discrete energy levels for the nucleus being bombarded. Two columns of data follow the energy level tabulation; the first is an energy list, and the second is the value of the Γ_γ / Γ_T ratio corresponding to the given energy. Next, the atomic mass numbers and the parameters for the level density function are displayed for all elements being considered on this run. On the next page, the total number of transitions between discrete energy levels is indicated. Then, there are four columns of tabulated data; two columns indicate the transition energies, EGP(I), and two columns exhibit the number of photons, PD(I), participating in the transitions. Below this tabulation, the continuous transition energy flux, the discrete transition energy flux, the total continuous initial energy, and the total discrete initial energy are displayed. On the next page, a tabulation of four columns is presented; two columns indicate photon energy, EG(I), and two columns indicate differential photon number flux, PS(I), with respect to energy. The next tabulation presents an equivalent to the discrete transition photon number flux, EFS(N), listed at integral energies, EGA(N), from one to ten Mev and the continuous transition photon differential number flux, EIS(N), in ten equally spaced energy intervals at the average energy, EGI(N). The last page of output for a given nucleus and bombarding energy displays the continuous transition photon differential number flux, PSS(L), at integral energy, GMA(L), values.

5. MULTI-SLAB GAMMA CODE (MSGAM)

CODE DESCRIPTION

The Lockheed Multi-Slab Gamma Code (MSGAM) estimates gamma dose rates at the exit face of a multi-layer shield; wherein the photon sources are generated by nucleon inelastic collisions within the shield. The photons are transmitted from the source location to the exit face by "line-of-sight" attenuation and appropriate build-up factors.[12]

The gamma dose rate at the shield exit face is estimated by:

$$D(E_\gamma) = F(E_\gamma)E_\gamma \sum_{i=1}^{N} \sum_{j=1}^{2} \int_0^{d_i} \int_0^{2\pi} \int_0^{\infty} \frac{S(d_i - x_{ij}, E_\gamma)}{4\pi \rho_{ij}^2} e^{-t_{ij}} \cdot B(t_{ij}, E_\gamma) r dr d\psi' dx \qquad (5\text{-}1)$$

In Equation (5-1),

N is the number of layers,

$F(E_\gamma)$ is the energy flux-to-dose conversion factor,

E_γ is the photon energy,

$S(d_i - x_{ij}, E_\gamma)$ is the source strength of photons with energy E_γ at the j^{th} source point in the i^{th} layer,

d_i is the thickness of the i^{th} layer,

x_{ij} is the normal distance from the j^{th} source point in the i^{th} layer to the exit face of the i^{th} layer,

ρ_{ij} is the "line-of-sight" distance from the j^{th} source point in the i^{th} layer to the exit face of the shield,

t_{ij} is the number of mean-free-paths from the j^{th} source point in the i^{th} layer to the exit face of the shield,

$B(t_{ij}, E_\gamma)$ is the build-up factor pertaining to the photon transmission from the j^{th} source point in the i^{th} layer to the exit face of the shield.

The range of source points per layer is limited to two in this code in order to make it compatible with the data obtainable from the Lockheed Proton Penetration Code (LPPC).

By fitting the product of the source strength, $S(d_i - x_{ij}, E_\gamma)$, and the build-up, $B(t_{ij}, E_\gamma)$, at two consecutive source points to an expression of the form $A_i e^{a_i x}$, the integrations indicated in Equation 5-1 may be performed analytically giving rise to the general equation:

$$D(E_\gamma) = \sum_{i=1}^{N} \frac{A_i E_\gamma F(E_\gamma)}{2a_i} \left\{ e^{a_i d_i} E_1(b_i d_i - c_i) \right.$$

$$- e^{-\frac{a_i b_i}{b_i}} E_1\left[\left(1 - \frac{a_i}{b_i}\right)(b_i d_i + c_i)\right] \qquad (5\text{-}2)$$

$$\left. - E_1(c_i) + e^{-\frac{a_i c_i}{b_i}} E_1\left[\left(1 - \frac{a_i}{b_i}\right)c_i\right] \right\}$$

where $b_i = \mu_i(E_\gamma)$, the mass attenuation coefficient for the i^{th} layer at the energy E_γ,

$$c_i = \sum_{k=i+1}^{N} \mu_k(E_\gamma) d_k$$

$$E_1(Z) = \int_1^\infty \frac{e^{-zt}}{t}\, dt$$

In addition to the general case, Equation 5-2, which is valid for most values of the a_i's, b_i's, and c_i's, there are six special cases arising from values and relations of the a_i's, b_i's, and c_i's:

Case I. $c_i = 0,\ a_i < b_i$

$$D(E_\gamma) = \sum_{i=1}^{N} \frac{A_i E_\gamma F(E_\gamma)}{2a_i} \left\{ e^{a_i d_i} E_1(b_i d_i) - E_1\left[\left(1 - \frac{a_i}{b_i}\right) b_i d_i\right] - \ln\left(1 - \frac{a_i}{b_i}\right) \right\} \tag{5-3}$$

Case II. $c_i = 0,\ 0 < b_i < a_i$

$$D(E_\gamma) = \sum_{i=1}^{N} \frac{A_i E_\gamma F(E_\gamma)}{2a_i} \left\{ e^{a_i d_i} E_1(b_i d_i) + \ln(b_i d_i) + \sum_{k=1}^{\infty} \frac{\left(\frac{a_i}{b_i} - 1\right)^k (b_i d_i)^k}{k \cdot k!} + 0.577216 \ldots \right\} \tag{5-4}$$

Case III. $c_i = 0,\ a_i = b_i$

$$D(E_\gamma) = \sum_{i=1}^{N} \frac{A_i E_\gamma F(E_\gamma)}{2a_i} \left\{ e^{a_i d_i} E_1(b_i d_i) + \ln(b_i d_i) + 0.577216 \right\} \tag{5-5}$$

Case IV. $c_i \neq 0,\ a_i = b_i$

$$D(E_\gamma) = \sum_{i=1}^{N} \frac{A_i E_\gamma F(E_\gamma)}{2a_i} \left\{ e^{a_i d_i} E_1(b_i d_i + c_i) - E_i(c_i) + e^{-c_i} \ln\left(\frac{b_i d_i + c_i}{c_i}\right) \right\} \tag{5-6}$$

Case V. $c_i \neq 0,\ 0 < b_i < a_i$

$$D(E_\gamma) = \sum_{i=1}^{N} \frac{A_i E_\gamma F(E_\gamma)}{2a_i} \left\{ e^{a_i d_i} E_1(b_i d_i + c_i) + e^{-\frac{a_i c_i}{b_i}} \left[\ln(b_i d_i + c_i) \right.\right.$$

$$\left.\left. + \sum_{k=1}^{\infty} \frac{\left(\frac{a_i}{b_i} - 1\right)^k (b_i d_i + c_i)^k}{k \cdot k!} - \sum_{k=0}^{\infty} \frac{\left(\frac{a_i}{b_i} - 1\right)^k c_i^k}{k \cdot k!} - \ln(c_i) \right] - E_1(c_i) \right\} \quad (5\text{-}7)$$

Case VI. $a_i = 0$

$$D(E_\gamma) = \sum_{i=1}^{N} \frac{A_i E_\gamma F(E_\gamma)}{2b_i} \left\{ E_2(c_i) - E_2(b_i d_i + c_i) \right\} \quad (5\text{-}8)$$

The build-up factors used for photon dose transmission through a multi-layer shield are calculated by one of three methods. First, the shield is considered as being composed of one material; the attenuation and numbers of mean-free-paths are calculated using the mass attenuation coefficients[20] of the actual materials, and the build-up is calculated using the equivalent material. Second, the shield is considered as consisting of two layers of different materials, the first layer of a "light" material and the second layer of a "heavy" material. Third, the shield is considered as consisting of two layers of different materials, the first layer of a "heavy" material and the second layer of a "light" material. For methods 2 and 3, the attenuation and numbers of mean-free-paths are determined using the mass attenuation coefficients of the materials present; whereas, the build-up factors are computed using the formulae developed by M. H. Kalos as presented by H. Goldstein.[18] The build-up factors for single materials in all three methods are calculated from the polynomial representations presented by M. A. Capo.[12]

The code is designed to compute the gamma dose rate emerging from the first layer, the first two layers, the first three layers, etc.; therefore, there must be one "case card" for each set of layers (i.e., one case card for the first layer, one for the first two, one for the first three, etc.).

The "case cards" indicate which of the above three methods is to be used to calculate the build-up factors; that is, whether the layers under consideration are to be treated as one equivalent thickness, two equivalent thicknesses, light-heavy, or two equivalent thickness, heavy-light. Also to be indicated in the "case card" are the number of layers in each equivalent thickness and the material of equivalence for each equivalent thickness.

The number of layers, the thickness of each layer, and the source strength for each photon energy at each "interface" may be determined from the LPPC output. The step-size, DELTA (X), used in LPPC to step through the shield determines the number of layers in the shield. The number of interfaces is equal to the number of layers plus one.

GLOSSARY OF INPUT DATA TERMS

NTOT - The total number of elements for which mass attenuation and build-up tables are to be read.

Z(K) - The atomic numbers of the elements in the tables in the same sequence as the tables.

NRA(J) - An integer indicating the form of the polynomial used to calculate the build-up factor

= 1, B(X, 1/E) - a polynomial in X and 1/E

= 2, B(X, E) - a polynomial in X and E

= 3, B(X, 1/E) for $E \leq 4.0$ Mev; B(X, E) for $E > 4.0$ Mev

X - the number of mean-free-paths

E - energy (Mev)

NI(J) - The range of the subscript "K" in the coefficient, CB(J, K, L), of the build-up factor polynomial for the j^{th} element.

NJ(J) - The range of the subscript "L" in the coefficient, CB(J, K, L), of the build-up factor polynomial for the j^{th} element.

NFDCF - The number of entries in the energy flux-to-dose conversion factor table.

EC(I) - The energy (Mev) of the i^{th} energy flux-to-dose conversion factor entry.

CV(I) - The i^{th} energy flux-to-dose conversion factor entry. ($r\text{-}hr^{-1}\text{-}Mev^{-1}\text{-}cm^2\text{-}sec$)

NEL - An integer indicating the number of layers in the shield.

D(I) - The thickness in gm/cm^2 of the i^{th} layer.

NEIT(I) - The number of entries in the mass attenuation table for the i^{th} element.

EM(J, L) - The energy associated with the l^{th} mass attenuation entry for the j^{th} element (Mev).

FMU(J, L) - The l^{th} mass attenuation entry for the j^{th} element (cm^2/gm).

NCPT - The number of entries in the Compton scattering table.

EU(J, L) - The energy associated with the l^{th} Compton scattering entry for the j^{th} element (Mev).

FMUC(J, L) - The l^{th} Compton scattering entry for the j^{th} element (cm^2/gm).

CB(J, K, L) - The coefficient, C_{kl}, in the polynomial for computing the build-up factors in the j^{th} element.

$$B(X, 1/E) = \sum_{k=1}^{NI(J)} \sum_{l=1}^{NJ(J)} C_{kl} X^{k-1} (1/E)^{l-1}$$

$$B(X, E) = \sum_{k=1}^{NI(J)} \sum_{l=1}^{NJ(J)} C_{kl} X^{k-1} E^{l-1}$$

NEG - The number of source energies.

EG(I) - The i^{th} source energy.

SSS(K, L) - The source strength of the l^{th} energy at the k^{th} interface. (photons/gm-sec)

LNB(I) - An "ordinal" number indicating the location of the mass attenuation table for the i^{th} shield material.

NBO - An integer indicating the equivalence status of the shield -

= 1, one equivalent thickness;

= 2, two equivalent thicknesses, light-heavy;

= 3, two equivalent thicknesses, heavy-light.

NL1 - The number of layers in the first equivalent thickness.

NL2 - The number of layers in the second equivalent thickness.

LE1 - An "ordinal" number indicating the location of the build-up table of the material of equivalence for the first equivalent thickness.

LE2 - An "ordinal" number indicating the location of the build-up table of the material of equivalence for the second equivalent thickness.

INPUT DATA PREPARATION

Card Type 1 - Columns 1-5, the number, NTOT, of materials in the mass attenuation and build-up tables - including those elements that must be entered twice, such as tungsten. FORMAT (14I5).

Card Type 2 - Eight fields of nine columns per field, each field contains the atomic number of the elements in the attenuation tables. The number of entries must equal NTOT in card type 1. FORMAT (8E9.).

Card Type 3 - Columns 1-5, the integer NRA(J) for the j^{th} set in the attenuation tables; columns 6-10, the integer NI(J) for the same set; columns 11-15, the integer NJ(J). There must be a card type 3 for each entry in card type 2. The values for these integers may be obtained from Reference 3.

Card Type 4 - Columns 1-5, the number, NFDCF, of entries in the energy flux-to-dose conversion factor table.

Card Type 5 - Columns 1-9, the energy associated with the first energy flux-to-dose conversion factor; columns 10-18, the first energy flux-to-dose conversion factor; columns 19-27, the energy associated with the second energy flux-to-dose conversion factor; columns 28-36, the second energy flux-to-dose conversion factor; etc. Entries are continued, 9 columns per entry, until NFDCF energy flux-to-dose conversion factors have been read. FORMAT (I5/(8E9.)).

Card Type 6 - Columns 1-5, the number, NEL, of "layers" in the shield. A "layer" is defined as the region between two consecutive source points.

Card Type 7 - Six fields of 12 columns per field, each field contains the thickness, gm/cm^2, of a layer - in order from incident face to exit face. FORMAT (I5/(6E12.)).

Card Type 8 - Fourteen fields of five columns per field, each field contains an integer NEIT(I). FORMAT (14I5).

Card types 9, 10, 11, and 12 are read in a DO LOOP ranging from one to NTOT.

Card Type 9 - Columns 1-9, the energy associated with the first mass attenuation coefficient; columns 10-18, the first mass attenuation coefficient; columns 19-27, the energy associated with the second mass attenuation coefficient; columns 28-36, the second mass attenuation coefficient; etc. Entries are continued, 9 columns per entry, until NEIT(I) mass attenuation coefficients have been read. FORMAT (8E9.).

Card Type 10 - Columns 1-5, an integer, NCPT, indicating the number of entries in the Compton scattering table.

Card Type 11 - Columns 1-9, the energy associated with the first Compton scattering entry; columns 10-18, the first Compton scattering entry; columns 19-27, the energy associated with the second Compton scattering entry; columns 28-36, the second Compton scattering entry; etc. Entries are continued,

9 columns per entry, until NCPT Compton scattering entries have been read. FORMAT (I5/(8E9.))

Card Type 12 - Seven fields of ten columns per field, each field contains a CB(J, K, L). See Reference 3. FORMAT (7E10.)

Card Type 13 - Columns 1-5, the number, NEG, of source energies.

Card Type 14 - Eight fields of nine columns per field, each field contains a source energy. Entries are continued until NEG source entries have been read. FORMAT (I5/(8E9.))

Cards type 15 are read in a DO LOOP ranging over the number of interfaces; i.e., the number of layers plus one.

Card Type 15 - Six fields of twelve columns per field, each field contains the source strength, SSS(K, L), for the l^{th} energy at the k^{th} interface. The entries are order by energy and then by interface - from incident face to exit face. FORMAT (6E10.)

Card Type 16 - Fourteen fields of five columns per field containing the integers LNB(I). FORMAT (14I5)

Cards type 17 are "case cards". There should be one card for each cumulative set of layers - i.e., one card for the first layer, one for the first two, one for the first three, etc.

Card Type 17 - Columns 1-5, the integer NBO indicating the build-up factor calculation option; columns 6-10, the number, NL1, of layers in the first equivalent thickness; columns 11-15, the number, NL2, of layers in the second equivalent thickness; columns 16-20, the number, LE1, indicating the material of equivalence for the first equivalent thickness; columns 21-25, the number, LE2, indicating the material of equivalence for the second equivalent thickness.

OUTPUT FORMAT

The output of the MSGAM code consists of one output set for each cumulative set of layers - i.e., one for the first layer, one for the first two layers, one for the first three layers, etc. Each output set has the following format.

First, the build-up factor option is indicated, either single equivalent thickness, two equivalent thicknesses, light-heavy, or two equivalent thicknesses, heavy-light. Next, the total number of layers pertaining to the output set is indicated; for the single equivalent thickness case, this is followed by the material of equivalence; for the two equivalent thicknesses cases, the total number of layers is followed by the number of layers in the first equivalent thickness, and then the materials of equivalence for the first and second thicknesses are indicated. Next, the total number of source points which contribute to this output set. Following this are the thicknesses of each layer. Then the layer materials are indicated. The source energies are displayed in a row of ten entries. Below the source energies are the dose rates resulting from each layer at each energy - each row represents a layer and each column represents the dose rate at the energy above it. Next, the total dose rate at each energy is output, summed over layer. Finally, the total dose rate, summed over energy, is indicated.

6. NUCLEAR CONSTANTS CODE (NCON)

CODE DESCRIPTION

The input values for the Nuclear Constants Code are defined by their association with the following equations. These equations determine the nuclear cascade production used in the Lockheed Proton Penetration Code.

$$G_{pp} = \frac{E_B\left(\frac{E_p + E_n}{E_B}\right)\frac{1}{\left[1 + \left(\frac{E_n}{E_p}\right)_p\right]}}{N\bar{E}(E_B, C_{pp}, K_{pp})} \tag{6-1}$$

$$G_{pn} = \frac{E_B\left(\frac{E_p + E_n}{E_B}\right)\left(\frac{E_n}{E_p}\right)_p\frac{1}{\left[1 + \left(\frac{E_n}{E_p}\right)_p\right]}}{N\bar{E}(E_B, C_{pn}, K_{pn})} \tag{6-2}$$

$$G_{np} = \frac{E_B\left(\frac{E_p + E_n}{E_B}\right)\frac{1}{\left[1 + \left(\frac{E_n}{E_p}\right)_n\right]}}{N\bar{E}(E_B, C_{np}, K_{np})} \tag{6-3}$$

$$G_{nn} = \frac{E_B\left(\frac{E_p + E_n}{E_B}\right)\left(\frac{E_n}{E_p}\right)_n\frac{1}{\left[1 + \left(\frac{E_n}{E_p}\right)_n\right]}}{N\bar{E}(E_B, C_{nn}, K_{nn})} \tag{6-4}$$

where

$$N\bar{E}(E_B, C_{xy}, K_{xy}) = \int_0^{E_B} \frac{E\,dE}{(E + C_{xy})^{K_{xy}}} \qquad (6\text{-}5)$$

For an incident particle, x, with energy E_B, the number, τ_{xy}, of secondary particles of type y, with energy E_S is given by

$$\tau_{xy}(E_B, E_S) = G_{xy}(E_B) \cdot \frac{1}{(E_S + C_{xy})^{K_{xy}}} \qquad (6\text{-}6)$$

GLOSSARY OF INPUT DATA TERMS

CPP - The "C_{pp}" in Equation 6-1.

CNP - The "C_{np}" in Equation 6-3.

CPN - The "C_{pn}" in Equation 6-2.

CNN - The "C_{nn}" in Equation 6-4.

RPP - The "K_{pp}" in Equation 6-1.

RNP - The "K_{np}" in Equation 6-3.

RPN - The "K_{pn}" in Equation 6-2.

RNN - The "K_{nn}" in Equation 6-4.

A - Atomic mass number for the element.

T - The nuclear transparency of the element.

IGO1 - Control Number: If IGO1 = 1, other elements to follow.
If IGO1 = 2, no other elements to follow.

E_B - Kinetic energy of incident particle.

R1 - $\left(\frac{E_p + E_n}{E_B}\right)$, the ratio of the total cascade energy to the bombarding energy.

R2 - $\left(\frac{E_n}{E_p}\right)_p$, the ratio of total neutron cascade energy to total proton cascade energy due to an incident proton.

R3 - $\left(\frac{E_n}{E_p}\right)_n$, the ratio of total neutron cascade energy to total proton cascade energy due to an incident neutron.

IGO2 - Control Number:

If IGO2 = 1, more EB's, R1's, R2's, and R3's to follow for this element.

If IGO2 = 2, no more data for this element.

The values K_{xy}, C_{xy}, T, R1, R2, and R3 may be obtained from graphs in NR-140;[6] these graphs are contained in this report for convenience.

K_{xy} - Figure 15
C_{xy} - Figure 16
T - Figure 17
R1 - Figure 18
R2 & R3 - Figure 19

INPUT DATA PREPARATION

Card Type 1 - Columns 1-7, CPP;
Columns 8-14, CNP;
Columns 15-21, CPN;
Columns 22-28, CNN;
Columns 29-35, RPP;
Columns 36-42, RNP;
Columns 43-49, RPN;

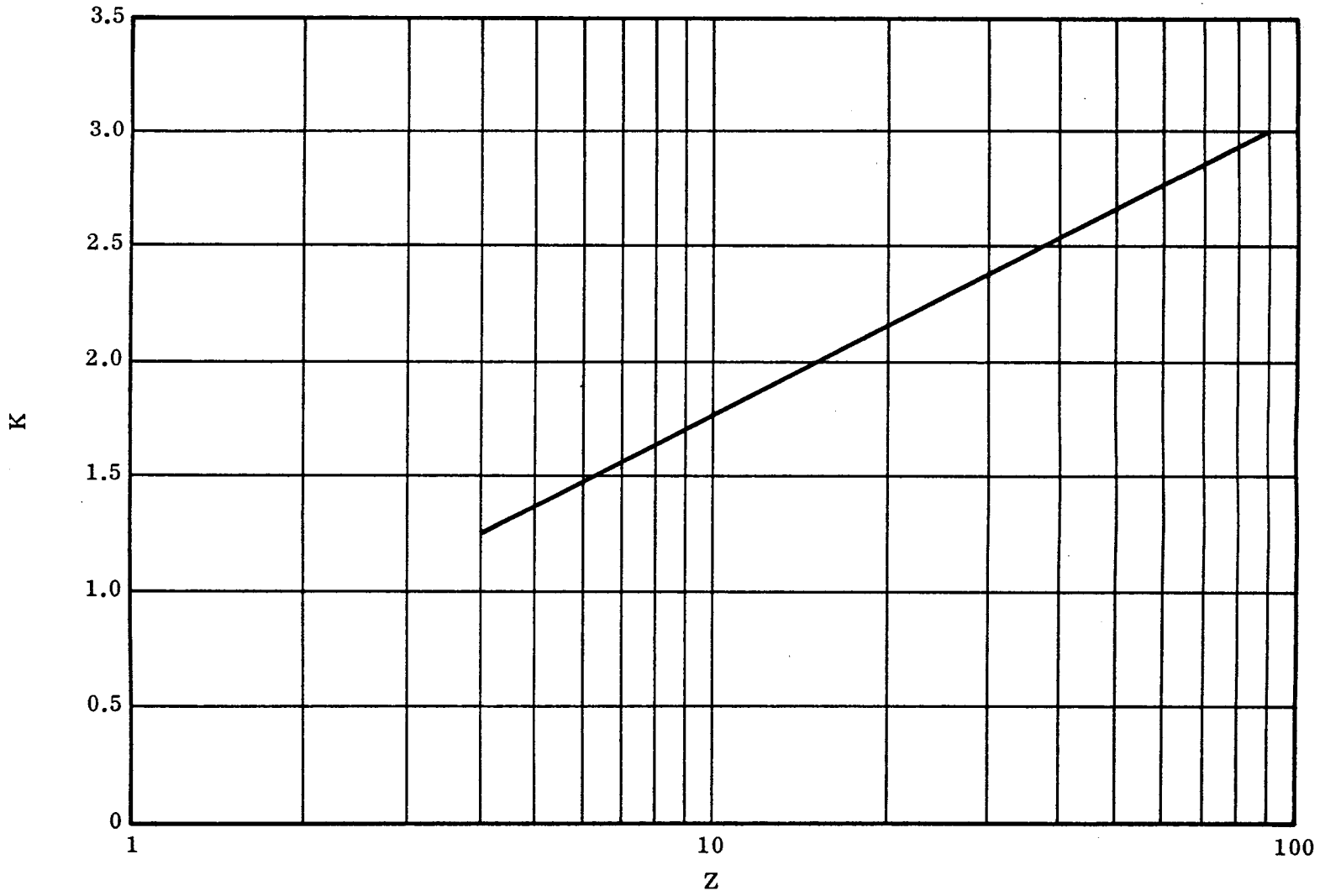

FIGURE 15 K AS FUNCTION OF MATERIAL (Z)

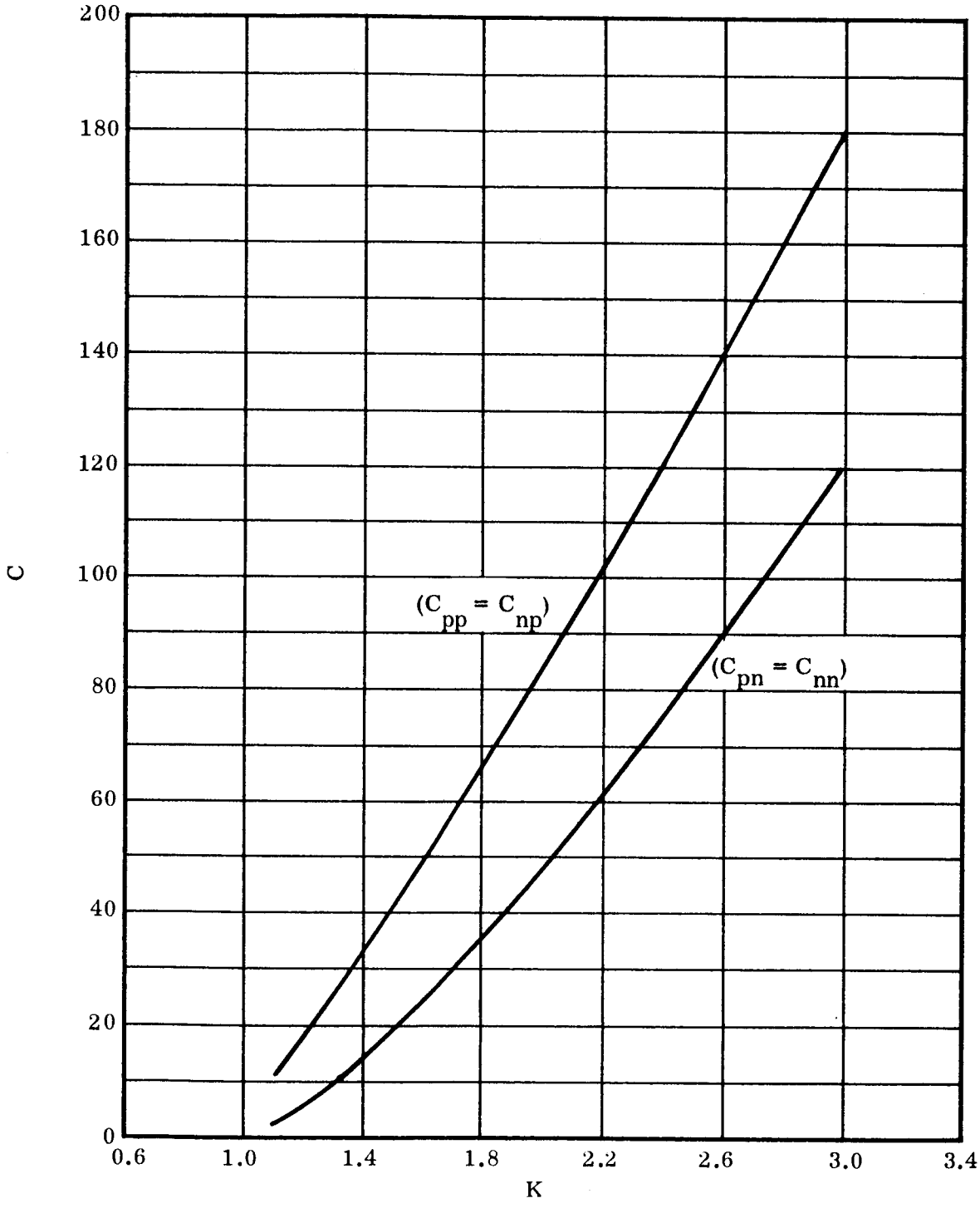

FIGURE 16 C VS K REQUIRED TO GIVE $\bar{E}/E_B = 0.22$ AND 0.17 FOR E_B = 460 MEV

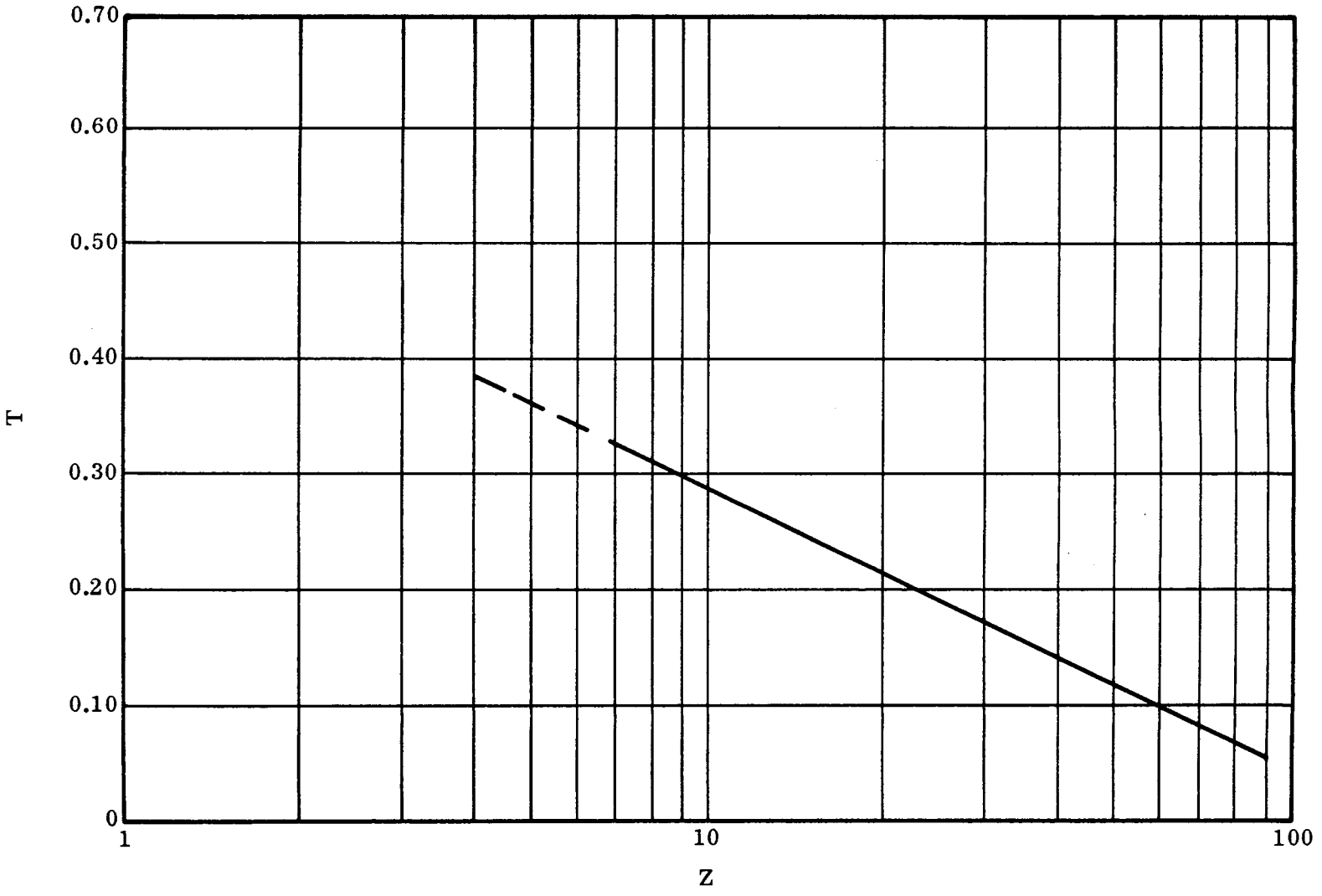

FIGURE 17 NUCLEAR TRANSPARENCIES FOR PROTON BOMBARDMENTS VS MATERIAL (Z)

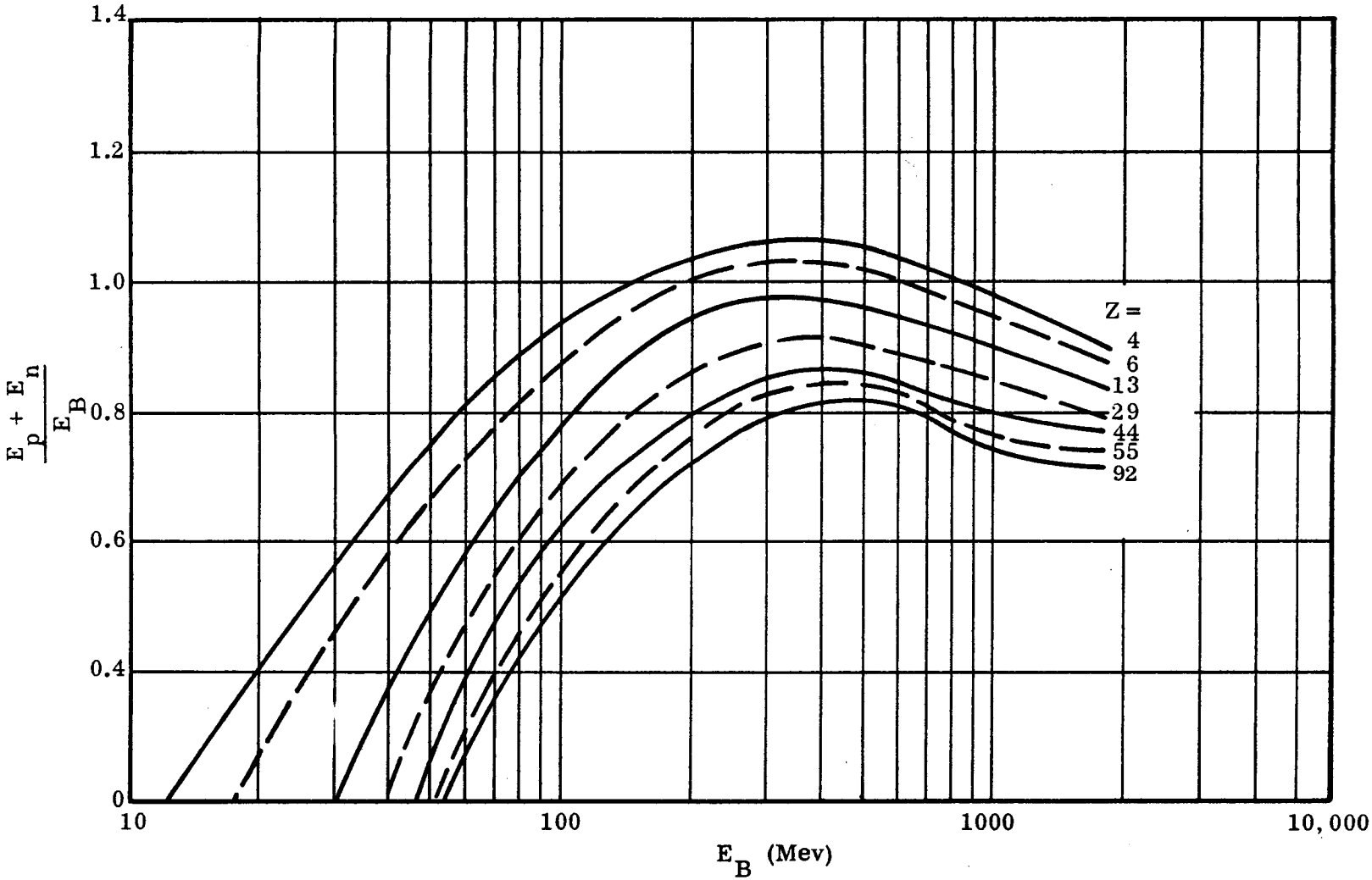

FIGURE 18 ENERGY DEPENDENCE OF SECONDARY PROTONS (E_p) AND NEUTRONS (E_n) UPON BOMBARDING ENERGY (E_B) FOR MATERIALS (Z)

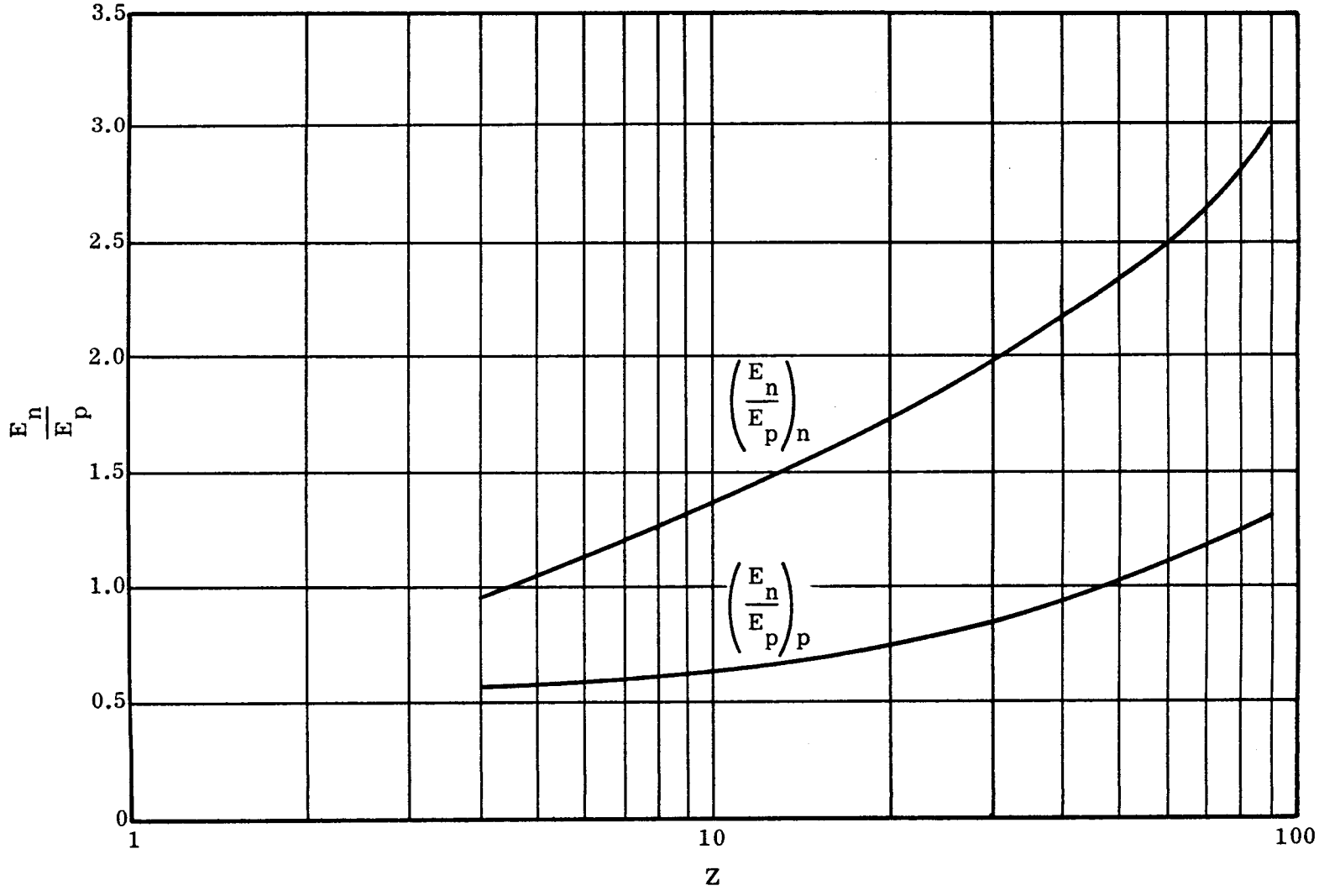

FIGURE 19 ENERGY RATIO OF CASCADE NEUTRONS (E_n) TO CASCADE PROTONS (E_p) AS FUNCTION OF MATERIAL (Z)

Columns 50-56, RNN;
Columns 57-63, A;
Columns 64-70, T;
Columns 71, IGO1.

Card Type 2 - Columns 1-8, EB;
Columns 9-16, R1;
Columns 17-24, R2;
Columns 25-32, R3;
Column 33, IGO2.

Note: Each card type 1 indicates an element for which the cascade constants are to be calculated. Following each card type 1, there should be cards type 2 - one for each bombarding energy to be considered.

OUTPUT FORMAT

The output from the NCON contains, in the heading, input information such as the atomic mass number, A, and the nuclear transparency, T, of the element and the constants, C and K, for p-p, n-p, p-n, and n-n reactions.

The main body of the output contains nine columns of information. The first column lists the kinetic energies, EB, of the incident particle in units of Mev. The second column lists the ratios, (EP + EN)/EB, of the total kinetic energy, of cascade protons plus the cascade neutron, to the kinetic energy of cascade protons for proton bombardment. The fourth column lists the ratios, (EN/EP)N, of the total kinetic energy of cascade neutrons to the total kinetic energy of cascade protons for neutron bombardment. The fifth column lists the G values necessary to give the proper total kinetic energy for a secondary nucleon from a p-p reaction. The sixth column lists the G values necessary to give the proper total kinetic energy of a secondary nucleon from an n-p reaction. The seventh column lists the G values necessary to give the proper total kinetic energy of secondary nucleon from a p-n reaction. The eighth column lists the G values necessary to give the proper total kinetic energy of a secondary nucleon from an n-n reaction. The ninth column lists the removal cross sections, TC, for the element as a function of the kinetic energy of the incident particle.

7. RANGE AND STOPPING POWER CALCULATOR (LRSPC)

CODE DESCRIPTION

The Lockheed Range and Stopping Power Calculator (LRSPC) is a computer code designed to estimate the energy loss, due to ionization and excitation, of charged particles passing through matter. This energy loss (i.e., stopping power) is calculated as a function of kinetic energy for charged particles penetrating materials composed of ten or less elements. Appropriate correction factors are introduced in the stopping power calculation to account for the "density effect", the "shell effect" and the "physical state effect". Protons with kinetic energies ranging from 2 Mev to 100 Gev are considered in the calculations.

The range of protons in matter is given by:

$$R(E) = R(2\ \text{Mev}) + \int_{E(2\ \text{Mev})}^{E} \frac{dE}{SP(E)} \qquad (7\text{-}1)$$

where R(E) is the range of a proton with kinetic energy (E);

R(2 Mev) is the experimentally determined range of protons with kinetic energy of 2 Mev;

SP(E) is calculated stopping power of protons with kinetic energy (E).

The stopping power, SP(E), is calculated from the Bethe-Bloch formula.

$$SP(E) = -\left(\frac{dE}{dx}\right)\left(\frac{1}{\rho_t}\right) = \frac{2\ Ne^4}{mc^2\ \beta^2} \sum \frac{Z_k\ \rho_k}{A_k\ \rho_t}\ (\text{BRAK}) \qquad (7\text{-}2)$$

where -(dE/dx) is the proton energy loss rate due to ionization in the material; ρ_t is the density of the stopping material in units of gm/cm^3; N is Avogadro's number in units of atoms/mole; e is the electronic charge in units of (Mev-cm)$^{1/2}$; mc^2 is the electron rest mass in units of Mev; β is the ratio of the velocity of the incident proton to the velocity of light; Z_k is the atomic number of the k^{th} element of the stopping material; ρ_k is the partial density of the k^{th} element of the stopping material in units of gm/cm^3; A_k is

the atomic weight of the k^{th} element of the stopping material; and BRAK is a term of convenience defined below.

$$BRAK = \ln\left[\frac{2mc^2\beta^2}{I^2(1-\beta^2)} W_{max}\right] - 2\beta^2 - U - \delta \qquad (7\text{-}3)$$

where I is the mean ionization potential of the stopping material in units of Mev; U is the "shell effect" correction term; δ is the "density effect" correction term; and W_{max} is maximum energy transfer from the incident proton to an atomic electron. W_{max} is defined by:

$$W_{max} = \frac{E_t^2 - \mu^2 c^4}{\mu c^2\left[(\mu/2m) + (m/2\mu) + (E_t/\mu c^2)\right]} \qquad (7\text{-}4)$$

where E_t is the total energy of the incident proton; μ is the rest mass of the incident proton; c is the speed of light; and m is the rest mass of the electron.

The mean ionization potential, I, is given by:

$$I = Exp\left[\frac{\sum_k (Z_k \rho_k/A_k) \ln I_k}{\sum_k (Z_k \rho_k/A_k)}\right] \qquad (7\text{-}5)$$

where I_k is the mean ionization potential of the k^{th} element in the stopping material.

The "shell effect" correction term (U) is introduced to prevent an overestimation of the stopping power of a material when the velocity of the incident charged particle is not much greater than the velocity of the inner electrons of the elements present.

$$U = 2C_K/Z + 2C_L/Z \qquad (7\text{-}6)$$

where C_K is the correction term for the ineffectiveness of the K shell electrons; Z is the atomic number of the stopping material; C_L is the correction term for the ineffectiveness of the L shell electrons.

The stopping number (B_i) for any atomic shell when η_i is large is,

$$B_i(\theta_i, \eta_i) = S_i(\theta_i) \ln \eta_i + T_i(\theta_i) - C_i(\theta_i, \eta_i) \qquad (7\text{-}7)$$

where i indicates the atomic electron shell (K, L, . . . etc.); θ_i is the ratio of the observed binding energy of the i^{th} atomic electron shell to the "ideal" ionization potential, which ignores screening by the outer electron shells; η_i is proportional to the energy of the incident particle divided by the "ideal" ionization potential; S_i is an η_i dependent term and T_i is an η_i independent term when the electrons of the i^{th} shell are considered motionless; and C_i is the correction term for the i^{th} shell electrons in motion. The stopping number, B, for a material is determined by the sum of the stopping numbers of each shell from all elements present.

$$B = \sum_{j=1}^{M} \sum_{i=1}^{N_j} B_{ij}(\theta_i, \eta_i) \qquad (7\text{-}8)$$

where B_{ij} is the stopping number for the i^{th} shell of the j^{th} atom; N_j is the number of electron shells in the j^{th} atom; and M is the number of elements in the material.

To determine the stopping number (B_K) of the K shell electrons, the expressions for θ_K and η_K are

$$\theta_K = \frac{I_K}{\left(\frac{mc^2}{2n^2}\right)\left(\frac{Z - 0.3}{137.0372}\right)^2} \qquad (7\text{-}9)$$

where I_K is the observed binding energy of the K shell, n is the principal quantum number (1) of the K shell, and (Z - 0.3)/137.0372 is the non-relativistic "ideal" ionization potential, of the K shell, times the fine structure constant and ignores screening by all but the other K electron, and

$$\eta_K = \beta^2 \Big/ \left[\left(\frac{1}{n^2}\right)\left(\frac{Z - 0.3}{137.0372}\right)^2\right] \qquad (7\text{-}10)$$

To determine the stopping number (B_L) of the L shell electrons, the expressions for θ_L, which is the weighted average of the energy states of the L level, and η_L are

$$\theta_L = \frac{2(\theta_{L1})(HOF_{L1}) + 3(\theta_{L2} + \theta_{L3})(HOF_{L2})}{2(HOF_{L1}) + 6(HOF_{L2})} \qquad (7\text{-}11)$$

where θ_{L1}, θ_{L2}, and θ_{L3} correspond to the three relativistic energy states in the L electron shell,

$$\theta_{L1} = \frac{I_{L1}}{\left(\frac{mc^2}{2n^2}\right)\left(\frac{Z - 4.15}{137.0372}\right)^2} - \frac{5}{16}\left(\frac{Z - 4.15}{137.0372}\right)^2$$

$$\theta_{L2} = \frac{I_{L2}}{\left(\frac{mc^2}{2n^2}\right)\left(\frac{Z - 4.15}{137.0372}\right)^2} - \frac{5}{16}\left(\frac{Z - 4.15}{137.0372}\right)^2 \qquad (7\text{-}12)$$

$$\theta_{L3} = \frac{I_{L3}}{\left(\frac{mc^2}{2n^2}\right)\left(\frac{Z - 4.15}{137.0372}\right)^2} - \frac{1}{16}\left(\frac{Z - 4.15}{137.0372}\right)^2$$

I_{L1}, I_{L2}, and I_{L3} are the observed binding energies of the L shell electrons, n is the principal quantum number (2) of the L shell, and (Z - 4.15)/137.0372 is the non-relativistic "ideal" ionization potential of L shell times the fine structure constant. HOF_{L1} is the Hönl[24] oscillator strength for the 2s electron states of the L shell, and HOF_{L2} is the Hönl oscillator strength for the 2p electron states of the L shell.

Values of η_K are calculated using Equation 7-10, and values of θ_K are calculated using Equation 7-9. Values of the stopping number, $B_K(\theta_K, \eta_K)$, are determined graphically from data presentations of Brown[9] and Walske[47]. This method is used to determine the stopping number when η_K is small. A plot of the $C_K(\theta_K, \eta_K)$ versus $1/\eta_K$ by Walske[47] is used to determine the C_K correction term to the K electron shell stopping number for small values of η_K. Three point interpolation in θ_K is used to get the proper value of B_K and C_K from these graphs and tables for the η_K of the incident proton. For large values of η_K, the asymptotic formulas for $B_K(\theta_K, \eta_K)$ of the K shell electrons given by Walske[47] are used,

$$B_K(0.7,\ \eta_K) = 1.8133 \ln \eta_K + 2.4603 - 2.0662\,\eta_K^{-1} - 7.3246\,\eta_K^{-2} + 45\,\eta_K^{-3}$$

$$B_K(0.75,\ \eta_K) = 1.7223 \ln \eta_K + 2.4044 - 2.0999\,\eta_K^{-1} - 7.3194\,\eta_K^{-2} + 45\,\eta_K^{-3}$$

$$B_K(0.8,\ \eta_K) = 1.6457 \ln \eta_K + 2.3462 - 2.1196\,\eta_K^{-1} - 7.3191\,\eta_K^{-2} + 45\,\eta_K^{-3}$$

$$B_K(0.85,\ \eta_K) = 1.5807 \ln \eta_K + 2.2868 - 2.1290\,\eta_K^{-1} - 7.3218\,\eta_K^{-2} + 45\,\eta_K^{-3}$$

$$B_K(0.9,\ \eta_K) = 1.5250 \ln \eta_K + 2.2273 - 2.1309\,\eta_K^{-1} - 7.3263\,\eta_K^{-2} + 45\,\eta_K^{-3} \qquad (7\text{-}13)$$

where $C_K(\theta_K, \eta_K)$ to order η_K^{-3} is the negative of the last three terms of the asyptotic formulas.

Values of η_L, as a function of the kinetic energy of the incident protons, and θ_L, as a function of the stopping material, are calculated, and a plot of the values of B_L versus η_L for $\theta_L = 0.35,\ 0.45,\ 0.55,\ 0.65$ and for $0 \leq \eta_L \leq 2$ and a table of the values of $B_L(\theta_L, \eta_L)$ for $\theta_L = 0.35,\ 0.45,\ 0.55,\ 0.65$ and for $1.0 \leq \eta_L \leq 3.5$ by Walske[48] are used to determine the stopping number of materials for lower values of η_L. For large values of η_L, the asymptotic formulas for $B_L(\theta_L, \eta_L)$ of the L shell electrons given by Walske[48] are used.

$$B_L(0.35,\ \eta_L) = 10.0371 \ln \eta_L + 28.1449 - 1.5032\,\eta_L^{-1} - 1.543\,\eta_L^{-2} + 4.0\,\eta_L^{-3} - 4.43\,\eta_L^{-4}$$

$$B_L(0.45,\ \eta_L) = 7.9116 \ln \eta_L + 24.4501 - 1.8756\,\eta_L^{-1} - 1.506\,\eta_L^{-2} + 4.0\,\eta_L^{-3} - 4.43\,\eta_L^{-4} \qquad (7\text{-}14)$$

$$B_L(0.55,\ \eta_L) = 6.7451 \ln \eta_L + 21.9061 - 1.9890\,\eta_L^{-1} - 1.498\,\eta_L^{-2} + 4.0\,\eta_L^{-3} - 4.43\,\eta_L^{-4}$$

(Equation 7-14 continued)

$$B_L(0.65,\ \eta_L) = 6.0345 \ln \eta_L + 20.0154 - 2.0040\, \eta_L^{-1} - 1.500\, \eta_L^{-2} + 4.0\, \eta_L^{-3} - 4.43\, \eta_L^{-4}$$

where $C_L(\theta_L,\ \eta_L)$ to order η_L^{-4} is the negative of the last four terms of the asymptotic formulas.

The "density effect" is the reduction in the ionization loss of a charged particle due to polarization of the stopping media. The density effect correction term to be applied to the Bethe-Bloch formula is directly dependent on the value of the mean ionization potential of the stopping media and is calculated by a method similar to that of Sternheimer.[40, 41, 42] It differs chiefly in the large number of electron shells considered.[23]

$$\Delta\left(-\frac{dE}{dx}\right) = \frac{2\pi ne^4}{mv^2}\left(-\delta\right) \tag{7-15}$$

where dE/dx is the energy loss rate, n is the number of electrons per cubic centimeter in the stopping material, e is the electron charge, m is the electron mass, v is the velocity of the incident particle ($v = \beta c$), and δ is the density effect correction term.

The density effect correction term δ is given by:

$$\delta = \left\{ \sum_{i,k} f_{ik} \ln\left[(l_{ik}^2 + l^2)/l_{ik}^2 \right] - l^2(1 - \beta^2) \right\} \tag{7-16}$$

where l is the solution of

$$\frac{1}{\beta^2} - 1 = \sum_{i,k} \frac{f_{ik}}{\bar{\nu}_{ik}^2 + l^2} \tag{7-17}$$

and $l_{i,k}$ is given by

$$l_{ik} = (\bar{\nu}_{ik}^2 + f_{ik})^{1/2} \tag{7-18}$$

Here, f_{ik} is the oscillator strength of the i^{th} transition in the k^{th} element. Its value is given by the ratio of the number of electrons in the i^{th} subshell to the atomic number. The term $\bar{\nu}_{ik}$ is the effective oscillator frequency of the i^{th} shell electrons of the k^{th} element in units of the plasma frequency ν_p.

$$\bar{\nu}_{ik} = \left(\frac{\nu_{ik}}{\nu_p} G_k \right) \tag{7-19}$$

The ν_{ik} is i^{th} transition frequency for the k^{th} element. The plasma frequency of the mixture is given by

$$\begin{aligned} h\ \nu_p &= h(ne^2/\pi m)^{1/2} \\ &= 28.8203 \times 10^{-6} \left[\sum_k (Z_k \rho_k / A_k) \right]^{1/2} \end{aligned} \tag{7-20}$$

The symbol G_k represents a correction term due to the fact that transitions are made into the continum. It is evaluated by normalizing the calculated ionization potential to the experimental effective ionization potential, I_k, for the k^{th} element. For nonconductors, the value of G_k is:

$$G_k = \mathrm{Exp}\left[\frac{\ln I_k - \sum_{i=1}^{j} f_{ik} \ln(h\ \nu_{ik})}{\sum_{i=1}^{j} f_{ik}} \right] \qquad i \leq j \tag{7-21}$$

For metals, the value of G_k is:

$$G_k = \mathrm{Exp}\left\{ \frac{\ln I_k - f_{jk} \ln\ h\ \nu_p (f_{jk})^{1/2} - \sum_{i=1}^{j-1} f_{ik} \ln(h\ \nu_{ik})}{\sum_{i=1}^{j-1} f_{ik}} \right\} \tag{7-22}$$

where i is the number of subshells, j is the oscillator number of the conduction electrons, and k is the element number.

A third correction is needed if the mean ionization potential is measured for a material in a solid or liquid physical state, and the stopping power is desired for the gaseous state or vice versa.[49]

$$I_k^{gas} = I_k^{condensed}\, e^{D_k/2} \tag{7-23}$$

For metals the D_k term is

$$D_k = \sum_{i=1}^{j-1} f_{ik} \ln(1 + f_{ik}/\overline{\nu}_{ik}^2) + 2f_{jk} \ln\left[h\, \nu_p (f_{jk})^{1/2}/E_{jk} \right] \tag{7-24}$$

where E_{jk} is the optical transition energy of electrons in a gas. For nonconductors the D_k term is

$$D_k = \sum_{i=1}^{j} f_{ik} \ln(1 + f_{ik}/\overline{\nu}_{ik}^2) \tag{7-25}$$

GLOSSARY OF INPUT DATA TERMS

NEB - Number of fine mesh energy points.

EMIN - Minimum energy of mesh.

EBR(I) - Major energy break points in fine mesh.

DE(I) - Step size of fine mesh between major energy break points.

NS - Number of subshells per element.

HNU(J, I) - Observed binding energy of the atomic electrons in each subshell in units of Mev, for the j^{th} element and i^{th} subshell.

EJ(J) - Principal quantum number of the outer shell electrons for the j^{th} element.

II(J, I) - Number of electrons in the i^{th} subshell of the j^{th} element.

NBK - Number of entries in the K shell electron stopping number table per θ_K.

EBK(I) - Energy dependent variable, $\eta_K = \frac{\beta^2}{\left(\frac{Z - 0.3}{137.0372}\right)^2}$

BK(J, I) - Stopping number of K-shell electrons for $\eta_K \leq 10$.

BK(1, I) - value of stopping number when θ_K is 0.7;

BK(2, I) - value of stopping number when θ_K is 0.8;

BK(3, I) - value of stopping number when θ_K is 0.9.

Where θ_K is the energy difference between a K-electron in the ground state and the lowest unoccupied state in units of Z^2_{Keff} R_H, R_H is the ionization potential of hydrogen.

NBL - Number of entries in the L electron stopping number table per θ_L.

EBL(I) - Energy dependent variable, $\eta_L = \frac{4\beta^2}{\left(\frac{Z - 4.15}{137.0372}\right)^2}$

BL(J, I) - Stopping number of L-electrons when $\eta_L \leq 3.5$.

BL(1, I) - value of stopping number when $\theta_L = 0.35$;

BL(2, I) - value of stopping number when $\theta_L = 0.45$;

BL(3, I) - value of stopping number when $\theta_L = 0.55$;

BL(4, I) - value of stopping number when $\theta_L = 0.65$;

where θ_L is the observed energy difference between an L electron in the ground state and the lowest unoccupied state in units of Z^2_{Leff} R_H.

ZZ(I) - Atomic number of elements in the Hönl weighting function table for L-shell electrons.

OZ1(I) - Hönl weighting function to correct for relativistic effects in the 2s electron energy states.

OZ2(I) - Hönl weighting function to correct for relativistic effects in the 2p electron energy states.

ZR(I) - Atomic numbers of elements in the initial value table for range of particles at 2 Mev.

TPOR(I) - Initial values for range of particles at 2 Mev.

FIZ(I) - Atomic numbers of elements in the table of ionization potentials.

FIZP(I) - Values of experimentally determined ionization potential in units of ev.

NES - Total number of energy mesh points for punched card output.

ES(I) - Energy mesh points for punched card output.

KMAX - Number of elements present in material, KMAX $\leq$ 10.

I2 - State of final material; I2 = 1(metal), I2 = 2 (condensed nonconductor), I2 = 3 (gas).

I1K(I) - State of element when I/Z was measured; I1K = 1 (metal), I1K = 2 (condensed nonconductor), I1K = 3 (gas).

Z(I) - Atomic number of the element.

AW(I) - Atomic weight of the element.

FIP(I) - Ionization potential of the element in units of ev.

RHO(I) - Density of the element in units of gm/cm^3.

UAR(I) - Correction factor to the L-shell term.

INPUT DATA PREPARATION

Card type 1 through card type 8A are placed on Tape B6.

Card Type 1 - Columns 7-10 contain the number of occupied subshells per element (NS). Columns 11-70 contain six fields of ten

columns per field of values of the electron binding energy per subshell per element (HNU).

Card Type 1A - Continuation card contains six fields of ten columns per field of values of HNU beginning in Column 11

FORMAT (6xI4, 6E10./(10X6E10.))

Card Type 2 - Columns 1-10 contain the principal quantum number of the outer subshell electron per element (EJ). Columns 11-70 contain a maximum of thirty fields of two columns per field of the number of electrons in the occupied subshells per element (II).

FORMAT (EI0., 30I2)

Card Type 3 - Contains nine fields of eight columns per field of energy mesh points (E).

FORMAT (9E8.)

Card Type 4 - Columns 1 and 2 contain the number of Eta K entries (NBK) in the stopping number table for K electrons.

Card Type 4A - Contains four fields of ten columns per field. Columns 1-10 contain the value of Eta K (EBK), Columns 11-40 contain the values of the stopping number of K electrons (BK); Columns 11-20, value of BK when Theta K is 0.7, Columns 21-30, value of BK when Theta K is 0.8, Columns 31-40, value of BK when Theta K is 0.9.

FORMAT (I2/(4E10.))

Card Type 5 - Columns 1 and 2 contain the number of Eta L entries (NBL) in the stopping number table for L electrons.

Card Type 5A - Contains five fields of ten columns per field. Columns 1-10 contain the value of Eta L (EBL); columns 11-50 contain values of the stopping number for L electrons (BL); columns 11-20, value of BL when Theta L is 0.35; columns 21-30, value of BL when Theta L is 0.45; columns 31-40, value of BL when Theta L is 0.55; columns 41-50, value of BL when Theta L is 0.65.

FORMAT (I2/(5E10.))

Card Type 6 - Contains three fields of ten columns per field. Columns 1-10 contain the atomic number of the element composing the table, (ZZ); columns 11-20 contain the Hönl weighting function for the 2s state L electrons (OZ1); and columns 21-30 contain the Hönl weighting function for the 2p state L electrons (OZ2).

FORMAT (3E10.).

Card Type 7 - Contains nine fields of eight columns per field. Columns 1-8, 17-24, 33-40, 49-56, and 65-72 contain the atomic number of the elements (ZR) composing the initial range table while columns 9-16, 25-32, 41-48, and 57-64 contain the initial range values (TPOR) for 2 Mev protons.

Card Type 7A - Continuation card - contains nine fields of eight columns per field. Columns 1-8, 17-24, 33-40, 49-56, and 65-72 contain the initial range values (TPOR) for 2 Mev protons while columns 9-16, 25-32, 41-48, and 57-64 contain the atomic number of the elements (ZR) composing the initial range table.

FORMAT (9E8.)

Note: Initial values for range of 2 Mev protons are described by card type 7, card type 7A, and card type 7, card type 7A, etc., until all atomic numbers and their accompanying initial range values are read in.

Card Type 8 - Contains nine fields of eight columns per field. Columns 1-8, 17-24, 33-40, 49-56, and 65-72 contain the atomic number of the elements (FIZ) composing the table of experimentally determined ionization potentials while columns 9-16, 25-32, 41-48, and 57-64 contain the values of the experimentally determined ionization potentials (FIZP).

Card Type 8A - Continuation card - contains nine fields of eight columns per field. Columns 1-8, 17-24, 33-40, 49-56, and 65-72 contain the values of the ionization potential (FIZP) while columns 9-16, 25-32, 41-48, and 57-64 contain the atomic numbers (FIZ) of the elements composing the ionization potential table.

FORMAT (9E8.)

Note: Experimentally determined ionization potential values for elements are described by card type 8, card type 8A, card type 8, card type 8A, etc., until all atomic numbers and their accompanying experimental ionization potentials are read in.

Note: Card type 9 and card type 9A follow the asterisk data card which is directly behind the binary program cards.

Card Type 9 - Columns 1-5 contain the number of fine mesh energy points (NEB). Columns 6-15 contain the minimum energy of mesh (EMIN).

Card Type 9A - Continuation card - contains eight fields of nine columns per field. Columns 1-9, 19-27, 37-45, and 55-63 contain the major energy break points (EBR(I)) while columns 10-18, 28-36, 46-54, and 64-72 contain the step size of the fine mesh between major energy break points (DE(I)) where I = 1, NEB.

FORMAT (I5, E10./(8E9.))

Note: The total number of EBR(I) and DE(I) entries on cards type 9A must equal the number in columns 1-5 of card type 9.

Card Type 10 - Columns 1-3 contain the number of energy mesh points (NES) for punched card output.

Card Type 10A - Nine fields of eight columns per field containing the energy values (ES) for the energy mesh point table.

FORMAT (I3/(9E8.))

Note: The total number of energy entries on cards type 10A must equal the number in columns 1-3 card type 10.

Note: A set of cards composed of card type 11, card type 12, and if necessary card type 13 are input for each case to be evaluated. The sets of cards should equal the number of cases to be evaluated.

Card Type 11 - Case Identification Card - Alphameric identification or labeling of the case being evaluated.

FORMAT (12A6)

Card Type 12 - Three fields of five columns per field followed by five fields of ten columns per field. Columns 1-5 contain the number of elements present in a material (KMAX); columns 6-10 contain the state (I2) of the final material, 1 = metal, 2 = condensed nonconductor, 3 = gas. Columns 11-15 contain the state (I1K), 1 = metal, 2 = condensed nonconductor, 3 = gas, of the element at the time its ionization potential was determined. Columns 16-25 contain the atomic number (Z) of the element composing the material. Columns 26-35 contain the atomic weight (AW) of the element composing the material. Columns 36-45 contain the ionization potential (FIP) of the element. Columns 46-55 contain the partial density (RHO) of the element composing the material, and columns 56-65 contain the L shell correction factor (UAR).

FORMAT (3I5, 5E10.)

Card Type 13 - Continuation card for card type 12 - one field of five columns followed by five fields of ten columns per field. Columns 1-10 are left intentionally blank. Columns 11-15 contain the state (I1K) of the element at the time its ionization potential was determined; 1 = metal, 2 = condensed nonconductor, 3 = gas. Columns 16-25 contain the atomic number (Z) of an element composing the material, columns 26-35 contain the atomic weight (AW) of an element composing the material. Columns 36-45 contain the ionization potential (FIP) of an element composing the material and columns 46-55 contain the partial density (RHO) of an element composing the material. Columns 56-65 contain the L shell correction factor (UAR).

Note: The ionization potential, FIP, in cards type 12 and 13 may be left blank. In this circumstance, a value for FIP will be determined by interpolation in the FIZP table.

Note: Case input data cards are read in order of one card type 12 and zero to nine cards type 13 until the number of card type 12 and cards type 13 is equal to the number of elements composing the material, KMAX, columns 1-5 on card type 12.

OUTPUT FORMAT

The typical output from the LRSPC consists of a heading containing comments or labeling information and a subheading consisting of the atomic number(s), the atomic weight(s), the ratio(s) of the calculated excitation potential(s) divided by the atomic number(s), the partial densities in units of gms/cm^3, the total ionization potential in units of ev, and total density in units of gms/cm^3 for the element or material being evaluated.

The main body of the output contains eight columns for information. The first column lists the kinetic energies of the incident protons in units of Mev. The second column lists the values of (BRAK), from the Bethe-Bloch formula, which is defined in the LRSPC description. The third column lists the calculated shell correction factors for the K shell electrons. The fourth column lists the calculated shell correction factors for the L shell electrons. The fifth column lists the total "shell effect" correction factor. The sixth column lists the "density effect" correction factors. The seventh column lists the calculated stopping powers in units of $Mev\text{-}cm^2\text{-}gm^{-1}$. The eighth column lists the ranges in units of $gms\text{-}cm^{-2}$.

8. SOURCE SPECTRUM CODE (LSSC)

CODE DESCRIPTION

The Lockheed Source Spectrum Code (LSSC) was written to facilitate preparation of proton input spectra in a format suitable for the Lockheed Proton Penetration Code (LPPC).

Space radiation fluxes reported in the literature are presented in a variety of ways, and the reduction of this data to a common form suitable for comparison and calculation is often tedious. The code is intended to eliminate the laborious manual calculations involved in reducing a given spectrum to a differential number flux versus energy. In practice, the code has been found adequate for converting trapped and solar flare spectra in the energy range of interest to space radiation shielding studies.

The code, LSSC, may be used to convert five types of proton spectral data to differential number flux versus energy. These types are:

Option 1 - Integral number flux versus rigidity.

Option 2 - Integral number flux versus energy.

Option 3 - Differential number flux versus rigidity.

Option 4 - Power law representation of integral number flux versus rigidity.

Option 5 - Power law representation of integral number flux versus energy.

Option 1

For this option, a table of rigidity values and their corresponding integral number flux values are read into the computer. The rigidities are converted to energies through the relation given by Equation 8-1.

$$E = \sqrt{(Re)^2 + 938^2} - 938 \qquad (8\text{-}1)$$

where E represents kinetic energy in Mev, R represents rigidity in Mv, and e represents the proton charge (=1).

The data are, after the above conversion, a table of integral number fluxes versus energy and are treated as such by Option 2. The comments under Option 2 relating to optimum choice of input data values, to ensure stability, apply to this option also.

Option 2

In this option, a table of energy values and their corresponding integral number flux values are read into the computer. The integral number flux versus energy spectrum is assumed to be representable by an analytic power function on the interval E_i to E_{i+1}:

$$F(E) = \frac{C}{D-1} E^{1-D}, \quad E_i \leq E \leq E_{i+1} \tag{8-2}$$

By definition

$$\frac{dF(E)}{dE} = -f(E) \tag{8-3}$$

Differentiating Equation 8-2 and substituting into Equation 8-3, one obtains the differential number flux versus energy spectrum,

$$f(E) = CE^{-D} \tag{8-4}$$

From Equation 8-2

$$C = (D-1)\, F(E)/E^{1-D} \tag{8-5}$$

The value of "D" is obtained by evaluating Equation 8-2 at the end points:

$$D = 1 - \frac{\ln\left[F(E_i)/F(E_{i+1})\right]}{\ln(E_i/E_{i+1})} \tag{8-6}$$

The differential number flux versus energy spectrum is obtained by substituting Equations 8-5 and 8-6 in Equation 8-4:

$$f(E) = \frac{F(E)}{E} \cdot \frac{\ln\left[F(E_i)/F(E_{i+1})\right]}{\ln(E_i/E_{i+1})}, \quad E_i \leq E \leq E_{i+1} \tag{8-7}$$

The values of F(E) at the output energies are acquired by polynomial interpolation in a table of the logarithm of E and the logarithm of F(E) evaluated at the input energies. Special provisions are made at those energy points where the size of the energy interval changes.

Option 2 occasionally produces small oscillations in the output spectrum but is more satisfactory than a numerical or graphical differentiation scheme. This is especially true when crude graphs of integral fluxes are to be analyzed. If Option 1 or 2 is used, it is suggested that the values of F(E) be replotted and a smooth curve drawn; then 5 to a maximum of 50 points may be read from the graph. The replotted data are not more accurate than the original, but fluctuations caused by errors in reading coarse interval graphs are minimized. The derivative is very sensitive to fluctuations. For this reason, points should be selected so that differences between successive flux and energy (or rigidity) values are large compared to the graph reading error.

Option 3

In this option, a table of differential number fluxes versus rigidity is read into the computer. Rigidity is transformed to energy according to Equation 8-1. The differential number flux is transformed as:

$$f(E) = F(R)\,\frac{\sqrt{R^2 + 938^2}}{R} \tag{8-8}$$

Option 4

The power law representation of integral number flux versus rigidity is given by Equation 8-9.

$$F(R) = AR^{-B} \tag{8-9}$$

The differential number flux versus rigidity is obtained from Equation 8-9 and given by

$$f(R) = ABR^{-B-1} \tag{8-10}$$

The differential number flux versus energy is related to the differential number flux versus rigidity through

$$f(E) = f(R)\,\frac{dR}{dE} \tag{8-11}$$

dR/dE is obtained from Equation 8-1 giving

$$f(E) = ABR^{-B-2} \cdot \sqrt{R^2 + 938^2} \tag{8-12}$$

by substituting Equations 8-10 and 8-1 in Equation 8-11.

The rigidity values at the output energies are determined by solving Equation 8-1 for R,

$$R = \sqrt{E^2 + 1876E} \tag{8-13}$$

Option 5

The "power law" representation of integral number flux versus energy is given by

$$F(E) = AE^{-B} \tag{8-14}$$

The differential number flux versus energy is obtained by substituting Equation 8-14 into Equation 8-3:

$$f(E) = ABE^{-B-1} \tag{8-15}$$

Equation 8-15 is evaluated at the output energies to obtain a table of differential number flux versus energy.

With the exception of Option 3, the energy points at which the differential number flux will be output are determined by the nine values:

EMAX - the maximum energy to be considered.

EMIN - the minimum energy to be considered.

EB1 - the upper bound for the first energy range, EMIN to EB1.

EB2 - the upper bound for the second energy range, EB1 to EB2.

EB3 - the upper bound for the third energy range, EB2 to EB3. The fourth energy range is EB3 to EMAX.

DEL1 - the energy step size in the first energy range.

DEL2 - the energy step size in the second energy range.

DEL3 - the energy step size in the third energy range.

DEL4 - the energy step size in the fourth energy range.

The number, NE, of output energy points is given by:

$$NE = (EB1 - EMIN)/DEL1 + (EB2 - EB1)/DEL2 + (EB3 - EB2)/DEL3 + (EMAX - EB3)/DEL4 + 1$$

Output energy points will be computed until EMAX is reached or 250 points have been computed - whichever occurs first terminates computation of output energy points.

GLOSSARY OF INPUT DATA TERMS

H - Hollerith information identifying the source spectrum.

NEI - Number of entries in spectrum table.

IPT - Option number

IPT = 1, integral number flux versus rigidity.

IPT = 2, integral number flux versus energy.

IPT = 3, differential number flux versus rigidity.

IPT = 4, power law representation of integral number flux versus rigidity.

IPT = 5, power law representation of integral number flux versus energy.

R(I) - Rigidity entries in Mv (million volts).

EI(I) - Energy entries in Mev.

FEI(I) - Integral flux values at rigidity, R(I), or energy, EI(I), points.

PIR(I) - Differential flux values at rigidity points, R(I).

AA - The coefficient "A" in the integral rigidity power law spectrum, AR^{-B}.

BB - The exponent "B" in the integral rigidity power law spectrum.

AA - The coefficient "A" in the integral energy power law spectrum, AE^{-B}.

BB - The exponent "B" in the integral energy power law spectrum.

EMAX - Maximum energy for which the differential flux spectrum is to be calculated.

EMIN - Minimum energy for which the differential flux spectrum is to be calculated.

EB1 - Upper limit of first differential flux energy range, from EMIN to EB1.

EB2 - Upper limit of second differential flux energy range, from EB1 to EB2.

EB3 - Upper limit of third differential flux energy range, from EB2 to EB3. The fourth, and last, range runs from EB3 to EMAX.

DEL1 - Energy increment within the first range.

DEL2 - Energy increment within the second range.

DEL3 - Energy increment within the third range.

DEL4 - Energy increment within the fourth range.

INPUT DATA PREPARATION

Card Type 1 - 72 columns of Hollerith information available for identification of source spectrum.

FORMAT (12A6)

Card Type 2 - Columns 1-5, the number of entries in the flux table; columns 6-10, the option number.

FORMAT (14I5)

The data contained in card types 3 and 4 depend upon the option number in card type 2.

Card Type 3 (Option 1) - Eight fields of 9 columns per field, each field contains a rigidity value, R(I), in Mv. The number of these entries should equal the number in columns 1-5 of card type 2.

FORMAT (8E9.)

Card Type 4 (Option 1) - Eight fields of 9 columns per field, each field contains an integral number flux value corresponding to the rigidity value in card type 3.

FORMAT (8E9.)

Card Type 3 (Option 2) - Eight fields of 9 columns per field, each field contains an energy value, EI(I), in Mev. The number of these entries should equal the number in columns 1-5 in card type 2.

FORMAT (8E9.)

Card Type 4 (Option 2) - Eight fields of 9 columns per field, each field contains an integral number flux value corresponding to the energy value in card type 3.

FORMAT (8E9.)

Card Type 3 (Option 3) - Eight fields of 9 columns per field, each field contains a rigidity value, R(I), in Mv. The number of these entries should equal the number in columns 1-5 of card type 2.

FORMAT (8E9.)

Card Type 4 (Option 3) - Eight fields of 9 columns per field, each field contains a differential number flux value corresponding to the rigidity value in card type 3.

FORMAT(8E9.)

Card Type 3 (Option 4) - Columns 1-9, the "A" of AR^{-B}; columns 10-18, the "B" of AR^{-B}. (This is the integral number flux versus rigidity power law.) There are no cards type 4 for options 4 and 5.

FORMAT (8E9.)

Card Type 3 (Option 5) - Columns 1-9, the "A" of AE^{-B}; columns 10-18, the "B" of AE^{-B}. (This is the integral number flux versus energy power law.)

FORMAT (8E9.)

Card Type 5 - Columns 1-9, EMAX; columns 10-18, EMIN; columns 19-27, EB1; columns 28-36, EB2; columns 37-45, EB3; columns 46-54, DEL1; columns 55-63, DEL2; columns 64-72, DEL3; columns 1-9 (next card), DEL4.

FORMAT (8E9.)

Note: There is no card type 5 for option 3.

OUTPUT FORMAT

The output information from LSSC, for all five options, is initially the data on the heading card, card type 1, and the option number.

For options 1 and 2, the input energies and integral fluxes are listed - in the case of option 1 the energies are determined from the input rigidities. Following the input data, the computed energy values, the corresponding differential number fluxes, and the corresponding integral number fluxes are listed.

For options 3, 4, and 5, the output is the same as for options 1 and 2; however, the input data is not listed.

For all five options, the number of computed energy values, the heading from card type 1, the computed energies, and the differential number fluxes are punched on cards.

9. ELECTRON BREMSSTRAHLUNG CODE (LEBC)

The Lockheed Electron Bremsstrahlung Code considers photons generated by electrons incident upon a shield material. The photons are attenuated through the remainder of the shield and the resulting dose calculated.

The incident electron flux is assumed to be normal to the surface of the shield. The cross-section, differential in photon energy, for bremsstrahlung production is obtained from formula 3BN in a review article by H. W. Koch and J. W. Motz.[41] This formula retains validity under the conditions of three inequalities,

$$137Z^{-1/3} >> (E_o E/k) \tag{9-1}$$

$$2\pi Z/137\ \beta_o << 1 \tag{9-2}$$

$$2\pi Z/137\beta << 1 \tag{9-3}$$

where E_o = total electron energy before collision in $m_o c^2$ units

E = total electron energy after collision in $m_o c^2$ units

k = photon energy in $m_o c^2$ units.

Inequality 9-1 implies screening effects are considered negligible; inequalities 9-2 and 9-3 imply that the electron kinetic energy is in the range of validity for the Born approximation. The Born approximation underestimates the true cross section at very low energies and overestimates the true cross section at extreme relativistic energies. The energy region in which the Born approximation is only slightly in error is the range from 4 to 10 Mev. Roughly, the Born approximation is within 10% above 2 Mev and within a factor of two below 2 Mev. The cross section formula, 3BN, used in LEBC is:

$$\frac{d\sigma(k,E_o)}{dk} = \frac{z^2 r_o^2 p}{137 p_o k}\left\{\frac{4}{3} - 2E_oE\left(\frac{p^2+p_o^2}{p^2p_o^2}\right) + \frac{f_oE}{p_o^3} + \frac{fE_o}{p^2} - \frac{ff_o}{pp_o} + \right.$$

$$L\left[\frac{8E_oE}{3p_op} + k^2\frac{(E_o^2E^2+p_o^2p^2)}{p_o^3p^3} + \right. \qquad (9\text{-}4)$$

$$\left.\left.\frac{k}{2p_op}\left(\left(\frac{E_oE+p_o^2}{p_o^3}\right)f_o - \left(\frac{E_oE+p^2}{p^3}\right)f + \frac{2kE_oE}{p^2p_o^2}\right)\right]\right\}$$

where $L = 2\ln\left[\frac{E_oE + p_op - 1}{k}\right]$

$f_o = \ln\left[\frac{E_o + p_o}{E_o - p_o}\right]$

$f = \ln\left[\frac{E+p}{E-p}\right]$

$E_o = T_o + 1$

$E = T + 1 = E_o - k$

$p_o = \left[T_o(T_o+2)\right]^{1/2}$

$p = \left[T(T+2)\right]^{1/2}$

E_o, E = initial and final total energy of the electron in a collision, in m_oc^2 units

T_o, T = initial and final kinetic energy of the electron in a collision, in m_oc^2 units

k = energy of emitted photon in m_oc^2 units

z = atomic number of stopping material

$r_o = 2.82 \times 10^{-13}$ cm (classical electron radius).

The photon differential energy flux, I(k), due to an integral number flux of electrons incident normally upon the shield material is given by the relation:

$$I(k) = \frac{0.511\, N_o\, z^2}{A} \int_{k+1}^{E_{o,\max}} \frac{k\, d\sigma(k, E_o)}{z^2\, dk\, S(E_o)}\, N(E_o)\, dE_o \qquad (9\text{-}5)$$

where N_o = Avogadro's number

A, z = atomic weight and atomic number of stopping material.

$\frac{d\sigma(k, E_o)}{dk}$ = bremsstrahlung cross section, differential with respect to photon energy, k, in units of cm^2/atom per incident electron

$E_{o,\max}$ = maximum total energy of incident electrons, in $m_o c^2$ units

$S(E_o)$ = stopping power,[34] in units of Mev-cm^2/gm, for electrons of total energy, E_o, in units of $m_o c^2$

$N(E_o)$ = integral number flux of electrons with total energy equal to or greater than E_o.

The numerical constant, 0.511, converts stopping power in units of Mev-cm^2/gm to stopping power in units of $m_o c^2$-cm^2/gm.

With the photon differential energy flux determined, the bremsstrahlung dose rate emerging from the shield may be calculated.

$$D(x) = 0.511 \int_{k_{min}}^{k_{max}} I(k)\, F(E)\, e^{-\mu(k) \cdot x}\, B(k, x) dk \qquad (9\text{-}6)$$

where $F(E)$ = photon energy flux-to-dose conversion factor,[18] r-cm^2-sec-hr^{-1}-Mev^{-1}

$\mu(k)$ = mass attenuation coefficient,[20] in cm^2/gm

x = normal thickness of shield, in gm/cm^2

$B(k, x)$ = point isotropic source dose build-up factor.[19]

$D(x)$ = photon dose rate in r/hr.

The numerical constant, 0.511, in this equation, is to convert the Mev energy units in the flux-to-dose conversion factor to m_0c^2 energy units.

In the bremsstrahlung code, the dose rate integration is actually the sum of two integrations. In the first, the integration is from the minimum photon energy to the K-edge energy; and in the second, the integration is from the K-edge energy to the maximum photon energy. This is done in order not to integrate over the discontinuity generated in the attenuation coefficients at the K-edge.

GLOSSARY OF INPUT DATA TERMS

H	- Hollerith information identifying calculation.
NMUT	- Number of mass attenuation coefficient (μ) tables.
NST	- Number of stopping power tables.
NNT	- Number of electron integral flux spectrum tables.
ZSTAR(J)	- Atomic number of element of j^{th} μ-table.
NKMU(J)	- Number of entries in j^{th} μ-table.
FKMU(J, I)	- i^{th} photon energy (Mev) entry in j^{th} μ-table of j^{th} element.
FMUII(J, I)	- i^{th} mass attenuation coefficient (cm^2/gm) of j^{th} element.
WA(I)	- Atomic weight of i^{th} element (corresponding to i^{th} μ -table).
Z(I)	- Atomic number for element of i^{th} stopping power table.
NES(I)	- Number of entries in stopping power table for i^{th} element.
ESI(I, J)	- j^{th} electron energy (Mev) entry for i^{th} element stopping power table.
S(I, J)	- Stopping power (Mev^1-gm^{-1}-cm^2) entry at j^{th} energy for i^{th} element.

NFDC - Number of energy-flux-to-dose conversion factors.

FKDC(I) - i^{th} photon energy (Mev) entry.

FDCV(I) - Energy-flux-to-dose conversion factor (r^{1}-hr^{-1}-Mev^{-1}-cm^{2}-sec^{1}) entry at i^{th} energy.

NBEE - Number of energy entries in the kk^{th} buildup table. (Corresponding to the kk^{th} μ-table.)

NBXX - Number of mean free path entries in the kk^{th} buildup table.

BE(JJ, KK) - jj^{th} photon energy (Mev) entry in the kk^{th} buildup table.

BX(JK, KK) - jk^{th} number of mean free paths entry in the kk^{th} buildup table.

BUP(JK, JJ, KK) - Dose buildup factor entry for the jk^{th} number of mean free paths at the jj^{th} photon energy in the kk^{th} element.

NTN(I) - Number of entries in the i^{th} electron integral flux spectrum table.

ETNI(I, J) - j^{th} electron energy (Mev) in i^{th} integral flux table.

FNII(I, J) - Electron integral flux entry at j^{th} energy in i^{th} electron integral flux table.

IOPT - Integral spectrum option:

1 = monoenergetic electron flux

2 = exponential integral flux $\left[Q(E) = Ae^{-E/B}\right]$

3 = tabular integral flux.

ISHLD - Shield material number (indicating material loaction in the sequence of μ-tables).

ITAR - Target material number (indicating material location in the sequence of stopping power tables).

(ITAR determines the material that stops the electrons and generates the photons, ISHLD determines the material that attenuates the photons generated in ITAR.)

INTAB - An integer determining which of the integral flux tables is to be used in the calculation.

IPDR - A print option:

1 = print intermediate data before integrating

0 = omit above printing.

ISTOP - Compute option:

0 = compute

1 = stop

2 = dump, then stop.

NTH - Number of shield thicknesses.

A - The "A" of $Ae^{-E/B}$ for the exponential integral flux option.

B - The "B" for the exponential integral flux option.

ENM - Maximum electron total energy (mc^2 units) including rest mass.

BLIMIT - Lower limit (Mev) of integration above the "K-edge".

ULIMIT - Upper limit (Mev) of integration below "K-edge".

TH(I) - Thickness of i^{th} shield (gm/cm^2).

INPUT DATA PREPARATION

Card Type 1 - 72 columns of Hollerith information, H, to identify the case or cases being run. Format (12A6)

Card Type 2 - 1st 3 columns, 3 one digit integers:

(a) The first integer (NMUT) indicates the number of gamma ray mass attenuation coefficient (μ) tables;

(b) The second integer (NST) indicates the number of electron stopping power tables;

(c) The third integer (NNT) indicates the number of electron integral flux tables. Format (3I1)

Note: The dimensions set by the program limit the number of each kind of table to six.

Card types 3 and 4 are read in a "DO LOOP" ranging over the number of tables (NMUT).

Card Type 3 - Columns 1-10, the atomic number, ZSTAR(J), of the element applicable to the table to be read (card type 4); columns 11-12, the number, NKMU(I), of entries in the table. Format (E10.,I2)

Card Type 4 - Columns 1-10, the photon energy, FKMU(J,I), (Mev) for which the mass attenuation coefficient, FMUII(J,I), is tabulated; columns 11-20, the mass attenuation coefficient (cm^2/gm). Format (2E10.)

Note: The number of cards type 4 for each card type 3 should be equal to the number in columns 11 and 12 of card type 3. Further, the number of cards type 3 should be equal to NMUT (column 1, card type 2). The sequencing of the cards is: card type 3, cards type 4, card type 3, cards type 4, etc.

Cards types 5 and 6 are read in a "DO LOOP" ranging over the number of electron stopping power tables (NST).

Card Type 5 - Columns 1-10, the atomic weight, WA(I), of the element for which stopping powers are to be used from cards type 6; columns 11-20, the atomic number, Z(I), of the same element; columns 21 and 22, the number, NES(I), of entries in the stopping power table for this element. Format (2E10.,I2)

Card Type 6 - Columns 1-10, the electron kinetic energy, ESI(I, J) (Mev), for which the stopping power is tabulated; columns 11-20, the stopping power, S(I, J) ($Mev^1\ gm^{-1}\ cm^2$). Format (2E10.)

Note: The number of cards type 6 for each card type 5 should be equal to the number in columns 21 and 22 of card type 5. Further, the number of cards type 5 should be equal to NST (column 2, card type 2). The sequencing of the data cards is: card type 5, cards type 6, card type 5, cards type 6, etc.

Card Type 7 - Columns 1 and 2, the number, NFDC, of energy-flux-to-dose conversion factor entries (cards type 8).

Card Type 8 - Columns 1-10, photon energy, FKDC(I) (Mev), at which energy-flux-to-dose conversion factor is tabulated; columns 11-20, energy-flux-to-dose conversion factor, FDCV(I). Format (I2/(2E10.))

Card types 9, 10, 11 and 12 are read in a "DO LOOP" ranging over the number of μ-tables (NMUT). These cards are applicable to the dose buildup tables. There should be as many dose buildup tables as there are mass attenuation coefficient (μ) tables, and the order of the elements should be the same in both sets of tables.

Card Type 9 - Columns 1 and 2, the number, NBEE, of entries in the energy table; columns 3 and 4, the number, NBXX, of entries in the mean-free-path table.

Card Type 10 - Seven fields of ten columns per field, each field contains a photon energy, BE(JJ, KK) (Mev), for which the dose buildup factors are tabulated. These cards are continued until the number of entries is equal to the number in columns 1 and 2 in card type 9. The entries must be in increasing energy. Format (2I2/(7E10.))

Card Type 11 - Seven fields of ten columns per field, each field contains the number, BX(JK, KK), of mean free paths of material thickness for which the dose buildup factors are tabulated. These cards are continued until the number of entries is equal to the number in columns 3 and 4, card type 9. The entries must be in order of increasing magnitude. Format (7E10.)

Card Type 12 - Seven fields of ten columns per field, each field contains a photon dose buildup factor, BUP(JK, JJ, KK). For each energy in card type 10, dose buildup factors are entered corresponding to each of the number of mean free paths entered in card type 11. The total number of dose buildup entries should be equal to the product of the two numbers in card type 9. Format (7E10.)

Note: The sequencing of cards types 9, 10, 11 and 12: card type 9, card(s) type 10, card(s) type 11, cards type 12, card type 9, card(s) type 10, card(s) type 11, cards type 12, etc. The number of these sets should equal the number of μ-tables (NMUT).

Card types 13 and 14 are read in a "DO LOOP" ranging over the number of electron integral flux tables (NNT; column 3, card type 2).

Card Type 13 - Columns 1 and 2, the number, NTN(I), of entries in the electron integral flux table. Format (I2)

Card Type 14 - Columns 1-10, electron energy, ETNI(I, J) (Mev), for which the integral flux is tabulated; columns 11-20, the integral flux value, FNII(I, J), for the given electron energy. The number of these cards should be equal the number in columns 1 and 2, card type 13. Format (2E10.)

Note: The sequencing of card types 13 and 14 is: card type 13, cards type 14, card type 13, cards type 14, etc. The number of sets of card type 13 and cards type 14 should equal NNT (column 3, card type 2).

The following card types are case cards.

Card Type 15 - Column 1, spectrum option, IOPT:

1 = monoenergetic electron flux

2 = exponential integral flux, $Q(E) = Ae^{-E/B}$

3 = tabular integral flux;

Column 2, shield option, ISHLD - number indicates material location in sequence of μ-tables;

Column 3, target option, ITAR - number indicates material location in sequence of stopping power tables;

Column 4, option for tabulated integral fluxes, INTAB - integer locates position of integral flux table in sequence of integral flux tables;

Column 5, print option, IPDR:

1 = print intermediate data before integrating,

0 = omit above printing;

Column 6, compute option, ISTOP:

0 = compute,

1 = stop,

2 = dump, then stop;

Columns 9 and 10, number, NTH, of shield thicknesses (maximum of twenty);

Columns 11-20, the coefficient "A" of $Ae^{-B/E}$ for the exponential integral flux option,

Columns 21-30, the "B" of the exponential integral flux option;

Columns 31-40, the maximum electron total energy, ENM, (m_oc^2 units), including rest mass;

Columns 41-50, lower limit, BLIMIT (Mev), of integration above the "K-edge";

Columns 51-60, upper limit, ULIMIT (Mev), of integration below the "K-edge".

Card Type 16 - Seven fields of ten columns in which are entered the shield thicknesses, TH(I), to be investigated. Number of entries must equal number in columns 9 and 10 in card type 15. Format (6I1, 2XI2, 5E10./(7E10.))

Sequencing of card types 15 and 16 is: card type 15, card(s) type 16, card type 15, card(s) type 16, etc. A blank card should always follow a stop or dump card ("1" or "2" in column 6 of card type 15).

OUTPUT FORMAT

LEBC output consists of one page of information for each case card, card types 15 and 16, executed. Each page exhibits the following format. The heading card, card type 1, is printed at the top of the page. Below the heading, information is displayed consisting of the spectrum option (N(E) OPTION), the value of A, the value of B, the atomic weight (WA) of the photon shielding material, the atomic number (Z) of the electron stopping material, the atomic number (Z*) of the photon shielding material, the maximum total energy (EN(MAX)) of the incident electrons, and the integral flux table (N TABLE) used, if any. Immediately beneath the above, two columns indicate the thicknesses, gm/cm^2, of shielding material and the photon dose rate, r/hr., at each of the thicknesses. Last, twenty values of photon energy (K), in mc^2 units and the corresponding values of photon differential energy flux (I(K)) are printed.

10. MISSION FLUX CODE (LMFC)

CODE DESCRIPTION

The mapping of the trapped radiation belts is, as yet, incomplete. It is necessary, therefore, to assume certain symmetries. In particular, the altitudes corresponding to the lower edge of the proton belt at the geomagnetic equator are assumed to be independent of geomagnetic latitude. Variation of proton and electron flux densities with geomagnetic latitude and with distance above the bottom of the belt is assumed to be independent of longitude. With these assumptions, proton and electron flux densities are specified at all points as a function of geomagnetic coordinates.

The geomagnetic position of the vehicle is approximated by the following equations:

$$R_M(\lambda_G) = R_G + R_B(0) - R_B(\lambda_G) \tag{10-1}$$

$$\phi_M(\phi_G, \lambda_G) = \phi_G - \phi_E(\lambda_G) \tag{10-2}$$

$$\lambda_M(\phi_G, \lambda_G) = \lambda_G - K_1 \cdot \phi_G \cdot \sin(\lambda_G - K_2) \tag{10-3}$$

where R_M, R_G = magnitude of vehicle position vector in geomagnetic (M) and geographic (G) coordinates

R_B = distance to the bottom of the proton belt from the surface of the earth

ϕ_M, ϕ_G = geomagnetic (M) and geographic (G) north latitude of vehicle

ϕ_E = north geographic latitude of the geomagnetic equator

λ_M, λ_G = geomagnetic and geographic east longitude of vehicle.

K_1, K_2 = empirical constants, 0.25 and 111°, respectively. These constants are from an empirical fit to Vestine's data.[50]

The total flux incident on the vehicle at the completion of a specific time interval is

$$N(T) = \int_0^T \frac{dN}{dt}(R_M, \phi_M, \lambda_M)dt \qquad (10\text{-}4)$$

where dN/dt is the integral number flux rate, and the vehicle coordinates are given as functions of time.

Tables of integral number fluxes versus R_M and ϕ_M for both trapped protons and electrons are stored in the code library (input data). In addition to the flux tables, a table of R_B versus λ_G is also stored. Vehicle geographic coordinates tabulated at equal time intervals are input to describe a specific mission. These coordinates are transformed to geomagnetic coordinates by Equations 10-1 to 10-3 and dN/dt is obtained as a function of time. The total proton and total electron fluxes are determined by a numerical integration (Simpson's Rule) of Equation 10-4.

For vehicles describing closed orbits, it may be more convenient to have the code determine the vehicle geomagnetic coordinates as a function of time. Neglecting perturbations to the orbit, the equations of motion of an orbiting body may be expressed as:

$$\ddot{x} = Gx(x^2 + y^2 + z^2)^{-3/2} \qquad (10\text{-}5)$$

$$\ddot{y} = Gy(x^2 + y^2 + z^2)^{-3/2} \qquad (10\text{-}6)$$

$$\ddot{z} = Gz(x^2 + y^2 + z^2)^{-3/2} \qquad (10\text{-}7)$$

where x, y, and z = Cartesian coordinates with the origin at the geographic center of a non-rotating earth; and,

G = the universal gravitation constant multiplied by the mass of the earth, 3.985×10^{14} m^3/sec^2.

The solution of these equations is obtained from a subroutine of the main program. This subroutine is named "ORBIT".

A right handed coordinate system is selected such that the z-axis is coincident with the earth's axis of rotation, the y-axis lies in the orbital plane and has the same sense as the vehicle velocity vector at perigee.

The initial conditions are:

$$x(0) = R_{GP} \cos \alpha \tag{10-8}$$

$$y(0) = 0 \tag{10-9}$$

$$z(0) = R_{GP} \sin \alpha \tag{10-10}$$

$$\dot{x}(0) = 0 \tag{10-11}$$

$$\dot{y}(0) = \left[(1 - e)G/R_{GP}\right]^{1/2} \tag{10-12}$$

$$\dot{z}(0) = 0 \tag{10-13}$$

where R_{GP} = the magnitude of the position vector at perigee;

α = angle of inclination of orbital plane with respect to the equatorial plane; and,

e = eccentricity of the closed trajectory.

Subject to the initial conditions, Equations 10-8 through 10-13, numerical solutions of Equations 10-5 through 10-7 are obtained by the application of the Runge-Kutta-Gill integration formulae. The fourth iteration is accepted as a solution, and 200 equal time intervals are treated.

The time dependent Cartesian coordinates are transformed to earth geomagnetic coordinates, relative to a rotating earth, by the relations:

$$R_G = (x^2 + y^2 + z^2)^{1/2} \tag{10-14}$$

$$\phi_G = \arcsin (z/R_G) \tag{10-15}$$

$$\lambda_G = \lambda_{GP} - \lambda_E t - d_2 \arctan (y/x) \tag{10-16}$$

here $d_2 = \begin{cases} 1 \text{ when orbit is west to east} \\ -1 \text{ when orbit is east to west} \end{cases}$

Equations 10-1 to 10-3 are used to obtain the geomagnetic coordinates, and the time integrated flux is provided by Equation 10-4.

GLOSSARY OF INPUT DATA TERMS

PHIEM(I) - Magnetic latitude associated with electron integral flux values.

REM(I) - Altitude above the earth's magnetic center associated with electron integral flux values (kilometers).

EF(I, J) - Electron integral flux values.

PHIPM(I) - Magnetic latitude associated with proton integral flux values.

RPM(I) - Altitude above the earth's magnetic center associated with the proton integral flux values (kilometers).

PF(I, J) - Proton integral flux values.

FLT(I) - Geographic East longitude.

PHIB(I) - North geographic latitude of the geomagnetic equator at geographic east longitude FLT.

RB(I) - Distance of the bottom of the proton belt from the surface of the earth.

JDATA - Option to:

1. Read in geographic coordinates of points on vehicle trajectory.
2. Compute geographic coordinates of points on vehicle trajectory.
3. Call EXIT.

NT - Number of geographic coordinate points on vehicle trajectory to be read. (These points determine the intervals used in obtaining the integrated particle flux over the trajectory.)

T(I) - Vehicle time coordinate (seconds).

RG(I) - Vehicle geocentric radial coordinate (kilometers).

PHIG(I) - Vehicle geocentric latitudinal coordinate (degrees).

FLG(I) - Vehicle geocentric longitudinal coordinate (degrees).

E - Orbit eccentricity.

ALPHAI - Orbit plane angle of inclination (degrees) to geographic equator.

P - Perigee (meters).

OT - Time in trajectory (minutes). (If OT $\leq$ 0, code computes times for closed orbit.)

FLNO - Geocentric longitude, degrees, at T = 0 (perigee).

RSENSE - Direction of orbit: 1 = west to east
-1 = east to west

INPUT DATA PREPARATION

Card Type 1 - Seven fields of ten columns per field, each field contains a geomagnetic latitude (in degrees, in order of increasing magnitude). There should be nineteen of these latitudes - 7 on the 1st card, 7 on the second, and 5 on the third. Format (7E10.)

Card Type 2 - Seven fields of ten columns per field, each field contains a geomagnetic radius (in kilometers). There should be twelve of these radii - 7 on the first card and 5 on the second. Format (7E10.)

Card Type 3 - Seven fields of ten columns per field, each field contains an electron integral flux value associated with the above latitudes and radii. The first three cards type 3 contain nineteen electron integral fluxes associated with the nineteen latitudes and the first altitude; the second three cards type 3 contain nineteen electron integral fluxes associated with the nineteen latitudes and the second altitude; this sequencing is continued for twelve altitudes. Format (7E10.)

Card Type 4 - Seven fields of ten columns per field, each field contains a geomagnetic latitude (in degrees, in order of increasing magnitude). There should be 22 of these latitudes - 7 on the first 3 cards and 1 on the fourth. Format (7E10.)

Card Type 5 - Seven fields of ten columns per field, each field contains a geomagnetic radius (in kilometers). There should be twelve of these radii - 7 on the first card and 5 on the second. Format (7E10.)

Card Type 6 - Seven fields of ten columns per field, each field contains a proton integral flux value associated with the latitudes and radii in card types 4 and 5. The first four cards type 6 contain 22 proton integral fluxes associated with the 22 latitudes at the first altitude; the second four cards type 6 contain 22 proton integral fluxes associated with the 22 latitudes at the second altitude; this sequencing is continued for twelve altitudes. Format (7E10.)

Card Type 7 - Columns 1-10, geographic longitude; columns 11-20, north geographic latitude of the geomagnetic equator at the longitude in columns 1-10; columns 21-30, the altitude (in meters), from the surface of the earth, of the bottom of the belt at the longitude in columns 1-10. There should be 37 of these cards with longitudes from 0^{o} to 360^{o}. (All longitudes and latitudes are in degrees.) Format (3E10.)

Card Type 8 - Column 1, an integer: 1, 2 or 3.

If 1, obtain trajectory points by reading cards type 9 and 10.

If 2, obtain trajectory points by reading card type 11.

If 3, end computations.

Card Type 9 - Columns 1-3, an integer (right adjusted) signifying the number of cards type 10 to follow. Format (I3)

Card Type 10 - Columns 1-10, time (in seconds) of this point on trajectory; columns 11-20, geographic radius to trajectory at this time; columns 21-30, geographic latitude at this time; columns 31-40, geographic longitude at this time. The number of cards type 10 should equal the integer in card type 9. Format (4E10.)

Card Type 11 - Columns 1-10, eccentricity of orbit; columns 11-20, inclination angle of orbit; columns 21-30, perigree of orbit (in meters); columns 31-40, time in orbit (in minutes, should be less than or equal to one period; if zero or negative,

program will compute time for one period); columns 41-50, geographic longitude of perigee; columns 51-53, orbit direction (if 1., west to east; if -1., east to west). Format (5E10.,E3.)

OUTPUT FORMAT

The first data output by the LMFC is a two-dimensional array of the electron integral flux values. The first line of output is a list of the geomagnetic altitudes, and the first column on the left are the geomagnetic latitudes; the electron integral flux values are associated with the given altitudes and latitudes. The second two-dimensional array is the table of proton integral flux values, analogous to the electron table.

When JDATA = 2, card type 8, the values of the time, T (in seconds), and the geographic coordinates X, Y, and Z, computed by subroutine ORBIT, are listed in an array of eight columns. When JDATA $\neq$ 2, this information is not printed.

The next table displays the vehicle geocentric coordinates along the trajectory and the electron and proton integral flux values at these positions. Beneath this table, the time integrated electron and proton flux values along the vehicle flight path are exhibited.

APPENDIX A

PROTON RANGE AND

STOPPING POWER DATA

TABLE A1 PROTON ENERGY LOSSES IN MEV-CENTIMETER SQUARE PER GRAM AS A FUNCTION OF ENERGY IN MEV.

E	BE	C	MG	AL	FE	CU	AG	CS
2.	1.321E 02	1.406E 02	1.175E 02	1.117E 02	9.020E 01	8.172E 01	6.072E 01	5.849E 01
3.	9.753E 01	1.043E 02	8.766E 01	8.371E 01	6.936E 01	6.449E 01	4.906E 01	4.673E 01
4.	7.820E 01	8.394E 01	7.092E 01	6.786E 01	5.688E 01	5.350E 01	4.162E 01	3.931E 01
5.	6.563E 01	7.064E 01	6.003E 01	5.750E 01	4.853E 01	4.593E 01	3.629E 01	3.418E 01
6.	5.680E 01	6.126E 01	5.232E 01	5.015E 01	4.251E 01	4.040E 01	3.232E 01	3.035E 01
7.	5.021E 01	5.426E 01	4.652E 01	4.463E 01	3.795E 01	3.616E 01	2.924E 01	2.737E 01
8.	4.510E 01	4.881E 01	4.200E 01	4.030E 01	3.436E 01	3.281E 01	2.673E 01	2.499E 01
9.	4.101E 01	4.444E 01	3.837E 01	3.682E 01	3.146E 01	3.008E 01	2.472E 01	2.303E 01
10.	3.766E 01	4.084E 01	3.537E 01	3.396E 01	2.906E 01	2.782E 01	2.300E 01	2.140E 01
12.	3.247E 01	3.527E 01	3.068E 01	2.950E 01	2.530E 01	2.427E 01	2.028E 01	1.880E 01
14.	2.864E 01	3.114E 01	2.720E 01	2.615E 01	2.250E 01	2.160E 01	1.822E 01	1.684E 01
16.	2.568E 01	2.795E 01	2.449E 01	2.356E 01	2.031E 01	1.952E 01	1.657E 01	1.529E 01
18.	2.332E 01	2.540E 01	2.232E 01	2.148E 01	1.855E 01	1.784E 01	1.521E 01	1.403E 01
20.	2.139E 01	2.332E 01	2.054E 01	1.977E 01	1.710E 01	1.646E 01	1.405E 01	1.299E 01
22.	1.979E 01	2.159E 01	1.905E 01	1.834E 01	1.589E 01	1.530E 01	1.307E 01	1.212E 01
24.	1.843E 01	2.011E 01	1.778E 01	1.713E 01	1.486E 01	1.431E 01	1.223E 01	1.136E 01
26.	1.727E 01	1.885E 01	1.669E 01	1.608E 01	1.397E 01	1.346E 01	1.153E 01	1.070E 01
28.	1.625E 01	1.775E 01	1.574E 01	1.517E 01	1.319E 01	1.271E 01	1.094E 01	1.012E 01
30.	1.537E 01	1.679E 01	1.490E 01	1.436E 01	1.251E 01	1.206E 01	1.040E 01	9.611E 00
35.	1.356E 01	1.482E 01	1.319E 01	1.272E 01	1.111E 01	1.071E 01	9.286E 00	8.559E 00
40.	1.217E 01	1.331E 01	1.188E 01	1.145E 01	1.002E 01	9.674E 00	8.398E 00	7.756E 00
45.	1.107E 01	1.212E 01	1.083E 01	1.045E 01	9.159E 00	8.842E 00	7.673E 00	7.109E 00
50.	1.017E 01	1.114E 01	9.974E 00	9.624E 00	8.451E 00	8.161E 00	7.095E 00	6.576E 00
55.	9.432E 00	1.033E 01	9.262E 00	8.939E 00	7.859E 00	7.594E 00	6.612E 00	6.128E 00
60.	8.805E 00	9.650E 00	8.660E 00	8.359E 00	7.358E 00	7.113E 00	6.201E 00	5.745E 00
65.	8.268E 00	9.065E 00	8.143E 00	7.862E 00	6.928E 00	6.699E 00	5.847E 00	5.415E 00
70.	7.803E 00	8.558E 00	7.695E 00	7.430E 00	6.554E 00	6.338E 00	5.539E 00	5.130E 00
75.	7.397E 00	8.114E 00	7.303E 00	7.052E 00	6.226E 00	6.022E 00	5.268E 00	4.880E 00
80.	7.038E 00	7.723E 00	6.956E 00	6.717E 00	5.935E 00	5.742E 00	5.028E 00	4.658E 00
90.	6.433E 00	7.063E 00	6.370E 00	6.153E 00	5.444E 00	5.269E 00	4.621E 00	4.282E 00
100.	5.943E 00	6.527E 00	5.894E 00	5.694E 00	5.043E 00	4.884E 00	4.289E 00	3.975E 00
110.	5.537E 00	6.084E 00	5.499E 00	5.313E 00	4.711E 00	4.563E 00	4.013E 00	3.720E 00
120.	5.196E 00	5.711E 00	5.166E 00	4.992E 00	4.430E 00	4.293E 00	3.780E 00	3.504E 00
130.	4.904E 00	5.392E 00	4.882E 00	4.718E 00	4.189E 00	4.061E 00	3.579E 00	3.319E 00
140.	4.652E 00	5.117E 00	4.636E 00	4.481E 00	3.981E 00	3.861E 00	3.406E 00	3.158E 00
150.	4.432E 00	4.877E 00	4.421E 00	4.274E 00	3.799E 00	3.685E 00	3.254E 00	3.018E 00
160.	4.239E 00	4.665E 00	4.232E 00	4.091E 00	3.638E 00	3.530E 00	3.120E 00	2.894E 00
180.	3.914E 00	4.310E 00	3.914E 00	3.784E 00	3.367E 00	3.270E 00	2.894E 00	2.685E 00
200.	3.652E 00	4.024E 00	3.657E 00	3.536E 00	3.148E 00	3.058E 00	2.711E 00	2.516E 00
225.	3.388E 00	3.736E 00	3.398E 00	3.286E 00	2.927E 00	2.845E 00	2.525E 00	2.345E 00
250.	3.176E 00	3.504E 00	3.189E 00	3.085E 00	2.749E 00	2.673E 00	2.376E 00	2.207E 00
275.	3.001E 00	3.313E 00	3.018E 00	2.919E 00	2.602E 00	2.531E 00	2.253E 00	2.093E 00
300.	2.855E 00	3.154E 00	2.874E 00	2.781E 00	2.479E 00	2.412E 00	2.150E 00	1.998E 00

TABLE A1 PROTON ENERGY LOSSES IN MEV-CENTIMETER SQUARE PER GRAM AS A FUNCTION OF ENERGY IN MEV.

E	BE	C	MG	AL	FE	CU	AG	CS
325.	2.731E 00	3.019E 00	2.753E 00	2.663E 00	2.375E 00	2.311E 00	2.063E 00	1.917E 00
350.	2.625E 00	2.904E 00	2.649E 00	2.563E 00	2.286E 00	2.225E 00	1.988E 00	1.848E 00
375.	2.533E 00	2.804E 00	2.559E 00	2.476E 00	2.209E 00	2.150E 00	1.923E 00	1.788E 00
400.	2.453E 00	2.717E 00	2.480E 00	2.400E 00	2.141E 00	2.084E 00	1.867E 00	1.736E 00
450.	2.320E 00	2.573E 00	2.350E 00	2.274E 00	2.029E 00	1.976E 00	1.773E 00	1.649E 00
500.	2.214E 00	2.459E 00	2.246E 00	2.174E 00	1.940E 00	1.890E 00	1.699E 00	1.581E 00
550.	2.128E 00	2.366E 00	2.163E 00	2.093E 00	1.869E 00	1.820E 00	1.639E 00	1.526E 00
600.	2.058E 00	2.290E 00	2.094E 00	2.027E 00	1.809E 00	1.762E 00	1.589E 00	1.480E 00
700.	1.949E 00	2.174E 00	1.989E 00	1.925E 00	1.719E 00	1.675E 00	1.514E 00	1.412E 00
800.	1.870E 00	2.089E 00	1.913E 00	1.852E 00	1.654E 00	1.611E 00	1.460E 00	1.362E 00
900.	1.811E 00	2.026E 00	1.857E 00	1.798E 00	1.606E 00	1.564E 00	1.421E 00	1.327E 00
1000.	1.766E 00	1.978E 00	1.815E 00	1.757E 00	1.569E 00	1.529E 00	1.391E 00	1.300E 00
1250.	1.691E 00	1.898E 00	1.747E 00	1.691E 00	1.510E 00	1.472E 00	1.344E 00	1.258E 00
1500.	1.648E 00	1.853E 00	1.710E 00	1.655E 00	1.479E 00	1.440E 00	1.320E 00	1.238E 00
1750.	1.623E 00	1.826E 00	1.690E 00	1.635E 00	1.461E 00	1.423E 00	1.308E 00	1.229E 00
2000.	1.608E 00	1.811E 00	1.680E 00	1.625E 00	1.453E 00	1.415E 00	1.303E 00	1.226E 00
2250.	1.600E 00	1.802E 00	1.676E 00	1.621E 00	1.449E 00	1.412E 00	1.302E 00	1.227E 00
2500.	1.595E 00	1.798E 00	1.677E 00	1.621E 00	1.449E 00	1.411E 00	1.304E 00	1.231E 00
2750.	1.594E 00	1.797E 00	1.679E 00	1.623E 00	1.452E 00	1.414E 00	1.308E 00	1.236E 00
3000.	1.595E 00	1.798E 00	1.683E 00	1.627E 00	1.455E 00	1.417E 00	1.313E 00	1.242E 00
3500.	1.599E 00	1.803E 00	1.695E 00	1.637E 00	1.465E 00	1.427E 00	1.324E 00	1.256E 00
4000.	1.607E 00	1.812E 00	1.708E 00	1.649E 00	1.477E 00	1.438E 00	1.337E 00	1.271E 00
4500.	1.615E 00	1.821E 00	1.721E 00	1.662E 00	1.489E 00	1.450E 00	1.351E 00	1.286E 00
5000.	1.625E 00	1.832E 00	1.734E 00	1.674E 00	1.501E 00	1.462E 00	1.364E 00	1.300E 00
6000.	1.643E 00	1.852E 00	1.759E 00	1.698E 00	1.524E 00	1.485E 00	1.388E 00	1.328E 00
7000.	1.660E 00	1.872E 00	1.782E 00	1.719E 00	1.546E 00	1.506E 00	1.411E 00	1.353E 00
8000.	1.676E 00	1.890E 00	1.802E 00	1.738E 00	1.567E 00	1.526E 00	1.432E 00	1.376E 00
9000.	1.691E 00	1.907E 00	1.820E 00	1.756E 00	1.585E 00	1.544E 00	1.451E 00	1.396E 00
10000.	1.704E 00	1.922E 00	1.836E 00	1.771E 00	1.602E 00	1.560E 00	1.468E 00	1.415E 00
12500.	1.733E 00	1.955E 00	1.872E 00	1.806E 00	1.640E 00	1.597E 00	1.505E 00	1.456E 00
15000.	1.757E 00	1.983E 00	1.901E 00	1.834E 00	1.671E 00	1.627E 00	1.536E 00	1.490E 00
17500.	1.777E 00	2.007E 00	1.927E 00	1.858E 00	1.698E 00	1.653E 00	1.562E 00	1.518E 00
20000.	1.794E 00	2.027E 00	1.949E 00	1.880E 00	1.722E 00	1.676E 00	1.584E 00	1.543E 00
22500.	1.810E 00	2.045E 00	1.968E 00	1.898E 00	1.742E 00	1.696E 00	1.604E 00	1.565E 00
25000.	1.824E 00	2.061E 00	1.986E 00	1.915E 00	1.761E 00	1.714E 00	1.621E 00	1.584E 00
27500.	1.836E 00	2.076E 00	2.002E 00	1.931E 00	1.778E 00	1.731E 00	1.637E 00	1.602E 00
30000.	1.848E 00	2.089E 00	2.016E 00	1.945E 00	1.793E 00	1.746E 00	1.651E 00	1.617E 00
40000.	1.885E 00	2.132E 00	2.064E 00	1.991E 00	1.842E 00	1.795E 00	1.696E 00	1.669E 00
50000.	1.914E 00	2.165E 00	2.101E 00	2.027E 00	1.880E 00	1.832E 00	1.731E 00	1.709E 00
60000.	1.938E 00	2.192E 00	2.131E 00	2.055E 00	1.909E 00	1.861E 00	1.759E 00	1.740E 00
70000.	1.958E 00	2.215E 00	2.156E 00	2.080E 00	1.934E 00	1.886E 00	1.782E 00	1.766E 00
80000.	1.975E 00	2.234E 00	2.178E 00	2.100E 00	1.955E 00	1.906E 00	1.802E 00	1.787E 00
90000.	1.991E 00	2.252E 00	2.197E 00	2.118E 00	1.973E 00	1.924E 00	1.819E 00	1.806E 00
100000.	2.004E 00	2.267E 00	2.213E 00	2.134E 00	1.989E 00	1.940E 00	1.835E 00	1.823E 00

TABLE A1 PROTON ENERGY LOSSES IN MEV-CENTIMETER SQUARE PER GRAM AS A FUNCTION OF ENERGY IN MEV.

E	H	AU	PB	U	(CH2)N	H2O	TISSUE	GLASS
2.	5.084E 01	4.822E 01	4.731E 01	4.579E 01	1.725E 02	1.563E 02	1.567E 02	1.086E 02
3.	4.119E 01	3.854E 01	3.784E 01	3.756E 01	1.269E 02	1.154E 02	1.157E 02	8.179E 01
4.	3.487E 01	3.249E 01	3.192E 01	3.197E 01	1.016E 02	9.277E 01	9.296E 01	6.641E 01
5.	3.044E 01	2.834E 01	2.783E 01	2.797E 01	8.521E 01	7.804E 01	7.817E 01	5.633E 01
6.	2.713E 01	2.536E 01	2.488E 01	2.496E 01	7.371E 01	6.770E 01	6.779E 01	4.916E 01
7.	2.455E 01	2.300E 01	2.256E 01	2.261E 01	6.516E 01	5.995E 01	6.001E 01	4.376E 01
8.	2.248E 01	2.112E 01	2.071E 01	2.073E 01	5.853E 01	5.393E 01	5.398E 01	3.954E 01
9.	2.078E 01	1.958E 01	1.918E 01	1.917E 01	5.322E 01	4.909E 01	4.913E 01	3.614E 01
10.	1.935E 01	1.829E 01	1.791E 01	1.785E 01	4.886E 01	4.512E 01	4.515E 01	3.333E 01
12.	1.706E 01	1.623E 01	1.589E 01	1.576E 01	4.213E 01	3.897E 01	3.899E 01	2.896E 01
14.	1.531E 01	1.462E 01	1.434E 01	1.417E 01	3.715E 01	3.442E 01	3.442E 01	2.570E 01
16.	1.392E 01	1.335E 01	1.308E 01	1.291E 01	3.330E 01	3.090E 01	3.090E 01	2.316E 01
18.	1.280E 01	1.229E 01	1.206E 01	1.188E 01	3.024E 01	2.809E 01	2.808E 01	2.113E 01
20.	1.187E 01	1.142E 01	1.120E 01	1.102E 01	2.774E 01	2.579E 01	2.578E 01	1.946E 01
22.	1.107E 01	1.069E 01	1.048E 01	1.029E 01	2.566E 01	2.387E 01	2.386E 01	1.806E 01
24.	1.040E 01	1.005E 01	9.858E 00	9.664E 00	2.390E 01	2.224E 01	2.223E 01	1.687E 01
26.	9.809E 00	9.492E 00	9.311E 00	9.121E 00	2.239E 01	2.085E 01	2.084E 01	1.585E 01
28.	9.292E 00	9.008E 00	8.832E 00	8.647E 00	2.107E 01	1.963E 01	1.962E 01	1.495E 01
30.	8.835E 00	8.577E 00	8.410E 00	8.225E 00	1.992E 01	1.857E 01	1.856E 01	1.416E 01
35.	7.893E 00	7.682E 00	7.534E 00	7.352E 00	1.757E 01	1.640E 01	1.639E 01	1.256E 01
40.	7.160E 00	6.984E 00	6.849E 00	6.671E 00	1.577E 01	1.473E 01	1.472E 01	1.131E 01
45.	6.569E 00	6.423E 00	6.297E 00	6.123E 00	1.435E 01	1.341E 01	1.339E 01	1.032E 01
50.	6.081E 00	5.959E 00	5.844E 00	5.672E 00	1.319E 01	1.233E 01	1.232E 01	9.515E 00
55.	5.669E 00	5.566E 00	5.461E 00	5.294E 00	1.222E 01	1.144E 01	1.142E 01	8.841E 00
60.	5.319E 00	5.227E 00	5.133E 00	4.972E 00	1.141E 01	1.068E 01	1.067E 01	8.271E 00
65.	5.017E 00	4.929E 00	4.846E 00	4.694E 00	1.071E 01	1.003E 01	1.002E 01	7.781E 00
70.	4.755E 00	4.671E 00	4.592E 00	4.452E 00	1.011E 01	9.472E 00	9.459E 00	7.356E 00
75.	4.526E 00	4.443E 00	4.369E 00	4.238E 00	9.584E 00	8.981E 00	8.969E 00	6.983E 00
80.	4.325E 00	4.243E 00	4.171E 00	4.048E 00	9.119E 00	8.548E 00	8.536E 00	6.654E 00
90.	3.981E 00	3.909E 00	3.837E 00	3.724E 00	8.336E 00	7.818E 00	7.806E 00	6.097E 00
100.	3.699E 00	3.641E 00	3.573E 00	3.459E 00	7.700E 00	7.226E 00	7.214E 00	5.645E 00
110.	3.463E 00	3.413E 00	3.350E 00	3.238E 00	7.175E 00	6.735E 00	6.724E 00	5.269E 00
120.	3.263E 00	3.219E 00	3.161E 00	3.051E 00	6.733E 00	6.322E 00	6.311E 00	4.953E 00
130.	3.090E 00	3.051E 00	2.997E 00	2.892E 00	6.355E 00	5.970E 00	5.959E 00	4.682E 00
140.	2.942E 00	2.905E 00	2.854E 00	2.754E 00	6.029E 00	5.665E 00	5.655E 00	4.448E 00
150.	2.812E 00	2.775E 00	2.729E 00	2.633E 00	5.745E 00	5.399E 00	5.390E 00	4.243E 00
160.	2.698E 00	2.661E 00	2.617E 00	2.526E 00	5.495E 00	5.166E 00	5.156E 00	4.063E 00
180.	2.504E 00	2.471E 00	2.428E 00	2.345E 00	5.075E 00	4.773E 00	4.764E 00	3.760E 00
200.	2.348E 00	2.317E 00	2.277E 00	2.198E 00	4.736E 00	4.456E 00	4.447E 00	3.515E 00
225.	2.189E 00	2.162E 00	2.124E 00	2.048E 00	4.395E 00	4.137E 00	4.128E 00	3.268E 00
250.	2.061E 00	2.036E 00	2.000E 00	1.928E 00	4.121E 00	3.880E 00	3.872E 00	3.069E 00
275.	1.956E 00	1.932E 00	1.898E 00	1.829E 00	3.896E 00	3.669E 00	3.661E 00	2.905E 00
300.	1.867E 00	1.845E 00	1.813E 00	1.746E 00	3.708E 00	3.493E 00	3.486E 00	2.768E 00

TABLE A1 PROTON ENERGY LOSSES IN MEV-CENTIMETER SQUARE PER GRAM AS A FUNCTION OF ENERGY IN MEV.

E	W	AU	PB	U	(CH2)N	H2O	TISSUE	GLASS
325.	1.792E 00	1.772E 00	1.741E 00	1.676E 00	3.549E 00	3.344E 00	3.337E 00	2.653E 00
350.	1.728E 00	1.709E 00	1.679E 00	1.615E 00	3.412E 00	3.216E 00	3.209E 00	2.553E 00
375.	1.672E 00	1.654E 00	1.625E 00	1.563E 00	3.295E 00	3.106E 00	3.099E 00	2.468E 00
400.	1.624E 00	1.606E 00	1.578E 00	1.518E 00	3.192E 00	3.010E 00	3.003E 00	2.393E 00
450.	1.543E 00	1.527E 00	1.500E 00	1.442E 00	3.021E 00	2.850E 00	2.843E 00	2.268E 00
500.	1.479E 00	1.464E 00	1.439E 00	1.382E 00	2.886E 00	2.723E 00	2.717E 00	2.170E 00
550.	1.428E 00	1.414E 00	1.389E 00	1.334E 00	2.777E 00	2.621E 00	2.615E 00	2.090E 00
600.	1.385E 00	1.372E 00	1.348E 00	1.295E 00	2.688E 00	2.537E 00	2.531E 00	2.024E 00
700.	1.320E 00	1.309E 00	1.286E 00	1.235E 00	2.550E 00	2.409E 00	2.403E 00	1.924E 00
800.	1.274E 00	1.264E 00	1.242E 00	1.192E 00	2.450E 00	2.317E 00	2.311E 00	1.852E 00
900.	1.240E 00	1.231E 00	1.210E 00	1.161E 00	2.375E 00	2.249E 00	2.243E 00	1.798E 00
1000.	1.214E 00	1.206E 00	1.186E 00	1.137E 00	2.317E 00	2.197E 00	2.192E 00	1.757E 00
1250.	1.173E 00	1.167E 00	1.148E 00	1.101E 00	2.222E 00	2.115E 00	2.107E 00	1.692E 00
1500.	1.152E 00	1.148E 00	1.130E 00	1.084E 00	2.167E 00	2.068E 00	2.060E 00	1.656E 00
1750.	1.142E 00	1.139E 00	1.122E 00	1.076E 00	2.134E 00	2.040E 00	2.032E 00	1.636E 00
2000.	1.138E 00	1.135E 00	1.119E 00	1.074E 00	2.115E 00	2.024E 00	2.015E 00	1.626E 00
2250.	1.138E 00	1.136E 00	1.121E 00	1.075E 00	2.103E 00	2.015E 00	2.006E 00	1.621E 00
2500.	1.140E 00	1.138E 00	1.124E 00	1.078E 00	2.097E 00	2.011E 00	2.002E 00	1.620E 00
2750.	1.144E 00	1.142E 00	1.129E 00	1.083E 00	2.094E 00	2.010E 00	2.001E 00	1.622E 00
3000.	1.148E 00	1.147E 00	1.134E 00	1.089E 00	2.094E 00	2.011E 00	2.001E 00	1.626E 00
3500.	1.159E 00	1.158E 00	1.147E 00	1.101E 00	2.099E 00	2.017E 00	2.007E 00	1.635E 00
4000.	1.171E 00	1.171E 00	1.160E 00	1.114E 00	2.107E 00	2.025E 00	2.016E 00	1.647E 00
4500.	1.183E 00	1.183E 00	1.174E 00	1.127E 00	2.116E 00	2.035E 00	2.025E 00	1.659E 00
5000.	1.195E 00	1.195E 00	1.187E 00	1.140E 00	2.127E 00	2.046E 00	2.036E 00	1.672E 00
6000.	1.218E 00	1.218E 00	1.211E 00	1.164E 00	2.149E 00	2.067E 00	2.058E 00	1.697E 00
7000.	1.239E 00	1.239E 00	1.233E 00	1.186E 00	2.170E 00	2.088E 00	2.078E 00	1.719E 00
8000.	1.259E 00	1.258E 00	1.253E 00	1.206E 00	2.189E 00	2.107E 00	2.098E 00	1.740E 00
9000.	1.276E 00	1.275E 00	1.271E 00	1.224E 00	2.208E 00	2.125E 00	2.116E 00	1.759E 00
10000.	1.292E 00	1.291E 00	1.288E 00	1.240E 00	2.225E 00	2.142E 00	2.132E 00	1.777E 00
12500.	1.327E 00	1.326E 00	1.324E 00	1.276E 00	2.262E 00	2.179E 00	2.169E 00	1.815E 00
15000.	1.356E 00	1.355E 00	1.353E 00	1.305E 00	2.294E 00	2.211E 00	2.201E 00	1.847E 00
17500.	1.381E 00	1.379E 00	1.379E 00	1.329E 00	2.322E 00	2.238E 00	2.227E 00	1.873E 00
20000.	1.403E 00	1.400E 00	1.400E 00	1.350E 00	2.344E 00	2.261E 00	2.251E 00	1.897E 00
22500.	1.422E 00	1.419E 00	1.420E 00	1.369E 00	2.364E 00	2.282E 00	2.271E 00	1.917E 00
25000.	1.439E 00	1.436E 00	1.437E 00	1.385E 00	2.382E 00	2.301E 00	2.290E 00	1.935E 00
27500.	1.454E 00	1.451E 00	1.452E 00	1.400E 00	2.399E 00	2.318E 00	2.307E 00	1.951E 00
30000.	1.468E 00	1.465E 00	1.466E 00	1.414E 00	2.414E 00	2.333E 00	2.322E 00	1.966E 00
40000.	1.513E 00	1.510E 00	1.512E 00	1.457E 00	2.463E 00	2.384E 00	2.371E 00	2.014E 00
50000.	1.548E 00	1.544E 00	1.546E 00	1.491E 00	2.501E 00	2.422E 00	2.409E 00	2.050E 00
60000.	1.575E 00	1.571E 00	1.574E 00	1.517E 00	2.532E 00	2.453E 00	2.440E 00	2.079E 00
70000.	1.598E 00	1.593E 00	1.597E 00	1.539E 00	2.558E 00	2.479E 00	2.466E 00	2.104E 00
80000.	1.618E 00	1.613E 00	1.617E 00	1.558E 00	2.581E 00	2.501E 00	2.487E 00	2.125E 00
90000.	1.635E 00	1.629E 00	1.634E 00	1.574E 00	2.600E 00	2.521E 00	2.507E 00	2.143E 00
100000.	1.649E 00	1.644E 00	1.649E 00	1.589E 00	2.618E 00	2.538E 00	2.524E 00	2.159E 00

TABLE A2 PROTON RANGES IN GRAMS PER SQUARE CENTIMETER AS A FUNCTION OF ENERGY IN MEV.

E	BE	C	MG	AL	FE	CU	AG	CS
2.	9.100E-03	8.400E-03	1.106E-02	1.151E-02	1.767E-02	1.900E-02	2.630E-02	2.957E-02
3.	1.802E-02	1.676E-02	2.104E-02	2.198E-02	3.043E-02	3.287E-02	4.479E-02	4.884E-02
4.	2.955E-02	2.752E-02	3.381E-02	3.533E-02	4.645E-02	4.998E-02	6.701E-02	7.229E-02
5.	4.357E-02	4.056E-02	4.920E-02	5.141E-02	6.555E-02	7.022E-02	9.281E-02	9.964E-02
6.	6.000E-02	5.580E-02	6.709E-02	7.008E-02	8.762E-02	9.349E-02	1.221E-01	1.307E-01
7.	7.876E-02	7.318E-02	8.740E-02	9.126E-02	1.126E-01	1.197E-01	1.546E-01	1.655E-01
8.	9.981E-02	9.265E-02	1.101E-01	1.149E-01	1.403E-01	1.488E-01	1.904E-01	2.038E-01
9.	1.231E-01	1.141E-01	1.350E-01	1.409E-01	1.707E-01	1.806E-01	2.294E-01	2.455E-01
10.	1.486E-01	1.376E-01	1.622E-01	1.692E-01	2.039E-01	2.152E-01	2.713E-01	2.906E-01
12.	2.059E-01	1.905E-01	2.231E-01	2.325E-01	2.778E-01	2.924E-01	3.642E-01	3.905E-01
14.	2.717E-01	2.510E-01	2.924E-01	3.047E-01	3.618E-01	3.799E-01	4.685E-01	5.031E-01
16.	3.455E-01	3.189E-01	3.701E-01	3.854E-01	4.555E-01	4.775E-01	5.837E-01	6.279E-01
18.	4.274E-01	3.940E-01	4.557E-01	4.744E-01	5.587E-01	5.848E-01	7.097E-01	7.646E-01
20.	5.170E-01	4.763E-01	5.492E-01	5.716E-01	6.711E-01	7.016E-01	8.466E-01	9.128E-01
22.	6.143E-01	5.655E-01	6.504E-01	6.767E-01	7.925E-01	8.277E-01	9.944E-01	1.072E 00
24.	7.191E-01	6.615E-01	7.592E-01	7.896E-01	9.227E-01	9.630E-01	1.153E 00	1.243E 00
26.	8.313E-01	7.643E-01	8.754E-01	9.102E-01	1.062E 00	1.107E 00	1.321E 00	1.424E 00
28.	9.507E-01	8.737E-01	9.988E-01	1.038E 00	1.209E 00	1.260E 00	1.499E 00	1.617E 00
30.	1.077E 00	9.896E-01	1.129E 00	1.174E 00	1.365E 00	1.422E 00	1.687E 00	1.819E 00
35.	1.425E 00	1.307E 00	1.487E 00	1.545E 00	1.790E 00	1.862E 00	2.197E 00	2.372E 00
40.	1.814E 00	1.664E 00	1.887E 00	1.959E 00	2.264E 00	2.354E 00	2.764E 00	2.987E 00
45.	2.246E 00	2.058E 00	2.328E 00	2.417E 00	2.787E 00	2.896E 00	3.387E 00	3.661E 00
50.	2.717E 00	2.489E 00	2.810E 00	2.916E 00	3.356E 00	3.485E 00	4.066E 00	4.393E 00
55.	3.228E 00	2.955E 00	3.331E 00	3.456E 00	3.970E 00	4.120E 00	4.796E 00	5.181E 00
60.	3.777E 00	3.456E 00	3.889E 00	4.035E 00	4.628E 00	4.801E 00	5.578E 00	6.024E 00
65.	4.364E 00	3.991E 00	4.485E 00	4.652E 00	5.328E 00	5.526E 00	6.408E 00	6.921E 00
70.	4.987E 00	4.559E 00	5.117E 00	5.306E 00	6.071E 00	6.294E 00	7.287E 00	7.870E 00
75.	5.645E 00	5.159E 00	5.784E 00	5.997E 00	6.854E 00	7.103E 00	8.213E 00	8.870E 00
80.	6.338E 00	5.791E 00	6.486E 00	6.724E 00	7.677E 00	7.954E 00	9.185E 00	9.919E 00
90.	7.826E 00	7.147E 00	7.990E 00	8.282E 00	9.438E 00	9.774E 00	1.126E 01	1.216E 01
100.	9.445E 00	8.621E 00	9.624E 00	9.973E 00	1.135E 01	1.175E 01	1.351E 01	1.459E 01
110.	1.119E 01	1.021E 01	1.138E 01	1.179E 01	1.340E 01	1.387E 01	1.592E 01	1.719E 01
120.	1.306E 01	1.191E 01	1.326E 01	1.373E 01	1.559E 01	1.613E 01	1.849E 01	1.996E 01
130.	1.504E 01	1.371E 01	1.525E 01	1.580E 01	1.791E 01	1.852E 01	2.121E 01	2.289E 01
140.	1.713E 01	1.561E 01	1.735E 01	1.797E 01	2.036E 01	2.105E 01	2.408E 01	2.598E 01
150.	1.933E 01	1.762E 01	1.956E 01	2.026E 01	2.294E 01	2.370E 01	2.708E 01	2.922E 01
160.	2.164E 01	1.971E 01	2.188E 01	2.265E 01	2.563E 01	2.648E 01	3.022E 01	3.261E 01
180.	2.656E 01	2.418E 01	2.680E 01	2.774E 01	3.135E 01	3.237E 01	3.689E 01	3.979E 01
200.	3.185E 01	2.899E 01	3.209E 01	3.321E 01	3.750E 01	3.870E 01	4.403E 01	4.749E 01
225.	3.897E 01	3.544E 01	3.919E 01	4.056E 01	4.574E 01	4.718E 01	5.360E 01	5.780E 01
250.	4.660E 01	4.236E 01	4.679E 01	4.842E 01	5.456E 01	5.626E 01	6.381E 01	6.880E 01
275.	5.470E 01	4.970E 01	5.485E 01	5.675E 01	6.392E 01	6.588E 01	7.463E 01	8.044E 01
300.	6.325E 01	5.744E 01	6.335E 01	6.553E 01	7.376E 01	7.600E 01	8.599E 01	9.267E 01

TABLE A2 PROTON RANGES IN GRAMS PER SQUARE CENTIMETER AS A FUNCTION OF ENERGY IN MEV.

E	BE	C	MG	AL	FE	CU	AG	CS
325.	7.220E 01	6.554E 01	7.224E 01	7.472E 01	8.407E 01	8.659E 01	9.787E 01	1.054E 02
350.	8.154E 01	7.399E 01	8.150E 01	8.430E 01	9.480E 01	9.762E 01	1.102E 02	1.187E 02
375.	9.124E 01	8.275E 01	9.110E 01	9.422E 01	1.059E 02	1.091E 02	1.230E 02	1.325E 02
400.	1.013E 02	9.181E 01	1.010E 02	1.045E 02	1.174E 02	1.209E 02	1.362E 02	1.467E 02
450.	1.222E 02	1.107E 02	1.218E 02	1.259E 02	1.414E 02	1.455E 02	1.637E 02	1.762E 02
500.	1.443E 02	1.306E 02	1.435E 02	1.484E 02	1.666E 02	1.714E 02	1.925E 02	2.072E 02
550.	1.674E 02	1.514E 02	1.662E 02	1.719E 02	1.929E 02	1.984E 02	2.225E 02	2.394E 02
600.	1.913E 02	1.729E 02	1.897E 02	1.961E 02	2.201E 02	2.263E 02	2.535E 02	2.727E 02
700.	2.413E 02	2.177E 02	2.388E 02	2.468E 02	2.769E 02	2.846E 02	3.181E 02	3.420E 02
800.	2.937E 02	2.647E 02	2.901E 02	2.998E 02	3.362E 02	3.455E 02	3.853E 02	4.141E 02
900.	3.480E 02	3.133E 02	3.432E 02	3.547E 02	3.976E 02	4.085E 02	4.548E 02	4.886E 02
1000.	4.040E 02	3.633E 02	3.977E 02	4.110E 02	4.607E 02	4.732E 02	5.260E 02	5.647E 02
1250.	5.489E 02	4.926E 02	5.383E 02	5.563E 02	6.233E 02	6.402E 02	7.091E 02	7.605E 02
1500.	6.988E 02	6.260E 02	6.831E 02	7.059E 02	7.908E 02	8.120E 02	8.969E 02	9.610E 02
1750.	8.517E 02	7.620E 02	8.303E 02	8.579E 02	9.609E 02	9.867E 02	1.087E 03	1.164E 03
2000.	1.007E 03	8.995E 02	9.787E 02	1.011E 03	1.133E 03	1.163E 03	1.279E 03	1.367E 03
2250.	1.162E 03	1.038E 03	1.128E 03	1.165E 03	1.305E 03	1.340E 03	1.471E 03	1.571E 03
2500.	1.319E 03	1.177E 03	1.277E 03	1.320E 03	1.477E 03	1.517E 03	1.663E 03	1.775E 03
2750.	1.476E 03	1.316E 03	1.426E 03	1.474E 03	1.650E 03	1.694E 03	1.854E 03	1.978E 03
3000.	1.633E 03	1.455E 03	1.574E 03	1.627E 03	1.822E 03	1.871E 03	2.045E 03	2.179E 03
3500.	1.946E 03	1.733E 03	1.870E 03	1.934E 03	2.164E 03	2.222E 03	2.424E 03	2.580E 03
4000.	2.258E 03	2.009E 03	2.164E 03	2.238E 03	2.504E 03	2.571E 03	2.800E 03	2.975E 03
4500.	2.568E 03	2.285E 03	2.456E 03	2.540E 03	2.841E 03	2.918E 03	3.172E 03	3.367E 03
5000.	2.877E 03	2.558E 03	2.745E 03	2.840E 03	3.176E 03	3.261E 03	3.540E 03	3.753E 03
6000.	3.489E 03	3.101E 03	3.318E 03	3.433E 03	3.837E 03	3.940E 03	4.267E 03	4.514E 03
7000.	4.094E 03	3.638E 03	3.882E 03	4.018E 03	4.488E 03	4.609E 03	4.981E 03	5.260E 03
8000.	4.693E 03	4.170E 03	4.441E 03	4.597E 03	5.131E 03	5.268E 03	5.685E 03	5.993E 03
9000.	5.287E 03	4.697E 03	4.993E 03	5.169E 03	5.765E 03	5.920E 03	6.378E 03	6.715E 03
10000.	5.876E 03	5.219E 03	5.540E 03	5.736E 03	6.392E 03	6.564E 03	7.063E 03	7.426E 03
12500.	7.331E 03	6.508E 03	6.888E 03	7.134E 03	7.934E 03	8.148E 03	8.744E 03	9.167E 03
15000.	8.763E 03	7.777E 03	8.213E 03	8.507E 03	9.444E 03	9.699E 03	1.039E 04	1.086E 04
17500.	1.018E 04	9.030E 03	9.519E 03	9.861E 03	1.093E 04	1.122E 04	1.200E 04	1.253E 04
20000.	1.158E 04	1.027E 04	1.081E 04	1.120E 04	1.239E 04	1.272E 04	1.359E 04	1.416E 04
22500.	1.296E 04	1.150E 04	1.209E 04	1.252E 04	1.383E 04	1.421E 04	1.516E 04	1.577E 04
25000.	1.434E 04	1.271E 04	1.335E 04	1.383E 04	1.526E 04	1.567E 04	1.671E 04	1.736E 04
27500.	1.571E 04	1.392E 04	1.460E 04	1.513E 04	1.667E 04	1.712E 04	1.824E 04	1.892E 04
30000.	1.706E 04	1.512E 04	1.585E 04	1.642E 04	1.807E 04	1.856E 04	1.976E 04	2.048E 04
40000.	2.242E 04	1.986E 04	2.075E 04	2.150E 04	2.357E 04	2.421E 04	2.574E 04	2.656E 04
50000.	2.768E 04	2.451E 04	2.555E 04	2.648E 04	2.894E 04	2.972E 04	3.157E 04	3.248E 04
60000.	3.287E 04	2.910E 04	3.027E 04	3.138E 04	3.422E 04	3.514E 04	3.730E 04	3.828E 04
70000.	3.801E 04	3.364E 04	3.494E 04	3.621E 04	3.942E 04	4.047E 04	4.294E 04	4.398E 04
80000.	4.309E 04	3.813E 04	3.955E 04	4.100E 04	4.457E 04	4.575E 04	4.852E 04	4.961E 04
90000.	4.813E 04	4.259E 04	4.412E 04	4.574E 04	4.966E 04	5.097E 04	5.404E 04	5.517E 04
100000.	5.314E 04	4.702E 04	4.866E 04	5.044E 04	5.471E 04	5.614E 04	5.952E 04	6.068E 04

TABLE A2 PROTON RANGES IN GRAMS PER SQUARE CENTIMETER AS A FUNCTION OF ENERGY IN MEV.

E	W	AU	PB	U	(CH2)N	H2O	TISSUE	GLASS
2.	3.755E-02	3.970E-02	4.100E-02	4.526E-02	6.431E-03	7.277E-03	7.257E-03	1.290E-02
3.	5.954E-02	6.308E-02	6.481E-02	6.949E-02	1.328E-02	1.482E-02	1.478E-02	2.364E-02
4.	8.603E-02	9.148E-02	9.372E-02	9.846E-02	2.215E-02	2.455E-02	2.449E-02	3.729E-02
5.	1.168E-01	1.245E-01	1.274E-01	1.320E-01	3.295E-02	3.635E-02	3.627E-02	5.370E-02
6.	1.517E-01	1.619E-01	1.655E-01	1.699E-01	4.560E-02	5.015E-02	5.005E-02	7.276E-02
7.	1.905E-01	2.033E-01	2.077E-01	2.121E-01	6.006E-02	6.588E-02	6.576E-02	9.436E-02
8.	2.331E-01	2.488E-01	2.541E-01	2.583E-01	7.628E-02	8.350E-02	8.336E-02	1.184E-01
9.	2.794E-01	2.980E-01	3.043E-01	3.085E-01	9.422E-02	1.030E-01	1.028E-01	1.449E-01
10.	3.293E-01	3.509E-01	3.583E-01	3.626E-01	1.138E-01	1.242E-01	1.240E-01	1.738E-01
12.	4.397E-01	4.672E-01	4.771E-01	4.821E-01	1.581E-01	1.721E-01	1.719E-01	2.383E-01
14.	5.636E-01	5.972E-01	6.097E-01	6.162E-01	2.087E-01	2.268E-01	2.266E-01	3.118E-01
16.	7.008E-01	7.406E-01	7.560E-01	7.643E-01	2.657E-01	2.882E-01	2.880E-01	3.939E-01
18.	8.508E-01	8.969E-01	9.153E-01	9.259E-01	3.288E-01	3.562E-01	3.560E-01	4.844E-01
20.	1.013E 00	1.066E 00	1.088E 00	1.101E 00	3.979E-01	4.306E-01	4.304E-01	5.831E-01
22.	1.188E 00	1.247E 00	1.272E 00	1.289E 00	4.729E-01	5.113E-01	5.111E-01	6.899E-01
24.	1.374E 00	1.440E 00	1.469E 00	1.489E 00	5.538E-01	5.981E-01	5.980E-01	8.045E-01
26.	1.572E 00	1.645E 00	1.678E 00	1.703E 00	6.403E-01	6.910E-01	6.910E-01	9.269E-01
28.	1.782E 00	1.861E 00	1.899E 00	1.928E 00	7.324E-01	7.899E-01	7.899E-01	1.057E 00
30.	2.003E 00	2.089E 00	2.131E 00	2.165E 00	8.301E-01	8.947E-01	8.948E-01	1.194E 00
35.	2.603E 00	2.706E 00	2.760E 00	2.809E 00	1.098E 00	1.182E 00	1.182E 00	1.570E 00
40.	3.269E 00	3.390E 00	3.457E 00	3.524E 00	1.399E 00	1.504E 00	1.505E 00	1.990E 00
45.	3.999E 00	4.137E 00	4.219E 00	4.308E 00	1.732E 00	1.860E 00	1.861E 00	2.454E 00
50.	4.790E 00	4.946E 00	5.044E 00	5.157E 00	2.096E 00	2.250E 00	2.251E 00	2.959E 00
55.	5.643E 00	5.815E 00	5.930E 00	6.070E 00	2.490E 00	2.671E 00	2.673E 00	3.504E 00
60.	6.554E 00	6.742E 00	6.875E 00	7.045E 00	2.913E 00	3.124E 00	3.126E 00	4.089E 00
65.	7.522E 00	7.728E 00	7.878E 00	8.081E 00	3.366E 00	3.607E 00	3.610E 00	4.713E 00
70.	8.546E 00	8.770E 00	8.938E 00	9.175E 00	3.847E 00	4.120E 00	4.124E 00	5.374E 00
75.	9.624E 00	9.868E 00	1.005E 01	1.033E 01	4.355E 00	4.663E 00	4.667E 00	6.072E 00
80.	1.075E 01	1.102E 01	1.123E 01	1.153E 01	4.890E 00	5.233E 00	5.239E 00	6.806E 00
90.	1.317E 01	1.348E 01	1.373E 01	1.411E 01	6.038E 00	6.458E 00	6.465E 00	8.378E 00
100.	1.578E 01	1.613E 01	1.643E 01	1.690E 01	7.288E 00	7.790E 00	7.799E 00	1.008E 01
110.	1.857E 01	1.897E 01	1.933E 01	1.989E 01	8.634E 00	9.225E 00	9.236E 00	1.192E 01
120.	2.155E 01	2.199E 01	2.240E 01	2.307E 01	1.007E 01	1.076E 01	1.077E 01	1.388E 01
130.	2.470E 01	2.518E 01	2.565E 01	2.644E 01	1.160E 01	1.239E 01	1.240E 01	1.596E 01
140.	2.802E 01	2.854E 01	2.907E 01	2.999E 01	1.322E 01	1.411E 01	1.413E 01	1.815E 01
150.	3.150E 01	3.206E 01	3.266E 01	3.370E 01	1.492E 01	1.592E 01	1.594E 01	2.045E 01
160.	3.513E 01	3.575E 01	3.640E 01	3.758E 01	1.670E 01	1.781E 01	1.784E 01	2.286E 01
180.	4.283E 01	4.355E 01	4.435E 01	4.581E 01	2.049E 01	2.184E 01	2.188E 01	2.798E 01
200.	5.109E 01	5.192E 01	5.286E 01	5.463E 01	2.457E 01	2.618E 01	2.623E 01	3.349E 01
225.	6.213E 01	6.310E 01	6.424E 01	6.642E 01	3.006E 01	3.201E 01	3.207E 01	4.088E 01
250.	7.391E 01	7.503E 01	7.638E 01	7.901E 01	3.594E 01	3.826E 01	3.833E 01	4.878E 01
275.	8.637E 01	8.764E 01	8.922E 01	9.234E 01	4.218E 01	4.489E 01	4.497E 01	5.716E 01
300.	9.946E 01	1.009E 02	1.027E 02	1.063E 02	4.877E 01	5.188E 01	5.197E 01	6.598E 01

TABLE A2 PROTON RANGES IN GRAMS PER SQUARE CENTIMETER AS A FUNCTION OF ENERGY IN MEV.

E	W	AU	PB	U	(CH2)N	H2O	TISSUE	GLASS
325.	1.131E 02	1.147E 02	1.168E 02	1.210E 02	5.566E 01	5.919E 01	5.931E 01	7.521E 01
350.	1.273E 02	1.291E 02	1.314E 02	1.362E 02	6.285E 01	6.682E 01	6.695E 01	8.482E 01
375.	1.420E 02	1.440E 02	1.465E 02	1.519E 02	7.031E 01	7.473E 01	7.488E 01	9.478E 01
400.	1.572E 02	1.593E 02	1.622E 02	1.681E 02	7.802E 01	8.291E 01	8.308E 01	1.051E 02
450.	1.888E 02	1.913E 02	1.947E 02	2.019E 02	9.413E 01	0.	1.002E 02	1.265E 02
500.	2.219E 02	2.247E 02	2.287E 02	2.374E 02	1.111E 02	1.180E 02	1.182E 02	1.491E 02
550.	2.564E 02	2.595E 02	2.641E 02	2.742E 02	1.287E 02	1.367E 02	1.370E 02	1.726E 02
600.	2.919E 02	2.954E 02	3.007E 02	3.123E 02	1.471E 02	1.561E 02	1.564E 02	1.969E 02
700.	3.660E 02	3.701E 02	3.767E 02	3.914E 02	1.853E 02	1.966E 02	1.970E 02	2.476E 02
800.	4.431E 02	4.479E 02	4.559E 02	4.739E 02	2.253E 02	2.389E 02	2.395E 02	3.007E 02
900.	5.228E 02	5.281E 02	5.375E 02	5.590E 02	2.668E 02	2.828E 02	2.834E 02	3.555E 02
1000.	6.043E 02	6.102E 02	6.210E 02	6.461E 02	3.095E 02	3.278E 02	3.285E 02	4.118E 02
1250.	8.141E 02	8.212E 02	8.356E 02	8.698E 02	4.198E 02	4.439E 02	4.451E 02	5.570E 02
1500.	1.029E 03	1.037E 03	1.055E 03	1.099E 03	5.338E 02	5.636E 02	5.652E 02	7.065E 02
1750.	1.247E 03	1.256E 03	1.277E 03	1.330E 03	6.501E 02	6.854E 02	6.874E 02	8.585E 02
2000.	1.467E 03	1.476E 03	1.501E 03	1.563E 03	7.678E 02	8.084E 02	8.110E 02	1.012E 03
2250.	1.686E 03	1.696E 03	1.724E 03	1.796E 03	8.864E 02	9.322E 02	9.354E 02	1.166E 03
2500.	1.906E 03	1.916E 03	1.947E 03	2.028E 03	1.006E 03	1.056E 03	1.060E 03	1.320E 03
2750.	2.125E 03	2.135E 03	2.169E 03	2.259E 03	1.125E 03	1.181E 03	1.185E 03	1.474E 03
3000.	2.343E 03	2.354E 03	2.389E 03	2.490E 03	1.244E 03	1.305E 03	1.310E 03	1.628E 03
3500.	2.776E 03	2.788E 03	2.828E 03	2.947E 03	1.483E 03	1.553E 03	1.559E 03	1.935E 03
4000.	3.205E 03	3.217E 03	3.261E 03	3.398E 03	1.720E 03	1.801E 03	1.808E 03	2.240E 03
4500.	3.630E 03	3.642E 03	3.690E 03	3.844E 03	1.957E 03	2.047E 03	2.056E 03	2.542E 03
5000.	4.050E 03	4.062E 03	4.113E 03	4.285E 03	2.193E 03	2.292E 03	2.302E 03	2.842E 03
6000.	4.879E 03	4.891E 03	4.947E 03	5.153E 03	2.661E 03	2.778E 03	2.790E 03	3.436E 03
7000.	5.693E 03	5.705E 03	5.765E 03	6.003E 03	3.124E 03	3.260E 03	3.274E 03	4.021E 03
8000.	6.493E 03	6.506E 03	6.569E 03	6.839E 03	3.583E 03	3.736E 03	3.753E 03	4.600E 03
9000.	7.282E 03	7.296E 03	7.361E 03	7.662E 03	4.037E 03	4.209E 03	4.228E 03	5.171E 03
10000.	8.061E 03	8.075E 03	8.143E 03	8.474E 03	4.488E 03	4.678E 03	4.698E 03	5.736E 03
12500.	9.968E 03	9.985E 03	1.006E 04	1.046E 04	5.603E 03	5.835E 03	5.860E 03	7.128E 03
15000.	1.183E 04	1.185E 04	1.192E 04	1.240E 04	6.700E 03	6.974E 03	7.004E 03	8.493E 03
17500.	1.366E 04	1.368E 04	1.375E 04	1.430E 04	7.784E 03	8.097E 03	8.134E 03	9.837E 03
20000.	1.545E 04	1.548E 04	1.555E 04	1.616E 04	8.855E 03	9.209E 03	9.250E 03	1.116E 04
22500.	1.722E 04	1.725E 04	1.733E 04	1.800E 04	9.917E 03	1.031E 04	1.036E 04	1.247E 04
25000.	1.897E 04	1.900E 04	1.908E 04	1.982E 04	1.097E 04	1.140E 04	1.145E 04	1.377E 04
27500.	2.070E 04	2.073E 04	2.081E 04	2.161E 04	1.202E 04	1.248E 04	1.254E 04	1.506E 04
30000.	2.241E 04	2.245E 04	2.252E 04	2.339E 04	1.306E 04	1.356E 04	1.362E 04	1.634E 04
40000.	2.911E 04	2.917E 04	2.923E 04	3.035E 04	1.715E 04	1.779E 04	1.788E 04	2.136E 04
50000.	3.565E 04	3.572E 04	3.577E 04	3.713E 04	2.118E 04	2.195E 04	2.206E 04	2.628E 04
60000.	4.205E 04	4.214E 04	4.218E 04	4.378E 04	2.515E 04	2.606E 04	2.618E 04	3.112E 04
70000.	4.835E 04	4.845E 04	4.848E 04	5.032E 04	2.908E 04	3.011E 04	3.026E 04	3.590E 04
80000.	5.457E 04	5.469E 04	5.470E 04	5.678E 04	3.297E 04	3.413E 04	3.430E 04	4.063E 04
90000.	6.072E 04	6.086E 04	6.085E 04	6.316E 04	3.683E 04	3.811E 04	3.830E 04	4.532E 04
100000.	6.680E 04	6.697E 04	6.694E 04	6.948E 04	4.067E 04	4.206E 04	4.228E 04	4.996E 04

REFERENCES

1. Albert, R. D.; Welton, T. A.: A Simplified Theory of Neutron Attenuation and Its Application to Reactor Shield Design, WAPD-15, 1950.

2. Allen, F. J.; Futter, A.; Wright, W.: Neutron Reflection and Flux Versus Depth for Concrete, BRL Report No. 1189, 1963.

3. Allen, F. J.; Futter, A.; Wright, W.: Neutron Reflection and Flux Versus Depth for Iron, BRL Report No. 1199, 1963.

4. Allen, F. J.; Futter, A.; Wright, W.: Neutron Reflection and Flux Versus Depth for Water, BRL Report No. 1204, 1963.

5. Allen, R. I.; Dressler, A. J.; Perkins, J. F.; Price, H. C.; Shielding Problems in Manned Space Vehicles, NR-104, Lockheed-Georgia Company, 1960.

6. Allen, R. I.; Bly, F. T.; Diressler, A. J.; Douglass, C. C.; Perkins, J. F.; Price, H. C.; Schofield, W. M.; Smith, E. C.: Shielding Problems in Manned Space Vehicles, NR-140, Lockheed-Georgia Company, 1961.

7. Alsmiller, F. S.; Alsmiller, R. G., Jr.; Trubey, D. K.: Comparison of Primary Proton Dose With the Dose from Gamma Rays Produced by Inelastic Scattering of Solar Flare Protons, Proceedings of the Symposium on the Protection Against Radiation Hazards in Space, Gatlinburg, Tenn., November 5-7, 1962, TID7652, Book 2.

8. Blatt, J. M.; Weisskopf, V. F.: Theoretical Nuclear Physics, John Wiley and Sons, New York, N. Y., 1952.

9. Brown, L. M.: Phys. Rev. 79, 297, 1950.

10. Burrell, M. O.; Cribbs, D. L.: A Monte Carlo Calculation of Neutron Penetration Through Iron Slabs, Vol. III, NR-82, Lockheed-Georgia Company, 1960.

11. Cameron, A. G. W.: Nuclear Radiation Widths, Can. J. Phys. 35, 666, 1957.

12. Capo, M. A.: Polynomial Approximation of Gamma Ray Buildup Factors for a Point Isotropic Source, APEX 510, 1958.

13. Case, K. M.; de Hoffman, F.; Placzek, G.: Introduction to the Theory of Neutron Diffusion, Vol. I, U. S. Government Printing Office, Washington, D. C., 1953.

14. Certaine, J.; Goldstein, H.; Kalos, M.; Mittleman, P. S.: Penetration of Neutrons From a Point Fission Source Through Carbon and Hydrocarbons, NDA 12-18, 1956.

15. Dostrovsky, I.; Fraenkel, F.; Friedlander, G.: Monte Carlo Calculations of Nuclear Evaporation Processes, III, Application of Low Energy Reactions, Phys. Rev. 116, 683, 1959.

16. Dostrovsky, I.; Fraenkel, F.; Winsberg, L.: Monte Carlo Calculations of Nuclear Evaporation Processes, IV, Spectra of Neutrons and Charged Particles from Nuclear Reactions, Phys. Rev. 118, 781, 1960.

17. Gibson, W. A.: Energy Removed from Proton and Neutron Beams by Tissue, ORNL 3260, 1962.

18. Goldstein, H.: Fundamental Aspects of Reactor Shielding, Addison-Wesley, Reading, Mass., 1959.

19. Goldstein, H.; Wilkins, J. E.: Calculations of the Penetration of Gamma Rays, NYO 3075, 1954.

20. Grodstein, G. W.: X-ray Attenuation Coefficients from 10 kev to 100 Mev, NBS Circular 583, 1957.

21. Gross, E.: The Absolute Yield of Low-Energy Neutrons from 90 Mev Proton Bombardment of Gold, Silver, Nickel, Aluminum, and Carbon, UCRL-3330, 1956.

22. Grover, J. R.: Effect of Competition Between Gamma Ray and Particle Emission on Excitation Functions, Phys. Rev. 123, 267, 1961.

23. Hill, Church; Mihelick: Rev. Mod. Phys. 30, 594, 1958.

24. Hönl, H.: Fur Dispersions Theorie der Roentgen Strahlen, Z. Physik 84, 1, 1933.

25. Koch, H. W.; Motz, J. W.: Bremsstrahlung Cross-Section Formulas and Related Data, Rev. Mod. Phys. 31, 920, 1959.

26. LeCouteur, K. J.; Long, D. W.: Neutron Evaporation and Level Densities in Excited Nuclei, Nuc. Phys. 13, 32, 1959.

27. LeCouteur, K. J.; Long, D. W.: Pairing Energy Effects in Excited Nuclei, Nuc. Phys. 14, 21, 1959-60.

28. LeCouteur, K. J.: The Evaporation Theory of Nuclear Disintegrations, Pro. Phys. Soc. (London) A 63, 259, 1950.

29. Liedtke, R. A.; Steinberg, H. A.: A Monte Carlo Code for Gamma Ray Transmission Through Laminated Slab Shields, WADC 58-80, 1958.

30. Madey, R.; Duneer, A. G., Jr.; Krieger, T. J.: Gamma Dose from Solar Flare Protons Incident on an Aluminum Shield, Presented at the Annual Meeting of the American Nuclear Society, June 18-21, 1962, Boston, Mass.

31. Metropolis, N.; Bivins, R.; Storm, M.; Turkevich, A.; Miller, J. M.; Friedlander, G.: Monte Carlo Calculations on Intranuclear Cascades, I, Low Energy Studies, Phys. Rev. 110, 185, 1958.

32. Metropolis, N.; Bivins, R.; Storm, M.; Miller, J. M.; Friedlander, G.; Turkevich, A.: Monte Carlo Calculations on Intranuclear Cascades, II, High Energy Studies and Pion Processes, Phys. Rev. 110, 204, 1958.

33. Mollenauer, J. F.: Effects of Angular Momentum on Gamma Ray Production in Compound Nucleus Reactions, UCRL9724, 1960.

34. Nelms, A. T.: Energy Loss and Range of Electrons and Positrons, NBS Circular 577, 1956.

35. Nuclear Data Sheets, National Academy of Science, National Research Council, Washington, D. C.

36. O'Brien, B. J.; Van Allen, J. A.; Laughlin, C. D.; Frank, L. A.: Absolute Electron Intensities in the Heart of the Earth's Outer Radiation Zone, J. Geo. Res. 67, 391, 1962.

37. Pik-Pichack, G. A.: Nucleon Emission by A Rotating Nucleus, Soviet Phys. - JETP 11, 557, 1960.

38. Schofield, W. M.; Smith, E. C.; Hill, C. W.: Shielding Problems in Manned Space Vehicles, ER-5997, Lockheed-Georgia Company, 1962.

39. Serber, R.: Nuclear Reactions at High Energies, Phys. Rev. 72, 114, 1947.

40. Sternheimer, R. M.: Range-Energy Relations for Protons in Be, C, Al, Cu, Pb, and Air, Phys. Rev. 115, 137, 1959.

41. Sternheimer, R. M.: Density Effect for the Ionization Loss in Various Materials, Phys. Rev. 103, 511, 1956.

42. Sternheimer, R. M.: The Density Effect for the Ionization Loss in Various Materials, Phys. Rev. 88, 851, 1952.

43. Stolovy, A.; Harvey, J. A.: Radiation Widths of Levels in Nuclei Near Closed Shells, Phys. Rev. 108, 353, 1957.

44. Troubetzkoy, E. S.: Continuum Theory of Gamma Ray Spectra Following Inelastic Scattering, NDA2111-3, Vol. B, 1959.

45. Varshni, Y. P.: Comparison of Three Equations for the Spacing of Nuclear Levels, Il Nuovo Cimento XXII, 145, 1961.

46. Wakatsuki, T.; Sugimoto, K.; Mizobuchi, A.: Gamma Rays from Several Elements Bombarded by 10 and 14 Mev Protons, J. Phys. Soc. Japan, 15, 1141, 1960.

47. Walske, M. C.: The Stopping Power of K-Electrons, Phys. Rev. 88, 1283, 1952.

48. Walske, M. C.: The Stopping Power of L-Electrons, Phys. Rev. 101, 940, 1956.

49. Wick, G. C.: Del Nuovo Cimento (9), 1, 302, 1943.

50. Vestine, E. H.; et al: Description of the Earth's Main Magnetic Field and Its Secular Change 1905-1945, Carnegie Institute of Washington Pub. No. 578, Washington, D. C., 1947.

51. Fichtel, C. E.; Guss, D. E.; and Ogilvie, K. W.: Details of Individual Solar Particle Events, Proceedings of the Symposium on the Protection Against Radiation Hazards in Space, Gatlinburg, Tenn., Nov. 5-7, 1962, TID 7652, Book 1.